Development of Simultaneous Pressure and Velocity Measurements Using Multi-Luminophore Microspheres for Wind Tunnel Application

Lillian Pryor

A thesis submitted in partial fulfillment of the
requirements for the degree of

Master of Science

University of Washington

2015

Committee:

Dana Dabiri, Chair

Gamal Khalil

Program Authorized to Offer Degree:
Aeronautics and Astronautics

University of Washington

Abstract

Development of Simultaneous Pressure and Velocity Measurements Using Multi-Luminophore Microspheres for Wind Tunnel Application

Lillian Pryor

Chair of the Supervisory Committee:
Associate Professor Dana Dabiri
Aeronautics and Astronautics

The development of pressure-sensitive microbeads allows for simultaneous measurement of pressure and velocity. These aerosolized microbeads are loaded with a pressure-sensitive dye coupled with a pressure-insensitive reference dye to provide pressure measurements. Methods of fabricating these particles and the results from their response times, characterized using a shock tube facility, are presented and discussed. Imaging techniques of these particles are developed and are used for creating Stern-Volmer plots for each of the particle types developed by measuring the intensities of the pressure-sensitive dye normalized to those of the reference dye and then to a baseline condition intensity ratio. Light intensity from the microspheres is measured using EMCCD cameras and processed to back-calculate pressure. A PIV camera is used to measure light intensity from the reference dye and in the future will be used to track the particles velocities. Further results regarding technique development will be discussed.

The views expressed are those of the author and do not reflect the official policy or position of the US Air Force, Department of Defense or the US Government.

TABLE OF CONTENTS

Page

List of Figures iii

List of Tables vii

Glossary viii

Chapter 1: Introduction 1
1.1 Background 1
1.1.1 Development of PSP 1
1.1.2 Development of Microbeads 2
1.1.3 Particle Image Velocimetry and Simultaneous Pressure Measurements 2
1.2 Theory 4
1.2.1 Mechanism 4
1.2.2 Intensity-Based Method 5
1.2.3 Lifetime Method 12
1.3 Research at University of Washington 14
1.3.1 Dual-Dye Polystyrene Particles 14
1.3.2 Particle Fabrication for Single-dye Fast Response Particles . . 15
1.3.3 Test Setup 15

Chapter 2: Experimental Setup 18
2.1 Initial Stern Volmer Tests 18
2.2 Shock Tube 20
2.3 Finalized Stern Volmer Tests 22

2.4 Illumination Source . . . 26
2.5 Dichroic filter and its Ghost Image . . . 27
2.6 Aerosolizing Undyed particles . . . 29

Chapter 3: Fabrication of Viable Dual-Dye Options . . . 31
3.1 Particle Dispersion Method . . . 39
3.1.1 Particles for 532 nm Laser . . . 39
3.1.2 Particles for 355 nm Laser . . . 53
3.1.3 Uncharacterized Peak . . . 59
3.2 Forced Dye Loading Through Complete Evaporation . . . 63

Chapter 4: Experimental Results . . . 66
4.1 Response Time Characterization . . . 66
4.2 Stern-Volmer . . . 70
4.3 Particle Summary and Discussion . . . 73
4.3.1 Polystyrene Particles from Previous Researches . . . 74
4.4 Spatially Resolved Film of Particles . . . 76
4.4.1 Setup Using the Dichroic Filter . . . 76
4.4.2 Setup Using Cameras on Either Side of the Pressure Chamber 82
4.5 Spatially Resolved Individual Particles on Quartz Slide . . . 85

Chapter 5: Software Development . . . 88
5.1 Driver code . . . 88
5.1.1 Flat-field Correction . . . 89
5.1.2 Image Registration . . . 89
5.1.3 Interpolation . . . 90

Chapter 6: Conclusions . . . 91
6.1 Recommendations for Future Work . . . 93

Bibliography . . . 95

LIST OF FIGURES

Figure Number Page

1.1 Theoretical setup for PIV 4
1.2 Schematic of a Luminescent Paint (PSP or TSP) on a Surface 5
1.3 Jablonsky energy-level diagram 6
1.4 Theoretical Shock tube and x-t diagram 12
1.5 modRLD method 13
1.6 Kimura's uncertainties in oxygen concentration 14
1.7 Schematic of Fletcher Kimura's setup 16
1.8 Schematic of Fletcher Kimura's setup for aerosolized particles 17
1.9 Dan Lacroix's setup using a two-camera system and dichroic 17

2.1 Schematic of the shock tube assembly 19
2.2 Theoretical example of a Stern-Volmer linear fit 20
2.3 Aluminum diaphragm before rupture 21
2.4 Aluminum diaphragm after rupture 22
2.5 Setup with dichroic 23
2.6 Comparison between emissions of glass and quartz from 355 nm absorbance 24
2.7 Solidworks design of new pressure-chamber 25
2.8 Setup with PIV camera 26
2.9 Ghost image in A/SiOEP polystyrene sample 28
2.10 Dichroic filter optics for a ghost image 29
2.11 Setup for aerosolizing particles 30
2.12 Aerosolized undyed silica particles 30

3.1 Absorption/Emission Spectra for A, B, and D Dyes 34
3.2 Absorption/Emission Spectra for E, F, and G Dyes 35

3.3 Absorption/Emission Spectra for H, I, and J Dyes 36
3.4 Absorption/Emission Spectra for R and SiOEP Dyes 37
3.5 Absorption/Emission Spectra for O and D+ Dyes 38
3.6 Setup used for particle fabrication 39
3.7 Dye B (650 nm) Si02 41
3.8 Spectra of 1400:1 B (650 nm)/Rhodamine (570 nm) dyes 0-100 kPa . 43
3.9 Spectra of Rose Bengal (550-725 nm) dye 44
3.10 Spectra of 20:1 B (650 nm)/Sulforhodomine (605 nm) Dyes 0-100 kPa 45
3.11 Spectra of 1:2 B (650 nm)/SiOEP (580 nm) dyes 0-100 kPa 46
3.12 Spectra of 2:1 A (650 nm)/SiOEP (580 nm) $Al0_2$ dyes 47
3.13 Timed temperature change of hot plates 49
3.14 Timed temperature change for left hot plates 49
3.15 Absorption spectra of solution, Test 1 50
3.16 Absorption spectra of solution, Test 2 51
3.17 Absorption spectra of solution, Test 3 51
3.18 Absorption spectra of solution, Test 4 52
3.19 Absorption spectra of solution, Test 5 52
3.20 Absorption spectra of solution, Test 6 53
3.21 Spectra of pressure sensitivity for 50:1 A/H $Zn0_2$ particle 54
3.22 Spectra of $Zn0_2$ particle, concentration $\frac{8 \text{ mg dye A}}{100 \text{ mg particles}}$, heated 2 hr 55
3.23 Spectra of $Zn0_2$ particle, concentration $\frac{8 \text{ mg dye A}}{100 \text{ mg particles}}$, heated 7 hr 56
3.24 Spectra of $Zn0_2$ particle, concentration $\frac{8 \text{ mg dye A}}{100 \text{ mg particles}}$, heated 10 hr 56
3.25 Spectra of $Zn0_2$ particle, concentration $\frac{1 \text{ mg dye A}}{100 \text{ mg particles}}$, heated 7 hr 57
3.26 Spectra of $Zn0_2$ particle, concentration $\frac{1 \text{ mg dye A}}{100 \text{ mg particles}}$, heated 10 hr 57
3.27 Spectra of $Zn0_2$ particle, concentration $\frac{0.27 \text{ mg dye A}}{100 \text{ mg particles}}$, heated 10 hr 58
3.28 Spectra of 50:1 B (650 nm)/H (530 nm) $Zn0_2$ particle with uncharacterized peak (778.5 nm) 60

3.29 Spectra of 50:1 A (650 nm)/H (530 nm) $Zn0_2$ particle with uncharacterized peak (763.5 nm) . . . 61
3.30 Spectra of B (650 nm) $Zn0_2$ particle with uncharacterized peak (780.7 nm) . . . 61
3.31 Spectra of A (650 nm)/SiOEP (580 nm) polystyrene particle without uncharacterized peak . . . 62
3.32 Spectra of B (650 nm)/H (530 nm)-1 silica particle with uncharacterized peak (775 nm) . . . 62
3.33 Spectra of B (650 nm)/H (530 nm)-3 silica particle with uncharacterized peak (722 nm) . . . 63
3.34 Spectra of pressure sensitivity for ruthenium (640 nm)/H (C480)(530 nm) on silica particles . . . 64
3.35 Spectra of pressure sensitivity for ruthenium (640 nm)/fluorescein (580 nm) on silica particles . . . 65
4.1 Raw Labview data of intensity over time from shock tube test of a dye A $Al0_2$ particle fabricated in a previous research, conducted during a previous research . . . 67
4.2 Raw Labview data of intensity over time from shock tube test of a dye A $Al0_2$ particle fabricated in a previous research, conducted during current research . . . 67
4.3 Raw data: intensity values for shock tube test of ruthenium/H silica particle . . . 68
4.4 Filtered data: intensity values showing maximum, minimum, start time, and 63.2% and 90% response times for shock tube test of ruthenium/H silica particle . . . 68
4.5 Shock tube results for most successful particle samples . . . 69
4.6 Stern Volmer Comparison for 50:1 A/H $Zn0_2$ . . . 71
4.7 Stern Volmer for 50:1 B/H dye $Zn0_2$ particles . . . 71
4.8 Stern Volmer for dye A $Zn0_2$ and dye B $Zn0_2$ particles Without Heat 72
4.9 Stern Volmer Comparison for 50:1 A/H $Zn0_2$ and B/H $Zn0_2$ . . . 72
4.10 Summary of oxide particles and their slopes . . . 73
4.11 Stern Volmer for A polystyrene particles . . . 75
4.12 Stern Volmer for A/SiOEP polystyrene particles . . . 75

4.13 Windowed ratio-of-ratios plots for A/SiOEP polystyrene particles . . 77
4.14 Curve fit between ratio-of-ratios and pressure for A/SiOEP polystyrene particles 78
4.15 Windowed back-calculation of pressure for A/SiOEP polystyrene particle 78
4.16 Windowed ratio of ratios plots for D/J silica particles 79
4.17 Curve fit between ratio of ratios and pressure for D/J silica particles . 79
4.18 Windowed back-calculation of pressure for D/J silica particles 80
4.19 Windowed ratio-of-ratios plots for D/G silica particles 80
4.20 Curve fit between ratio-of-ratios and pressure for D/G silica particles 81
4.21 Pressure and reference intensity values and ratio of ratio versus pressure for D/G silica particles 81
4.22 Plots of pressure intensity values at each pressure (80-120 kPa) for ruthenium/fluorescein silica particles 83
4.23 Plots of reference intensity values at each pressure (80-120 kPa) for ruthenium/fluorescein silica particles 84
4.24 Scaled pressure and reference plot at atmospheric pressure for ruthenium/fluorescein silica particles 86
4.25 Plots of thresholded pressure intensity values at each pressure (70-130 kPa) for ruthenium/fluorescein silica particles 86
4.26 Plots of reference intensity values at each pressure (70-130 kPa) for ruthenium/fluorescein silica particles 87

LIST OF TABLES

Table Number Page

3.1 List of Pressure Dyes 32
3.2 List of Reference Dyes 33
3.3 Setup for Fabrication of Particles 39
3.4 Time Dependance of Stern-Volmer 55

GLOSSARY

PSP: Pressure-sensitive paint, a paint used in globally mapping pressure on a surface

PIV: Particle image velocimetry, a method for measuring velocity distributions in a flow

PSBEAD: Dual-dye particle

DCM: Dichloromethane

ISOPROPANOL: Isopropyl alcohol

ACKNOWLEDGMENTS

The author would like to thank the University of Washington and the Department of Aeronautics and Astronautics for giving her the opportunity to explore a fascinating subject and collaborate with imaginative and motivated peers. She expresses her appreciation to her professors, Professor Dana Dabiri and Professor Gamal Khalil, as well as her lab associates Trey Cottingham, Nick Dona, Josh Hunt, Gai Ogihara, and Jamie Lambie for their collaboration. A special thanks to Dr. Wei Hsin-Tien and Dan Lacroix for their indispensable help in the experimental setup, and to Professor Bob Breidenthal, for his advice on PSParticle application to flow fields.

DEDICATION

To my family, Dustin, McKenna, and Kaila, who helped keep me sane.

Chapter 1
INTRODUCTION

1.1 Background

1.1.1 Development of PSP

When testing the aerodynamics of a model in a wind tunnel for unsteady flow application, pressure is vital for fully diagnosing the flow. Pressure plays a role in determining boundary layer transition and separation characteristics, providing information about shocks, defining the distribution of aerodynamic loads for aircraft design, determining ambient conditions in the wind tunnel, and in validating computational fluid dynamics (CFD).[1] In unsteady flow, changes in the flow occur very quickly, along the order of microseconds.

Developing a fast-responding instrument to capture changes within small eddies can be very useful. Several methods of quantitatively measuring pressure have been developed. Pressure transducers with field taps provide a discrete measurement of the localized pressure, but its placement can interfere and tamper with the aerodynamic characteristics of the test subject. To create a sufficiently resolved pressure field on a complex aircraft model, Sullivan mentions that hundreds of pressure taps must be utilized.[1] Manufacturing a model with built-in tubing becomes very expensive and labor-intensive.[1]

Pressure-sensitive paint (PSP) in the U.S. was developed in 1989 at the NASA Ames Research Center using a coating developed by researchers at the University of

Washington and has become a well-established and commercialized test method used commonly in wind tunnel applications.[1–9] The facilities for AEDC, ARA, TsAGI, and DLR all have testing systems for use with PSP.[10]

PSP's use in unsteady flow applications has been demonstrated testing rotor blades.[11,12] Gregory et. al. provides useful instruction on the application of fast-response PSP.[13]

The benefits of dual dyes in PSP's in reducing systematic errors has been realized early on by labs such as ISSI of Dayton of Ohio, Mébarki of the NRC of Canada on automotive model testing, and by researchers such as Muhammet Kose at University of Florida.[14,15] Fletcher Kimura demonstrates the usefulness of a dual dye by calibrating the light intensity of polymer coupons to pressure.[14] PSP provides more spatial resolution on a test subject and is more cost-effective, but is limited to determining pressure along the surface of the test subject.

1.1.2 Development of Microbeads

Aerosolized fast-responding dual luminophore microbeads pose a viable solution to a more global pressure mapping of an unsteady environment. A substrate particle such as anodized aluminum oxide, silica, or zinc oxide ranging 3-19 μm are coated with two separate dyes. The pressure dye is sensitive to pressure and the reference dye is insensitive to pressure. When a light source is used to excite these particles, both dyes fluoresce in response. Using an intensity-based technique, the illumination of these dyes can be measured, ratioed, and calibrated to pressure.

1.1.3 Particle Image Velocimetry and Simultaneous Pressure Measurements

Particle Image Velocimetry (PIV) is a well-established technique and has previously been used to observe reflectance from a 2-D sheet of illuminated particles.[16,17] Fig-

ure 1.1 shows a theoretical representation of a typical PIV setup.[10] Tracer beads are seeded into the flow of interest and illuminated by a pulsed light source. Two consecutive images of the beads are taken using digital cameras with a known time difference, usually a few microseconds, between the two images. A cross-correlation method is used between the two images to determine the displacement, and the velocity distribution can then be determined.[10]

Airborne Particles in Nitrogen

Abe and co-workers researched PSParticles made of fumed silicon dioxide particles with porous outer shells loaded with the pressure-sensitive luminophor ($[Ru(bpy)^{2+}_{3}]$-Cl_2).[14] They injected the particles into a flow of mixed oxygen and nitrogen gas that emptied from a jet into an ambient air chamber and used rapid lifetime determination of the particles' luminescence to measure oxygen concentration.[14] When the oxygen concentration was more than 5%, their error increased to 16%.[18] The ruthenium-based pressure-sensitive luminophore has a high temperature dependence, so they needed careful monitoring of temperature.[8] They stated but did not demonstrate PIV.[8]

Ideally, the microbeads coated with pressure-sensitive dyes can simultaneously provide luminescence for use in pressure measurement and be used as tracer particles in the flow to allow for PIV to calculate velocity. This measurement technique would open the door to endless experimental opportunities and would offer a new method for determining flow properties within turbulent and unsteady flow applications.

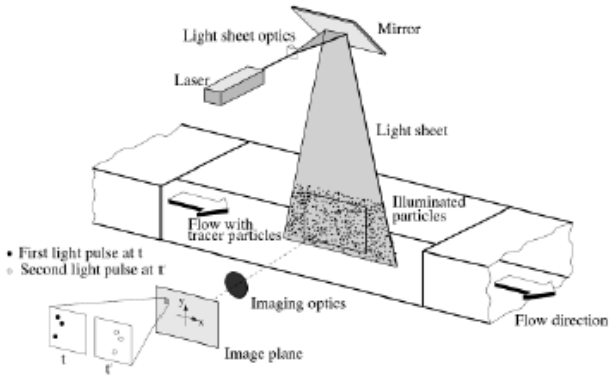

Figure 1.1: Theoretical setup for PIV[10]

1.2 Theory

1.2.1 Mechanism

The dyes coating the particles are composed of luminophores, molecules capable of absorbing light and re-emitting light at a lower energy level, as shown in Figure 1.2. The luminophores absorb light from a specific range of wavelengths and emit light at a known and higher range of wavelengths. When luminophores are energized with light energy, they enter an excited state. The excited electronic states involved are the singlet states S_1 and S_2 and the triplet state T_1. Each state has its own rotational states.[1] T_1 has a lower energy than the corresponding singlet state S_1.[1] The luminophores need to release the excess energy in order to return to their ground electronic state, S_0.[1,15] They can release that energy through radiative or nonradiative processes.[1,15] Nonradiative processes include vibrational energy, releasing of heat, or oxygen quenching.[8] One radiative process is luminescence, which is composed of fluorescence and phosphorescence. Fluorescence is the spin-allowed radiation transition from S_1 to S_0, states of the same multiplicity.[1] Phosphorescence is the transition from T_1 to S_0, an intersystem crossing process and "forbidden" transition.[1] For phospho-

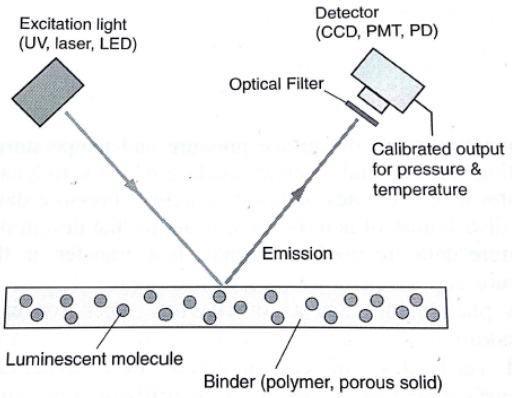

Figure 1.2: Schematic of a Luminescent Paint (PSP or TSP) on a Surface[1]

rescence to occur, the luminophore has to undergo an electron spin flip before relaxing to the singlet ground state, S_0.[19] For this reason, the phosphorescent lifetime is usually longer than that of fluorescence.[1] The Jablonsky energy-level diagram depicting this process in shown in Figure 1.3.

Phosphorescence typically has timescales on the order of milliseconds to seconds.[19,20] To measure the light emission of the luminophores, experiment setups use a measurement system which includes a monochromatic light source (LED or laser), a photodetector, and a pressure transducer. To determine spacial resolution of luminophore emission, a charge-coupled device (CCD) can be used.[19,21–23]

1.2.2 Intensity-Based Method

Due to their polarity, oxygen molecules in contact with luminophores will receive electrons from the luminophores, lowering their energy state and reducing the intensity of the luminescence emanating from the luminophores in a process called oxygen or luminescence quenching.[1,8] Light intensity of the luminophores is thus indirectly proportional to the concentration of oxygen. Henrys law states that the concentration of

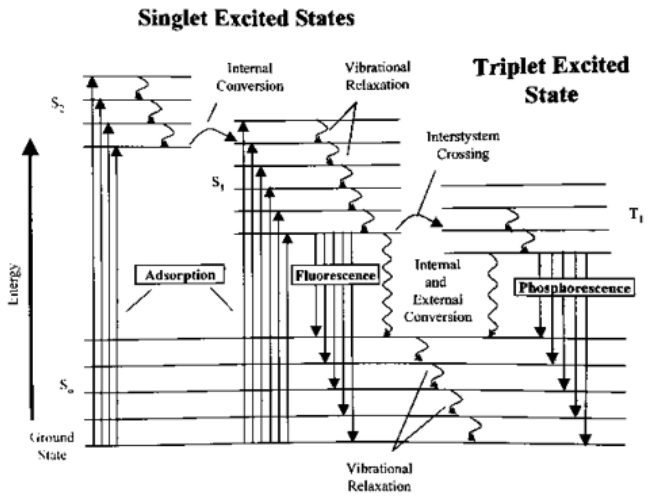

Figure 1.3: Jablonsky energy-level diagram[1]

oxygen within the dye is proportional to the partial pressure of oxygen or air pressure residing outside the dye, so luminescence is indirectly proportional to pressure.[1]

Stern-Volmer

The Stern-Volmer equation, shown by equation 1.1, describes the relationship between oxygen concentration and luminescent intensity.[1,4] The variables I and and P stand for luminescent intensity and air pressure, while I_{ref} and P_{ref} are the corresponding variables at the reference conditions.[1] I is typically known as the wind-on intensity, whereas I_{ref} is the wind-off intensity, typically taken at atmospheric conditions.[1] A and B are temperature-dependent coefficients that are determined empirically.[1]

$$\frac{I_{ref}}{I} = A + B\frac{P}{P_{ref}} \tag{1.1}$$

Ideally, the intensity ratio I_{ref}/I will remove any effects of uneven dye loading, illumination, or concentration of the particles, with the cost of the acquisition of an

additional image of the subject for referencing.

There are a variety of factors that affect the response time and intensity of the luminescence of the particles. The concentration of the dye, whether the particle is saturated or only coated with dye, the properties of self-quenching, the permeability of oxygen into the dye, etc. When the dye is oxygen-permeable, the oxygen molecules can interact with luminophores within the dye.[1,15]

Temperature usually affects the luminescent intensity of the particles inversely in a process known as thermal quenching.[10] Pressure-sensitive beads are inherently temperature-sensitive. Ideally, ratioing the pressure dye with a reference dye should help reduce temperature errors.

Ratiometric Method with Dual Dye

An issue with the aforementioned form of the Stern-Volmer equation is its application to airborne particles. The particles move in their environment, making a reference image for a single dye particle difficult to acquire. Dual-dye paints were developed to eliminate the need to take a wind-off reference image of the subject. With a dual dye, the reference intensities for the Stern-Volmer equation become those of the reference dye, which can be taken simultaneously with the pressure dye's using a second camera. The intensity-based ratiometric method thus requires the use of two cameras to image the luminescence from the reference dye and from the pressure dye. Ratioing pressure dye intensity to a reference dye helps to reduce the uncertainties due to temperature changes, particle size, particle density, light intensity, and other ambient variables.

Time Response in turbulent flow

The response time of the particles is an important characteristic because certain flow applications may require instrument response on the order of microseconds. An

understanding of the smallest-forming eddies in turbulent flow provides information about the minimum possible time requirement needed for particle response times. To find the timescale for the smallest eddies in a flow, certain characteristics must be considered. The energy dissipated per unit time per unit mass of fluid, ϵ, represents the "energy flux" continually transferring from large to small eddies.[24] Equation 1.2 shows Kolmogorov and Obukhov's law, which relates velocity variation to eddy size.[24]

$$v_\lambda \sim (\epsilon\lambda)^{\frac{1}{3}}, \tag{1.2}$$

where v_λ is the velocity of turbulent eddies and λ is the size of the given eddy.[24] The characteristic time of the flow for a given eddy size is $\tau_\lambda = \frac{\lambda}{v_\lambda}$. Reynold's number on the order of the smallest eddies, $Re_{\lambda 0}$, is expressed by $Re_{\lambda 0} \sim \frac{v_{\lambda 0}\lambda_0}{\nu}$. $Re_{\lambda 0}$ is similar to one.[24] After some manipulation, equation 1.3, revealing the time constant for small scale eddies, is found.[24]

$$\tau_{\lambda 0} \sim \frac{\delta}{v_\delta} {Re_\delta}^{-\frac{1}{2}}, \tag{1.3}$$

where $\tau_{\lambda 0}$ is the smallest eddy time scale, δ is the characteristic length for the larger eddies, and Re_δ is its corresponding Reynold's number.[24] Another form of this equation is equation 1.4.

$$\tau_{\lambda 0} \sim \frac{\delta^2}{\nu} {Re_\delta}^{-\frac{3}{2}}, \tag{1.4}$$

where ν is the kinematic viscosity of the fluid. An example for a typical time scale seen in turbulent flow would be a flow whose larger eddies have a Reynold's number of 70,000, a kinematic viscosity of 0.14 cm^2/sec, and a large eddy size of 25 cm (9.8 in), which would lead to a small eddy timescale of approximately 240 μs. The Kolmogorov timescale can be altered in an experimental setup by changing these conditions.

It should also be noted that the airborne particles have not been tested in their capability to follow along the movement of the smallest eddies and additional testing is necessary to optimize the particles' capability of following the flow. This is important for the purpose of PIV as well. Stokes number, a unitless number comparing the characteristic time of the particle to the flow's characteristic time scale and expressed in equation 1.5, quantifies the flow-following characteristics for a particle.[25]

$$St = \frac{\tau_p}{\tau_{\lambda 0}} \ll 1 \tag{1.5}$$

τ_p is the relaxation time of the particle or the time constant in the exponential decay of the particle velocity due to drag.[25,26] When Stokes number is far less than one, the particle is able to follow the flow. Equation 1.6 shows that a low τ_p, and therefore a low Stokes number, depends on minimizing particle size and density.[24] A balance must therefore be made between the desirability for a larger, brighter particle to measure pressure and the requirement for the particles to be small enough to follow the flow accurately.

$$\tau_p = \frac{\rho_p d_p^2}{18 \mu_f \rho_f} \tag{1.6}$$

In equation 1.6, ρ_p is the particle density, ρ_f is the fluid density, d_p is the particle diameter, and μ_f is the fluid dynamic viscosity.[25] The primary particles used in this research, silica particles, have a density of 1.67 g/cc and their maximum diameter is 19 μm. Air's density is 1.00 g/cc and its dynamic viscosity is 0.14 g/cm-s. The corresponding particle response time is 2.93 μs. To obtain a Stokes number of 0.01, the required large eddy Reynold's number is found to be approximately 70,000. Besides being able to kinematically follow the flow, the particles need to have a fast-enough pressure response time relative to the Kolmogrov time scale. A Stokes number for pressure response is given by using the 63.2% or 90% rise time of the particle rather

than τ_p in equation 1.5. Using a 63.2% and 90% rise time of 100 μs and 200 μs, respectively, the times associated with one of the best-performing particles, a Stokes number of 0.42 and 0.83, respectively, results. This means that the time it takes for the particle's luminosity to respond to pressure is less than the time for a Kolmogrov scale eddy to rotate once. If a Stokes number of 0.01 is desired for the 63.2% and 90% rise times, a maximum Reynold's number of 6,000 and 4,000, respectively, can be used.

There are many factors that contribute to the luminescent time response of a particle. Smaller particles tend to have shorter response times.[27] Response times of the particles are also dependent on the luminescent lifetime of the oxygen-sensitive luminophore, the thickness of the layer of dye on the particle, and the particle's oxygen diffusivity.[8] Because particles cannot respond faster than the lifetime of the luminophor used, experimentally useful oxygen-sensitive luminophors generally have lifetimes between 1 and 50 μs.[8] These lifetimes, however, tend to be shorter than time constants relating to oxygen diffusion for the particle.[8] For a thin layer of PSP, the 99% rise time is calculated using equation 1.7

$$\tau_{99\%} = \frac{12L^2}{\pi^2 D}, \tag{1.7}$$

where L is the thickness of the paint and D is the matrix's oxygen diffusion coefficient.[8] The response time for a spherical PSBead is shown by equation 1.8.

$$\tau_{99\%} = \frac{3d^2}{4\pi^2 D} \tag{1.8}$$

where d is the diameter of the bead.[8] Based on this principle, a PSbead with a thin coating of dye is ideal for faster time responses, at the cost of emission brightness.[8] Also, if D is too large, too much oxygen quenching can occur at atmospheric pressure.[8] PSP's capability at measuring fast-responding flow has been validated through

measuring vortex shedding and airflow over rotor blades.[8,12,28,29] However, polymer based matrices, which respond on the order of milliseconds, do not respond as quickly as anodized aluminum or silica gel.[30,31]

Shock Tube

The shock tube, a commonly used device for generating fast pressure changes, is used in this experiment for measuring the response time of the pressure-sensitive particles. It is composed of two sections with different pressures, separated by a diaphragm. While the driver side is kept at ambient pressure, air is vacuumed from the driven side of the chamber until the pressure difference forces the diaphragm to rupture. The resulting compression waves travel down the driven section while expansion waves move across the driver section. The compression waves superimpose to form a normal shock wave that propagates downstream and generates a near-instantaneous pressure rise. Gregory and Sullivan performed a time response study using a Fluidic Oscillator and discovered that paints respond faster to pressure decreases than pressure increases.[10,32] The shock tube test thus measures the time response in their worst case scenario. The speed of the shock generated is shown in equation 1.9.

$$V_s = a\left[\frac{\gamma_1 - 1}{2\gamma_1} + \frac{\gamma_1 + 1}{2\gamma_1}\frac{p_2}{p_1}\right]^{\frac{1}{2}}, \tag{1.9}$$

where p_1 and p_2 are the pressures before and after the shock respectively, a is the speed of sound, and γ_1 is the specific heat ratio of air, approximately 1.4.[33] A theoretical example of the shock tube device and an x-t diagram are shown in Figure 1.4.

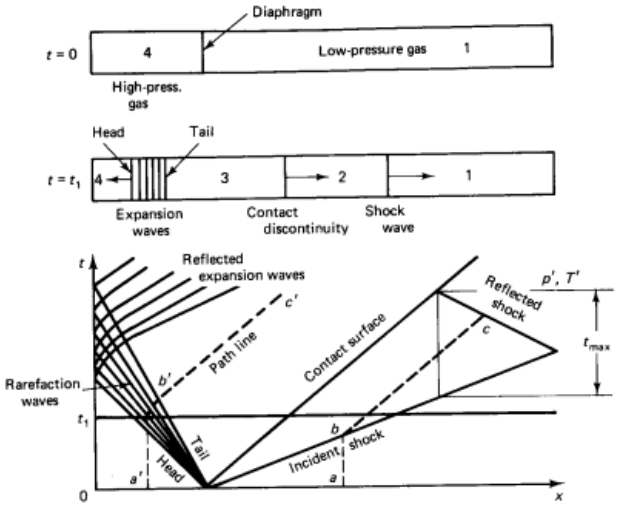

Figure 1.4: Theoretical Shock tube and x-t diagram[10,33]

1.2.3 Lifetime Method

Phosphorescence has a theoretical exponential decay, shown by equation 1.10.[19,34]

$$I = I_0 e^{-t/r} + D_0, \tag{1.10}$$

where I_0 is the luminophore's initial intensity after excitation, t is time, τ is the phosphorescent lifetime, and D_0 is the background signal.[19,34] The luminophors balance their loss of energy between oxygen quenching and luminescence. Smaller oxygen concentrations thus result in more phosphorescence and longer phosphorescent lifetimes. Through Henry's law, which relates oxygen concentration to oxygen's partial pressure, lifetimes can be used to determine the surrounding air pressure.[6,19] One technique for measuring lifetime is rapid lifetime determination (RLD).[19,35] Luminescence decay is integrated over two periods of time and the lifetime is found using the ratio of the integrals.[19] A modified version of the technique, modRLD, was developed and the decay curve was split into two regions I and II, split at time t_d.[19,21] Figure

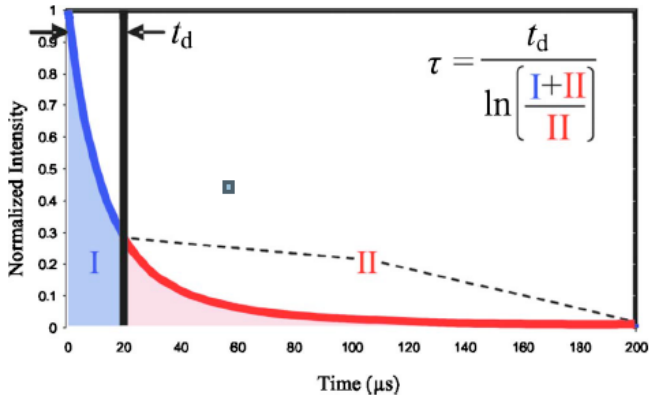

Figure 1.5: modRLD method for lifetime calculation[19,21]

1.5 shows an example decay curve.

Equation 1.11 shows how lifetime value is calculated with modRLD.[19,21]

$$\tau = \frac{\tau_d}{\ln \frac{I+II}{II}} \tag{1.11}$$

The main disadvantage for using the lifetime method with fast-responding aerosolized particles is the need for averaging intensity over a large area through pixel binning to reduce the uncertainties in measuring oxygen concentration, demonstrated in Kimura's research and Abe's research.[19] Kimura's uncertainties corresponding to different pixel binning are shown by Figure 1.6. Kimura, in his research with aerosolized particles, had pressure measurement errors as high as 0.5 atm with 2 x 2 binning, which he largely attributed to limitations in acquiring sufficient signal.[19] He was able to reduce these uncertainties to 0.003-0.005 atm with the use of 32 x 32 pixel binning.[19]

Abe et al. experienced high uncertainties in his airborne particles, particularly under conditions with higher oxygen concentration. His error was about 20% with 4 pixel averaging, and 10% with 16 pixel averaging.[18]

	δ_P (atm)			
% O_2	2×2 pixels	8×8 pixels	16×16 pixels	32×32 pixels
21	0.465	0.109	0.052	0.027
16.8	0.273	0.058	0.029	0.017
10.5	0.130	0.029	0.015	0.009
4.2	0.056	0.014	0.007	0.004
0	0.021	0.005	0.003	0.002

Figure 1.6: Kimura's uncertainties in oxygen concentration[19]

Low signal-to-noise signal was an added disadvantage to Kimura's approach. The intensity-based method for pressure measurement is better able to collect a stronger signal from the airborne particles because it is able to use a more sensitive low-light camera, as well as being able to image the full luminescence into the CCD.

1.3 Research at University of Washington

1.3.1 Dual-Dye Polystyrene Particles

Research has previously been performed on pressure-sensitive particles. In Kimura's research, oxygen-sensitive polystyrene microspheres (PSBeads) were doped with dual luminophores. These luminophores were platinum porphyrin (PtOEP, emitting at 650 nm), an oxygen-sensitive luminophore, and silicon porphyrin (SiOEP, emitting at 580 nm), an oxygen-insensitive reference dye.[14] The particles were highly uniform (1-5 microns) and could be made with high yield. Fletcher Kimura imaged the dual-dye polystyrene particles in an air suspension in a quartz chamber.[14] Kimura was able to take simultaneous velocity measurements using digital particle image velocimetry.[19]

While these particles have been shown to be very bright and highly responsive to pressure, they have a longer response time to pressure changes, occurring on the order of milliseconds. The 2.5μm diameter PSBeads showed a 1/e response time of 3.15

ms and a 99% response time of 8.8 ms.[8] Kimura tested some osmium-based silicon dioxide microspheres which showed a response time of 13.6-18.9 μs, but suffered from a significant decrease in signal-to-noise ratio.[8]

For the purposes of turbulent flow, this research seeks to discover particles that are fast-responding, on the order of microseconds, while maintaining sufficient brightness and pressure sensitivity.

1.3.2 Particle Fabrication for Single-dye Fast Response Particles

In an effort to increase the brightness for fast-response PSbeads, experimentation in the production of single dye microspheres was done by researcher Jonathan Howard. 2 mg of dye was dissolved into 10 mL of dichloromethanol in a glass vial and 500 mg of anodized aluminum oxide beads was added to the mixture. The mixture was sonicated for 1 hour, stirred for 24 hours, and heated to just below the boiling point. The sample was washed twice with deionized water through 5 minute centrifuging. A sample of the particles in solution was pipetted onto a glass slide.

These particles were shown to be sufficiently bright, but when a second reference dye was added, the overall brightness of the particle was diminished. This presented a challenge to be addressed in this research.

1.3.3 Test Setup

Previous researches at the University of Washington have tried multiple setups and methods to image luminescence. Fletcher Kimura used an image multiplexer known as the MultiSpec Imager, which has an internal beam splitter, to image dual-dye PSP's and particles on one CCD, shown in Figure 1.7.[14] Kimura's setup for aerosolizing particles is shown in Figure 1.8. An adaptation of this setup is used in this experimentation and described in detail in the experimental setup.

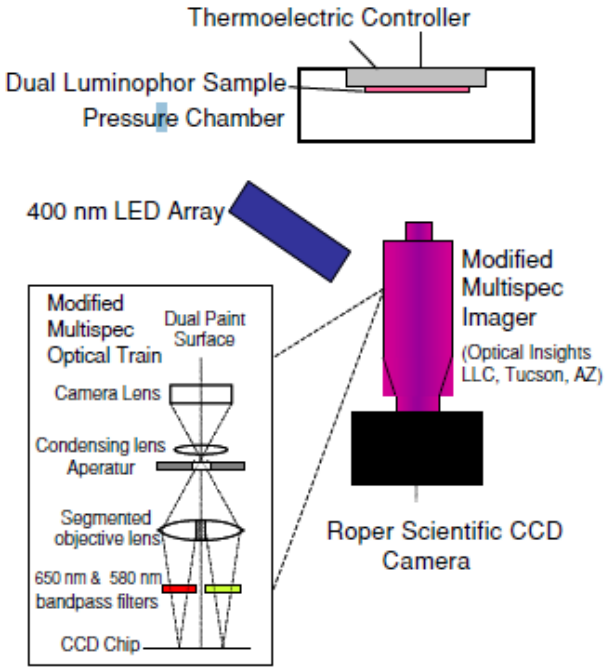

Figure 1.7: Schematic of Fletcher Kimura's setup[14]

Daniel Lacroix imaged dual and triple dye polystyrene particles using a 532nm YAG laser and dichroic beam splitter to send the emissions of the reference and pressure dyes separately to a Hamamatsu EM CCD camera and sCMOS camera.[10] His setup is shown by Figure 1.9. He performed shock tube and Stern-Volmer experiments for each of his particle sets.[10] His setup for shock tube and preliminary Stern-Volmer tests is used and adapted in this research, and detailed further in the experimental setup.

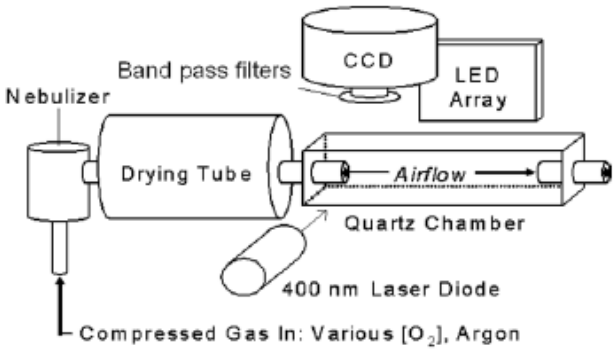

Figure 1.8: Schematic of Fletcher Kimura's setup for aerosolized particles[14]

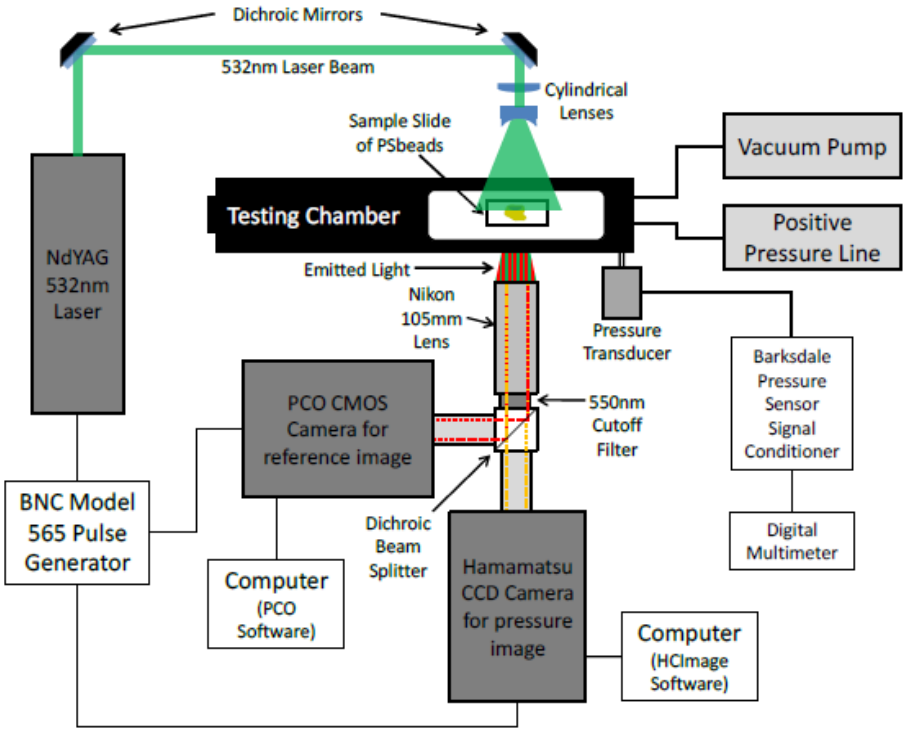

Figure 1.9: Dan Lacroix's setup using a two-camera system and dichroic[10]

Chapter 2

EXPERIMENTAL SETUP

2.1 Initial Stern Volmer Tests

Initial tests for Stern-Volmer and shock tube results used an LED or laser diode as an excitation source to illuminate the quartz-windowed test section of the shock tube. The setup is shown in Figure 2.1. The shock tube used is an aluminum square tube with 0.64 cm thick walls and a cross section of 3.9 x 3.9 cm. The driver section is 3.1 m long and the driven side is 1.8 m long. The chamber has two 1.9 x 3.8 cm test windows 0.58 m downstream of the diaphragm.[10] Two pressure transducers are mounted 0.12 m downstream of the test window in the driven section. Both transducers are mounted flush with the walls to avoid impedance of the flow.[10] Differential pressure was measured with a high-sensitivity dynamic pressure transducer (model 211B5, Kistler Instruments, Amherst, NY) attached to a power supply coupler (model 5114, Kistler Instruments, Amherst, NY), with a 90% rise time of 2 μs.[10,36] The absolute pressure measurements were taken using an Omega PX236 series pressure transducer with a recorded accuracy of 0.25% of the full scale.[10,36] The light emitted by the particles is focused through a plano-convex lens array into the photomultiplier (PMT Hamamatsu R928), which is mounted directly over the top quartz window and fitted with a filter to transmit solely the emission of the pressure dye. Its response time is 2.2 μs and its gain was adjusted to output a 1 volt signal from measured light emission at ambient conditions. The signals from the transducers and PMT were passed through a National Instruments data acquisition board (BNC-2120), sampling at 100k samples/sec, to a computer where data could be processed using Signal Ex-

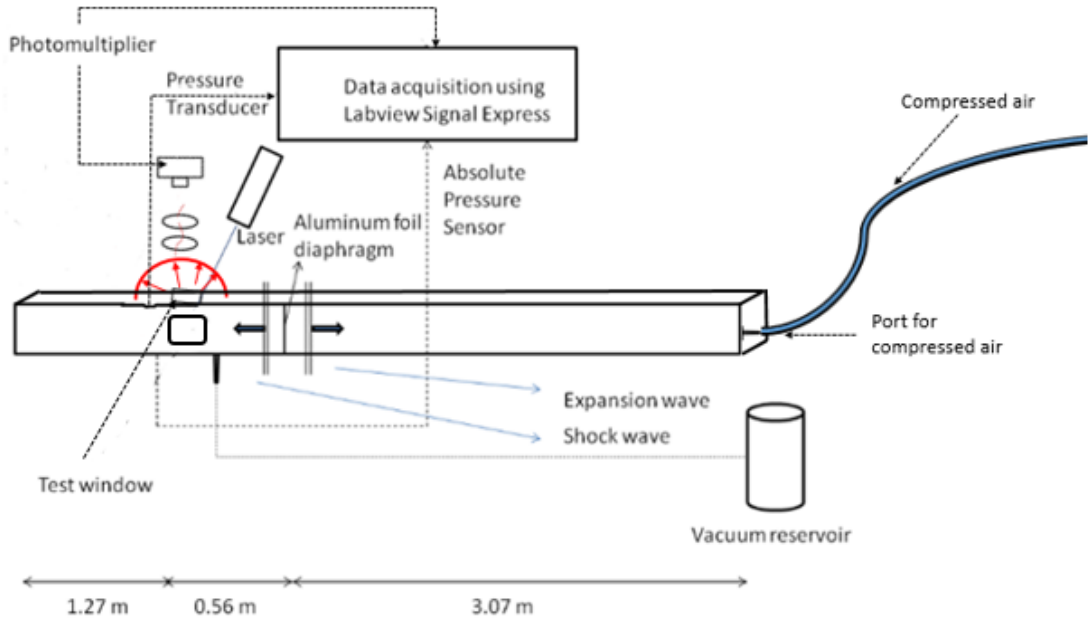

Figure 2.1: Schematic of the shock tube assembly[36]

press Labview.

In a Stern-Volmer test, a film of the sample was coated onto a piece of a microscope slide and secured face down on the top quartz window. Based on the optimal absorption wavelength of the dye, either a 365-405 nm or a 532 nm LED was used to excite the particles. With the PMT measuring the pressure dye's emission, air pressure was increased from atmospheric by opening a valve to allow compressed air to flow into the chamber, and then the air was vacated by sealing the valve and opening another connected to the vacuum reservoir. After removing effects of photodegradation using linear detrending, a linear curve was fit to the emission intensities normalized by the atmospheric condition and the pressure inside the chamber. An example is shown by Figure 2.2.

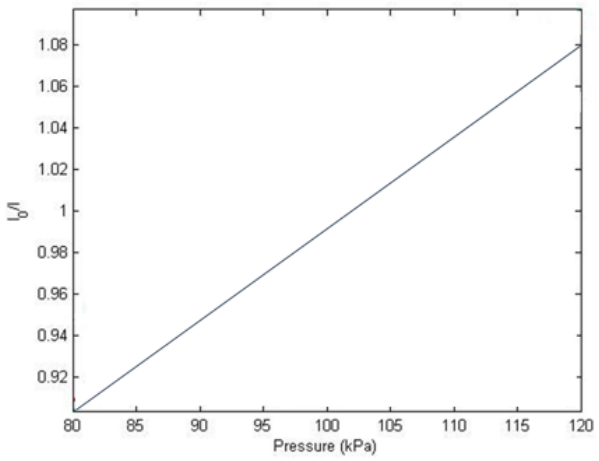

Figure 2.2: Theoretical example of a Stern-Volmer linear fit

2.2 Shock Tube

Pieces of microscope slide coated in the particles were mounted onto the inside portion of the top window face down so as to directly contact the shock wave. The samples were excited and their emission sampled from the same quartz window to prevent anomalies to due changes in index of refraction of the air caused by the passing shockwave.[8] A vacuum reservoir, fully vacuumed ahead of time using a vacuum pump, was used to decrease the pressure to 30-50 kPa on the driven section within a couple of seconds, resulting in the diaphragm rupturing. The driver side of the chamber was held at atmospheric pressure, approximately 100 kPa. The diaphragm for the shock tube is a 3.9 x 3.9 cm^2 square of heavy duty aluminum foil with a cross form etched using a slightly sharp tool such as tweezers. Care had to be taken not to etch the diaphragm so deeply that a through hole was made, which would prevent a shock form forming, or so shallow that the rupture no longer followed the perforations, and several iterations had to be performed to perfect the method. The

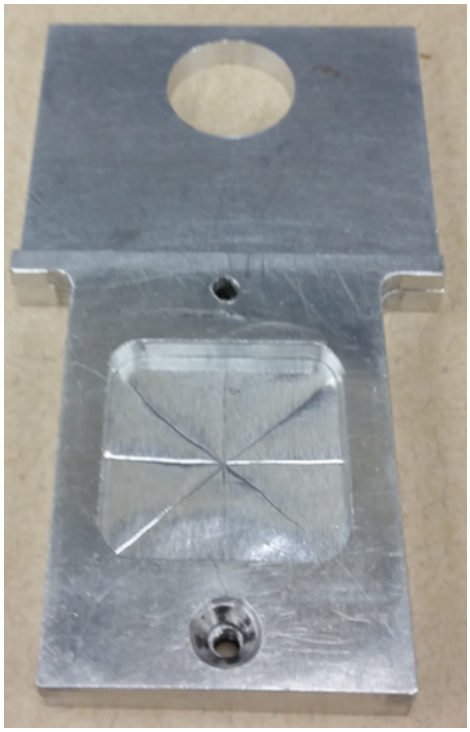

Figure 2.3: Aluminum diaphragm before rupture

diaphragm before rupture is shown in Figure 2.3. Figure 2.4 shows the diaphragm after it is ruptured. The data was processed through Matlab to calculate the 63.2% and 90% response times of the particles.

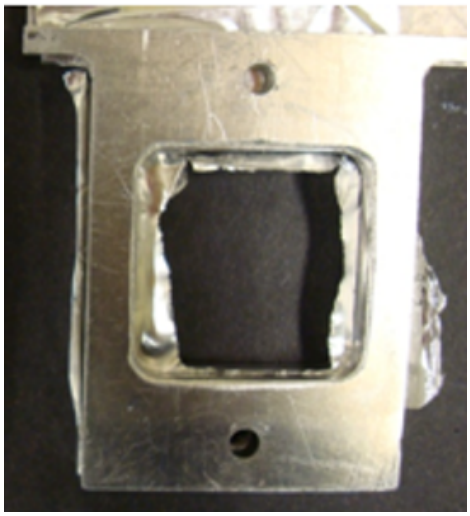

Figure 2.4: Aluminum diaphragm after rupture[36]

2.3 Finalized Stern Volmer Tests

Two different setups were used for testing pressure sensitivity with the cameras. In the first setup, an aluminum pressure chamber 35 x 5 x 5 cm with interior test section dimensions of 6 x 4 x 4 cm and quartz glass windows 6 x 2.5 cm on the top, front and bottom faces of the chamber was used.[10] A Barksdale 402h2 Series pressure transducer with a pressure range of 0-50 psi and an accuracy of 0.25% full scale attached to a Barksdale pressure sensor signal conditioner monitored the pressure throughout the experiment.[10] The particle samples were illuminated with a Quantel 355nm YAG laser. Their emission was captured through an 85 mm lens connected to a dichroic filter, which split the emission based on wavelength and passed the reference and pressure emissions separately into two EMCCD Hamamatsu cameras. The setup is shown by Figure 2.5. It was determined that using glass as a slide for the particles is not ideal because glass absorbs a portion of the laser light. Quartz has little to no absorption of the laser light and was used instead. Figure 2.6 compares the intensity

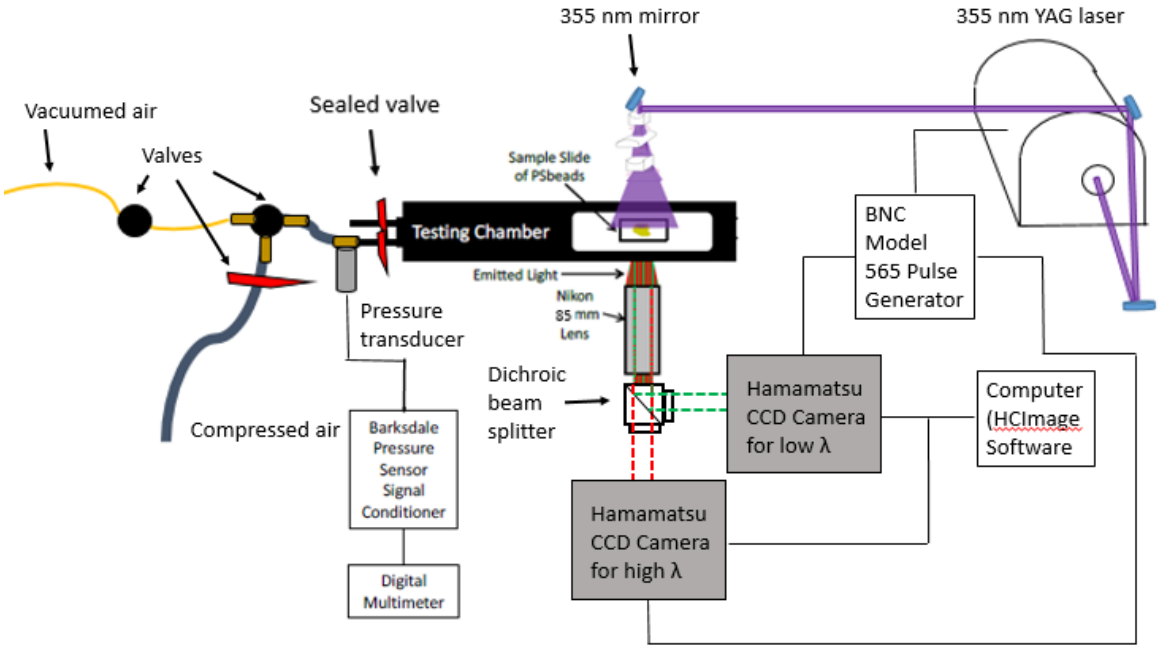

Figure 2.5: Setup with dichroic[10]

values seen between glass and quartz when a pulsed 355 nm YAG laser is shown on each.

In order to better validate the pressure-measuring capability of the particles in eventual wind tunnel use, it was speculated that tests with a larger size sample would be useful. The first setup was too small to fit a sample more than a couple of centimeters long. A fellow researcher, Trey Cottingham, discovered upon modification of the first setup that if the sample's size is increased to fill a higher portion of the field of view, vignetting and significant distortions around the edges of the sample occur. An image-quality lens array behind the dichroic filter becomes necessary to refocus the image. However, this significantly decreases the light signal received from the test setup.[25] Since signal-to-noise ratio is one of the limiting factors in luminescence experimentation, this poses a challenge to acquisition. To combat this issue

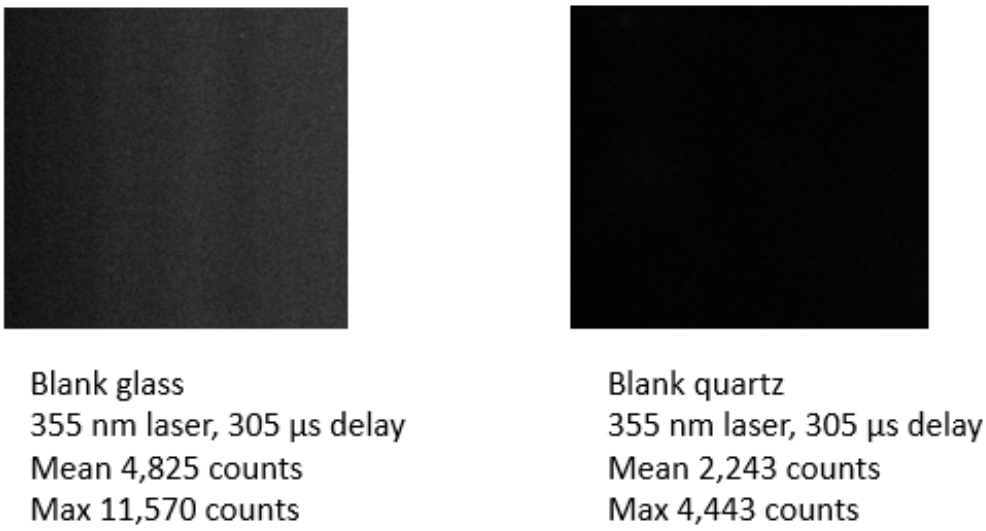

Figure 2.6: Comparison between emissions of glass and quartz from 355 nm absorbance

and better allow the capability for larger samples, a larger field of view, and simultaneous velocity measurements, a second test setup was made. In this setup, a new, larger aluminum pressure chamber was designed and built. The new chamber has four quartz windows with dimensions 4 x 4 x 0.25 in on the front and rear sides and 2 x 4 x 0.25 in on the top and bottom sides. More detailed dimensions are shown in Figure 2.7. The tests under this setup were run with an increased field of view of 4.1 cm.

The Barksdale pressure transducer used in the first setup has an uncertainty of approximately 860 Pa. Since the standard deviations being observed between the back-calculation of pressure from the particles and the measured pressure were 100-200 pascals for the A/SiOEP polystyrene particle, it is important to have a pressure transducer that can measure pressure with a lower uncertainty than the standard deviations. The equipment was upgraded in the second setup to a Mensor CPT 6100

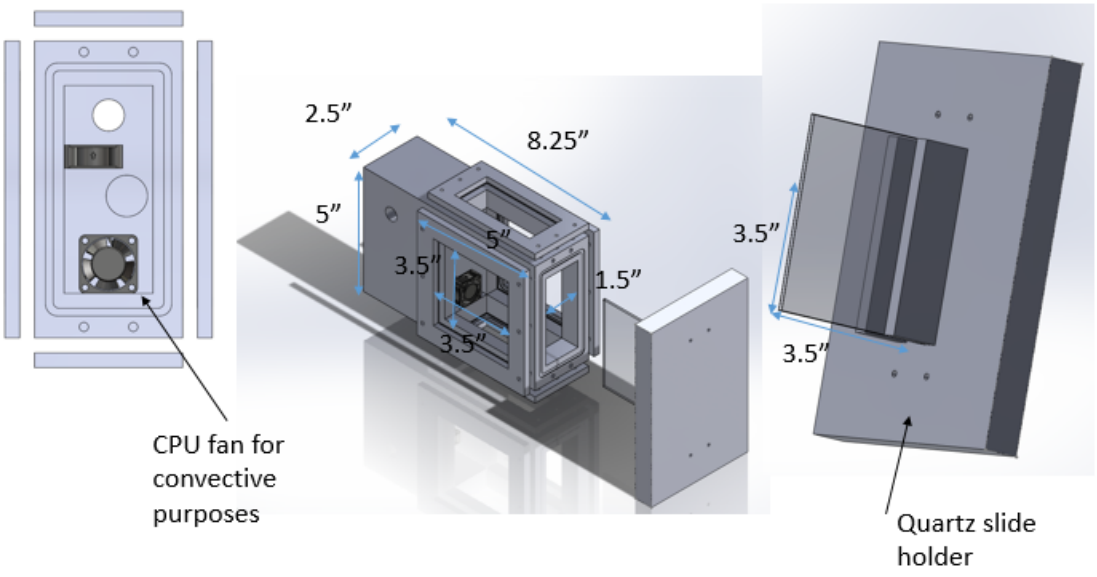

Figure 2.7: Solidworks design of new pressure-chamber

pressure transducer with a range 70-130 kPa and a full scale accuracy of 0.01%, or 6 pascals. It was read with a Keithley 9100 multimeter, which has an uncertainty of 0.00175 volts, adding an uncertainty of 10.5 pascals to the transducer and resulting in a total uncertainty of 16.5 pascals.

Temperature controllability was considered to be an attractive capability in the instance that temperature effects needed to be accounted for, or if temperature-sensitive particles needed to be tested. To allow for temperature controllability for future temperature measurements, two 1/4 in pipe screws with a hermetically sealed high-temperature cartridge heater (120 volts, 3/8 in diameter, 1-1/2 in length, 250 Watts) and a thermocouple were fitted to the chamber. A hermetically sealed DB-9 port was installed to allow the electrical wires of two small CPU fans (3010S WD, 12V DC, 0.10A, 4.1 CFM) usable for convection purposes to pass through. The additional quartz window in the chamber provides the capability to install a Particle Image

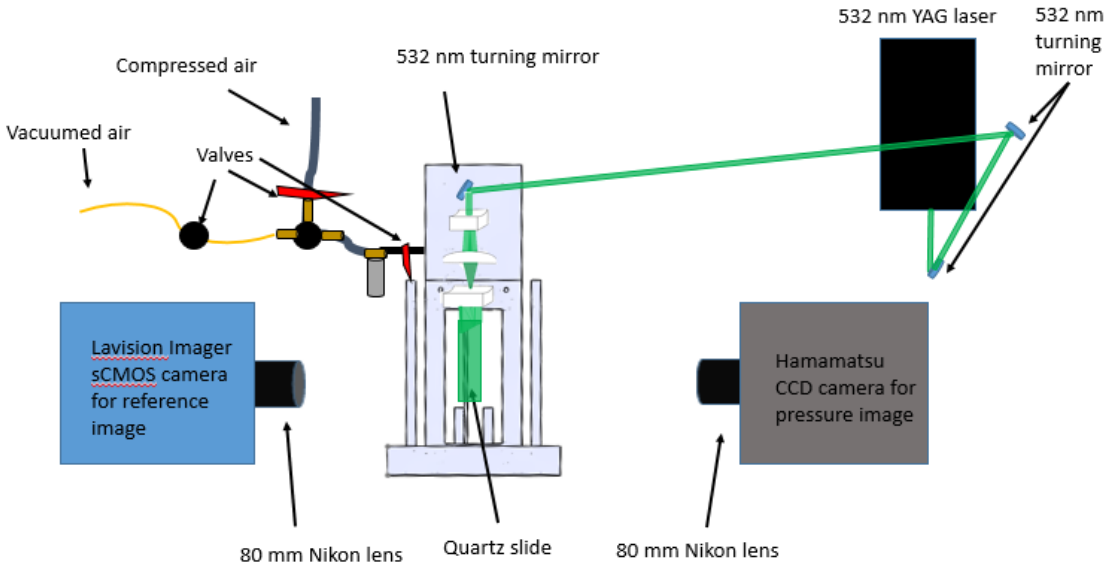

Figure 2.8: Setup with PIV camera[10]

Velocimetry (PIV) camera on the back side of the chamber. Furthermore, the PIV camera was used as the new reference camera to alleviate the need for a dichroic filter and light-diminishing lens array. This also eliminated the need for a third camera in a 2-dye system, reducing the image registration and alignment requirements. A schematic of the new setup is shown by Figure 2.8.

2.4 Illumination Source

In the first setup, a Quantel Brilliant B 532 nm pulsed YAG laser outfitted to supply a secondary 355 nm beam was used. This laser had a rated energy output of 400 mJ per pulse at 532 nm and outputted approximately 100 mJ per pulse at 355 nm. A delay of 305 μs was used between the flash lamp and q-switch for testing, and a frequency of 15 Hz was set using a BNC model 565 pulse generator. The use of a 355 nm laser is beneficial because it has a higher range of wavelengths above its emission than

a 532 nm laser does, allowing more flexibility in selecting a pressure/reference dye combination with spectral separation between their emission peaks. While the 355 nm laser was being used for another research project, the beam's diameter increased substantially and its intensity dropped. Upon inspection it was determined that an initial misalignment of the laser's internal optics had caused some of the optical components to be damaged over time, and once a critical point had been reached, the laser was no longer safely usable without the replacement of the damaged components. In the second experimental setup, a 532 nm pulsed dual Nd:YAG laser (New Wave Research, Solo PIV) was used instead. 532 nm laser line dichroic mirrors (Thorlabs, NB1-J12) were used to turn the beam as needed and direct its light into the pressure chamber.[10] Replacing the 355 nm laser with a 532 nm one presented a substantial challenge because all of the particles made in-house were designed for a 355 nm excitation source. This resulted in the need for developing a new particle that can work under 532 nm excitation.

2.5 Dichroic filter and its Ghost Image

When using the dichroic filter in the first setup to transmit the emission of an A/-SiOEP polystyrene particle sample excited by the 355 nm laser, an offset and dimmer ghost image of the object of interest could be seen on the camera viewing the reflected light from the dichroic filter, shown by Figure 2.9. The transmitted image from the dichroic filter did not show the ghost image. The phenomenon is described by Figure 2.10, where a theoretical dichroic filter is shown reflecting light from a cathode-ray tube.[37] The dashed lines depict the rays that form the ghost image. Ray 1 contains light of blue and yellow wavelengths. When the light contacts the dichroic coating, the lower-wavelength blue light reflects as ray 2. The yellow light continues as ray 3 until it contacts the back side of the dichroic filter, where a portion of its light

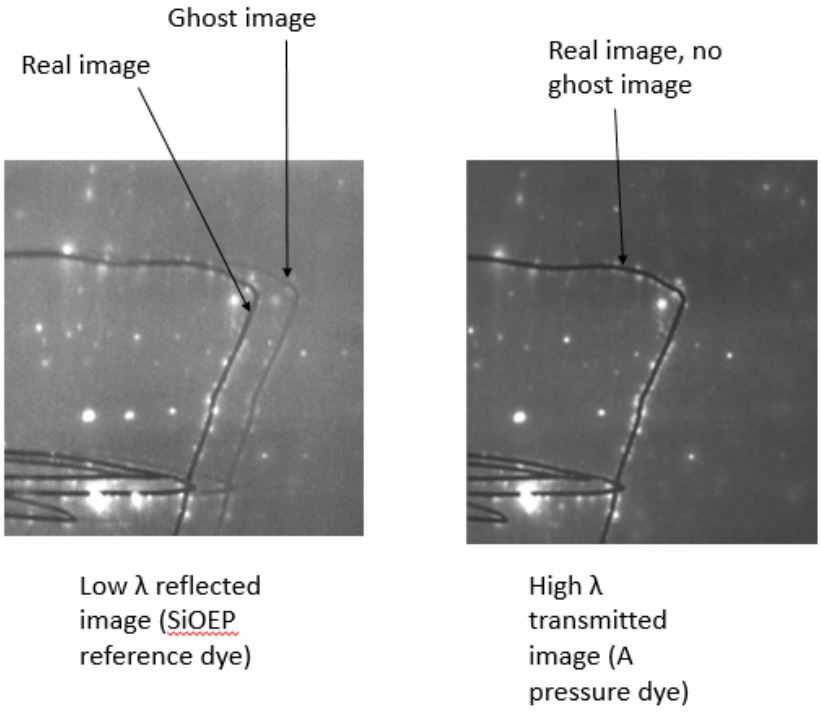

Figure 2.9: Ghost image in reflected image of an etched A/SiOEP polystyrene sample on the left, no ghost image seen in transmitted image on the right

reflects as ray 5 despite the anti-reflectance coating and transmits through the filter, offset as ray 6.[37] Ray 6 is the ghost image and is primarily higher-wavelength light. Because it is higher in wavelength than the transmitted light, the ghost image could be eliminated by adding a shortpass filter on the reflected side of the dichroic that only transmits the low-wavelength emission.

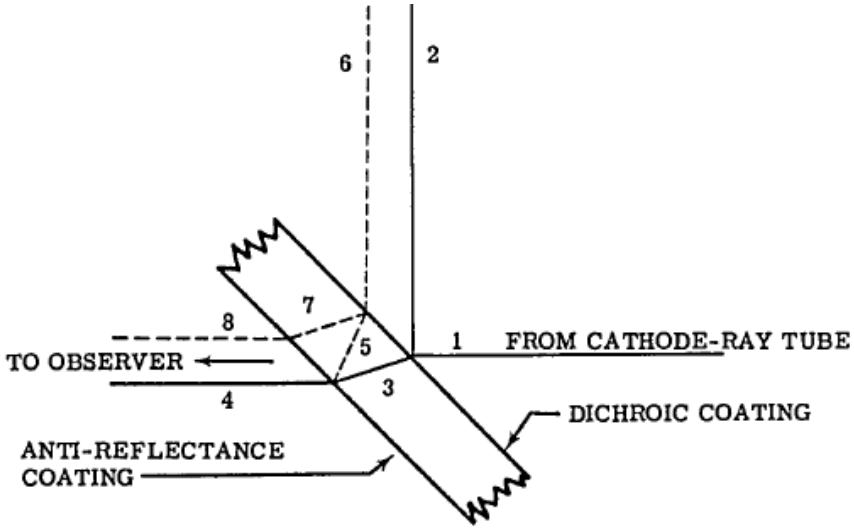

Figure 2.10: Dichroic filter optics for a ghost image[37]

2.6 Aerosolizing Undyed particles

In order to demonstrate the feasibility of imaging particles with the new setup, an aerosolized test of undyed silica particles was performed. A solution of the undyed silica particles of concentration 50 mg/10 mL hexane was placed in a nebulizer under 20-30 psi. The nebulizer generates a mist of particles which flows into a diffusion dryer (TSI Incorporated, Model 3062).[14] A T-shaped adapter has been added to this setup to allow for a small crossflow to aid in passing the aerosolized particles into the dryer. From the dryer, the particles pass into the quartz chamber to be imaged. For the purpose of aerosolizing particles, a side wall with an exit port connected to a particle filter was attached. The setup is shown by Figure 2.11. The aerosolized particles imaged from the Hamamatsu camera are shown in Figure 2.12.

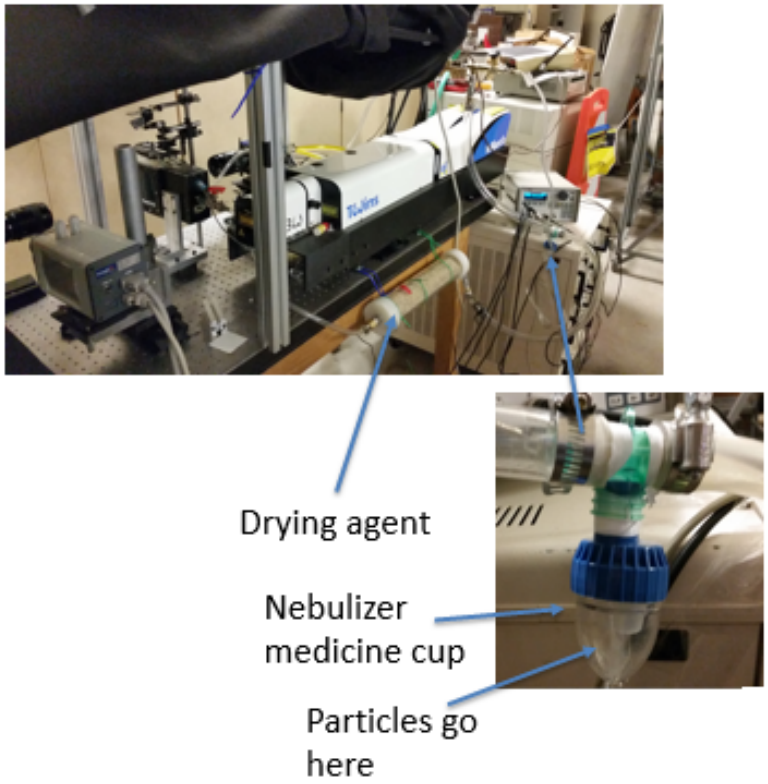

Figure 2.11: Setup for aerosolizing particles

Figure 2.12: Aerosolized undyed silica particles

Chapter 3

FABRICATION OF VIABLE DUAL-DYE OPTIONS

Previous research conducted by Daniel Lacroix discovered that the response times of PTSBeads made in a two-step process, where dye is coated onto pre-made particles, were shorter than particles made in a one-step process, where the particle is created while simultaneously loading it with dye.[10] He reported 63.2% and 90% response time values of 114 μs and 204 μs, respectively, with standard deviations of 69 μs and 117 μs for the one-step process, while his two-step PTSBeads had response times of 41 μs and 79 μs, with standard deviations of 25 μs and 66 μs, respectively.[10] In addition, it is easier to control size with pre-fabricated particles. In this research, the two-step method was used.

An effective bead-making process will load both dyes onto the particles homogeneously and in such a manner as to balance higher light intensity with a shorter time response. Particles with porous surfaces tend to provide higher surface area and more dye loading. While this can help make the particles brighter, saturating the particle with too many layers of dye will drastically decrease the particles' response time, which is dependent on the particle thickness and permeability. The two-step method is beneficial because it allows only a thin coating of the dye on the particle, which allows for faster time responses. However, it follows that the particles are less bright. The pressure dyes used in testing are shown in Table 3.1, and the reference dyes are shown in Table 3.2. Figures 3.1, 3.2, 3.3, 3.4, and 3.5 show the absorption and emission spectra for each dye.[25] Figure 3.6 shows the setup used in making the particles. Four hot plates with magnetic stirrers, called the left, mid-left, mid-right,

and right hot plates based on their location in this research, were used for heating and stirring the liquid dye solutions containing particles. A condenser was provided for each hot plate to reduce the rate of evaporation of the solutions. The boiling flasks containing the heated solutions were submerged in sand baths to help provide uniform heating. The manufacturers of the hot plates are given in Table 3.3.

Table 3.1: List of Pressure Dyes

	Dye	Name	Emission Wavelength (nm)	Manufacturer
Pressure	A	Pt (II) Octaethyl-porphine (PtOEP)	650	Frontier Scientific
	B	Pt (II) meso-Tetra (pentafluorophenyl) porphine	650	Frontier Scientific
	D+	Iridium (III) Bis(3-[2-benzothiazolyl] coumarin Hexafluoro-acetylacetone	585	N/A
	O	Acridine Orange	640	Molecular Probes
	R	tris-(Bathophe-nanthroline) Ruthenium (II) Chloride	595	GFS Organic Chemicals

Table 3.2: List of Reference Dyes

	Dye	Name	Emission Wavelength (nm)	Manufacturer
Reference	F	Rhodamine base B	570	N/A
	G	meso-Tetra(pentafluoro-phenyl)porphine chlorin free	700	Frontier Scientific
	SiOEP	Si (IV) R1, R2 Octaethylporphine (mixture of ligands R1, R2=0Me, OH, Cl)	580	Frontier Scientific
	RS	Sulforhodamine 101	605	N/A
	H	Coumarin 6, 440, 480	530	Lumtec, Exiton Chemical Co
	I	Aluminum (III) Phthalocyanine Chloride Tetrasulfonic Acid	685	Frontier Scientific
	J	Magnesium (II)meso-Tetra (penta-fluorophenyl)porphine	650	Frontier Scientific
		Rose Bengal	N/A	Aldrich
		Rhodamine 6G	570	N/A
		Fluorescein acid crystals	580	N/A

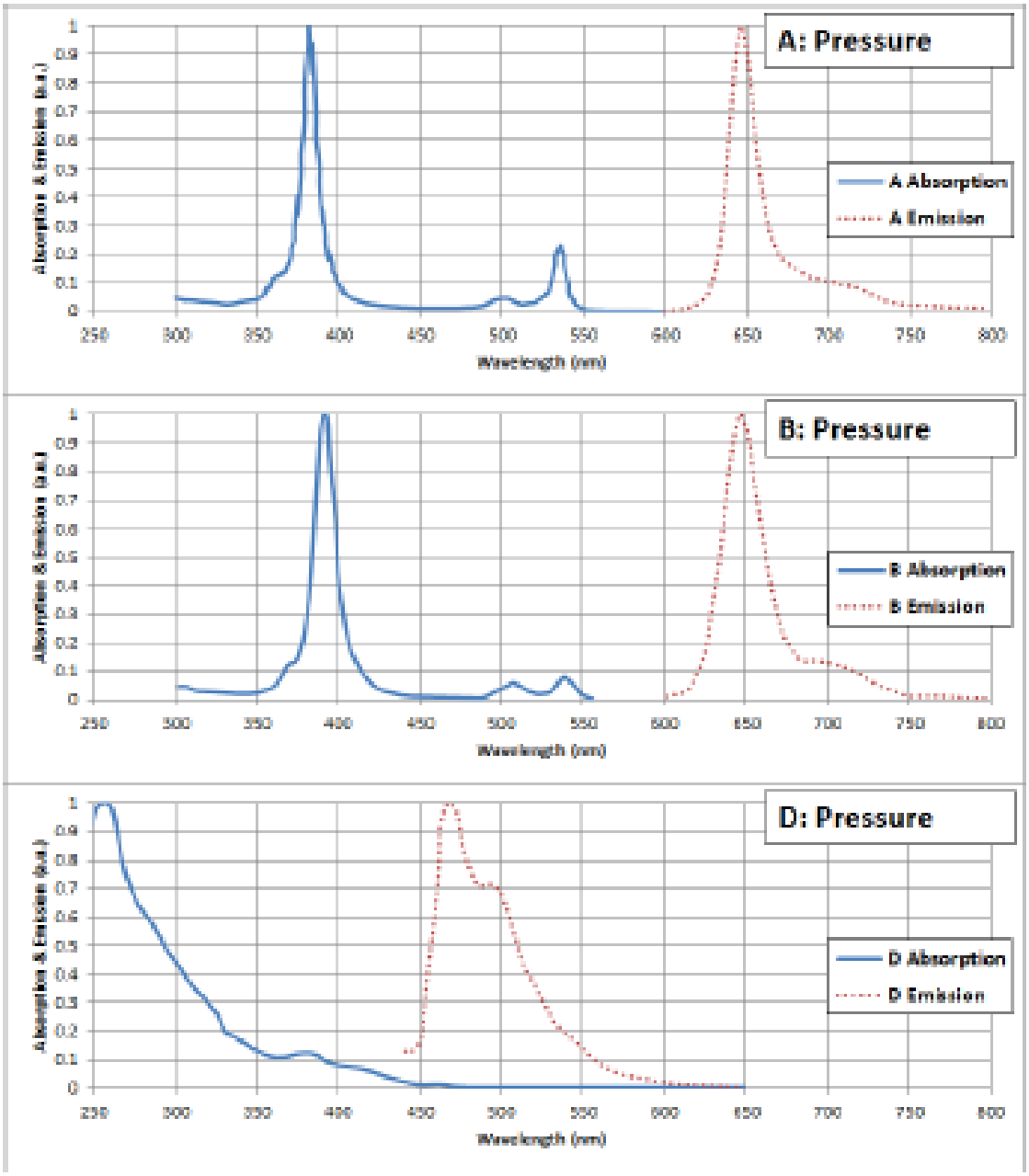

Figure 3.1: Absorption/Emission Spectra for A, B, and D Dyes[25]

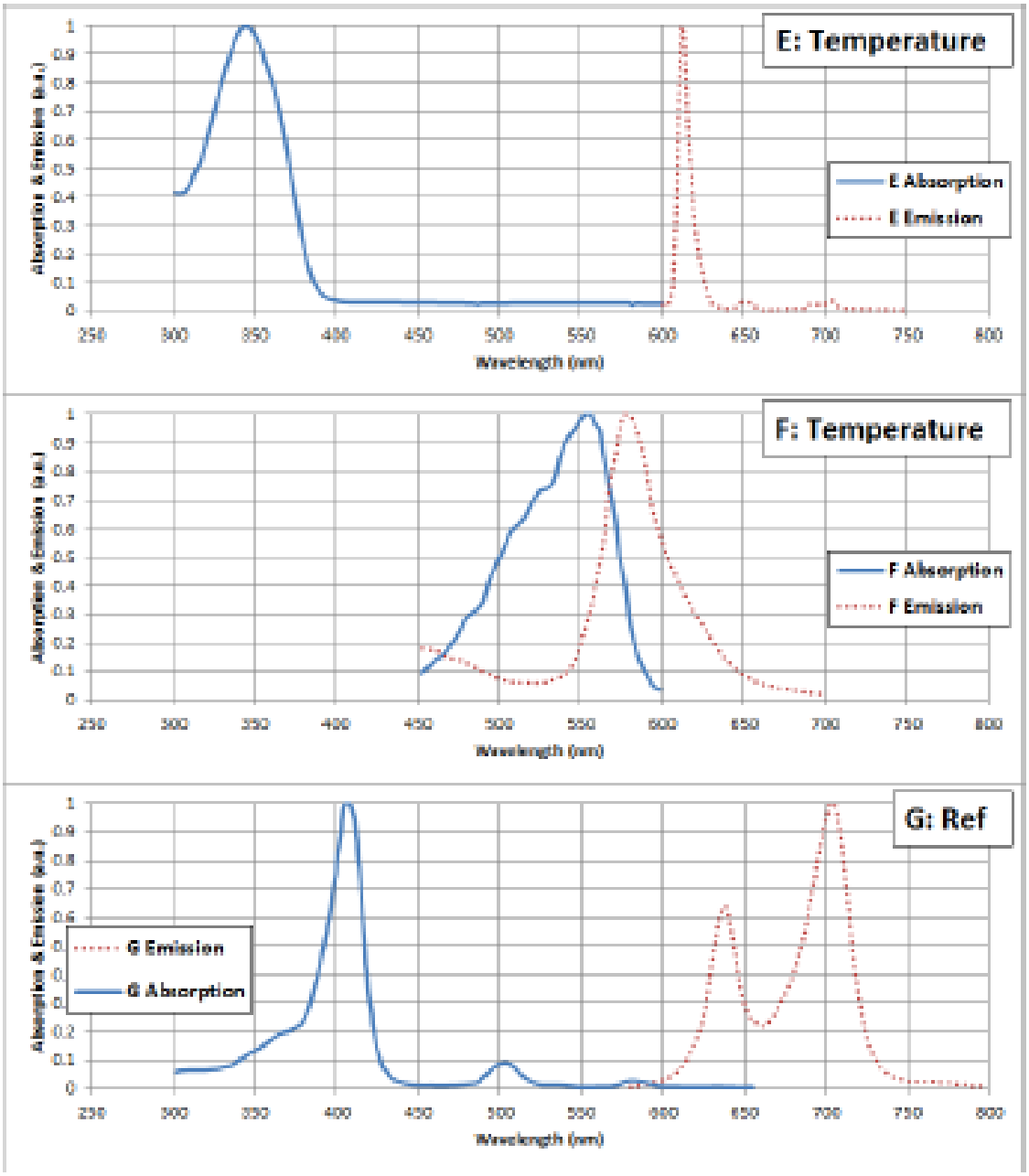

Figure 3.2: Absorption/Emission Spectra for E, F, and G Dyes[25]

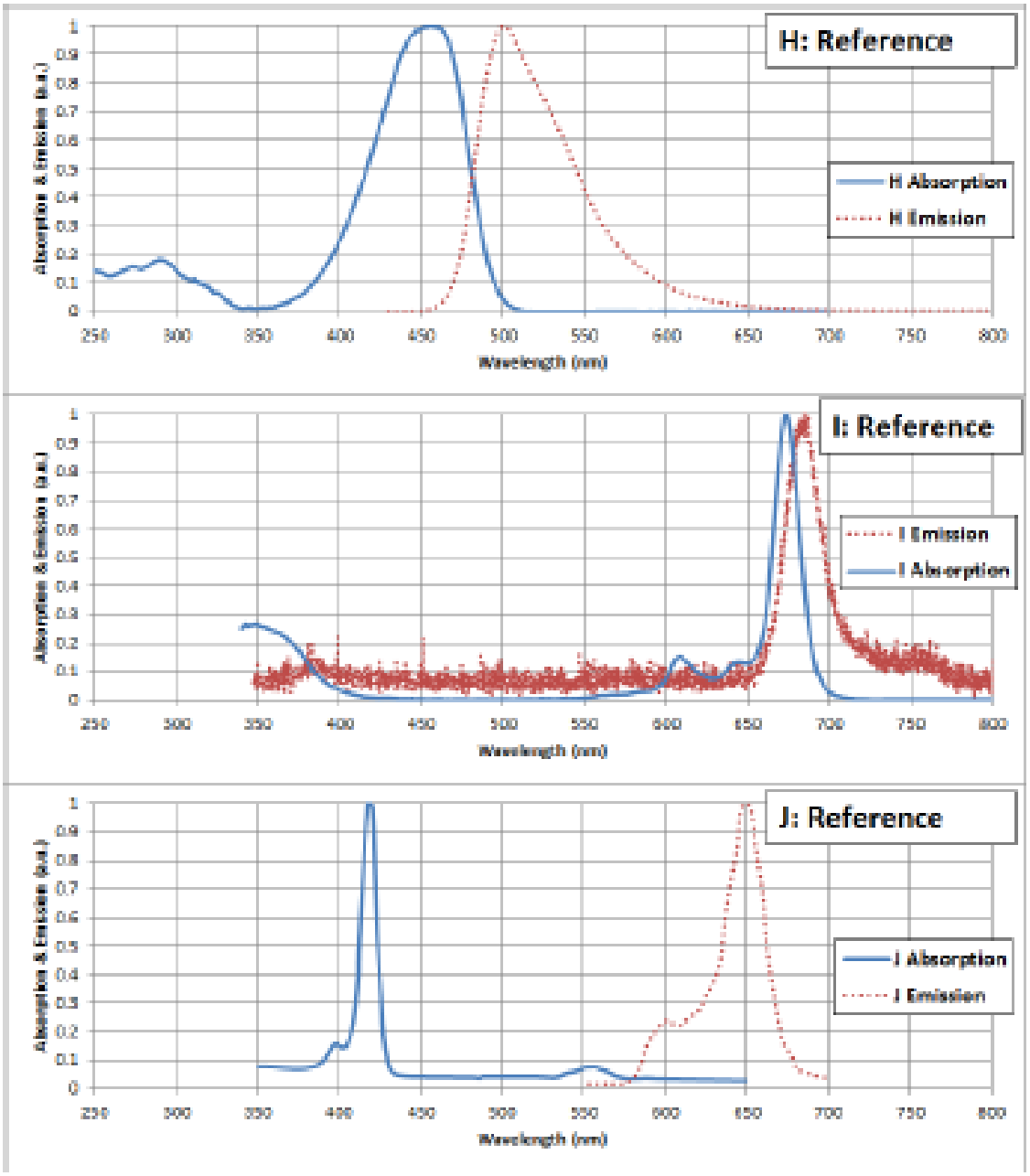

Figure 3.3: Absorption/Emission Spectra for H, I, and J Dyes[25]

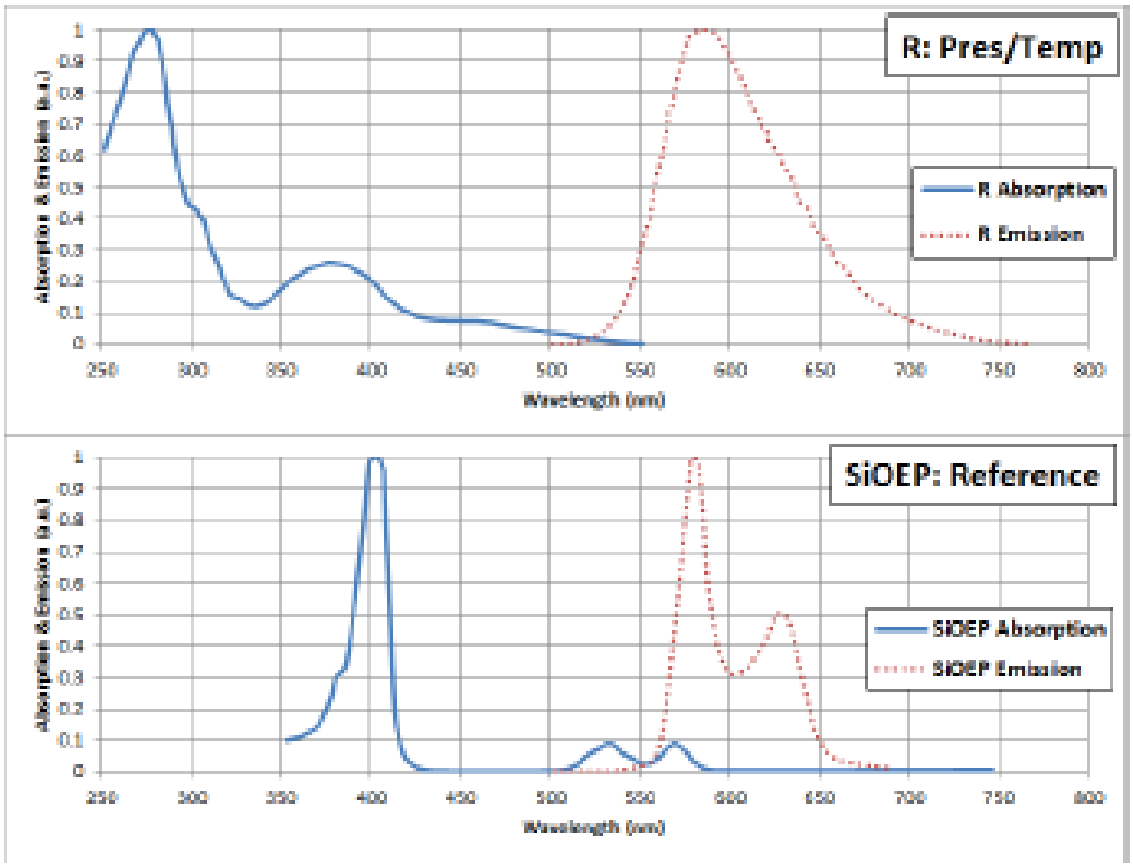

Figure 3.4: Absorption/Emission Spectra for R and SiOEP Dyes[25]

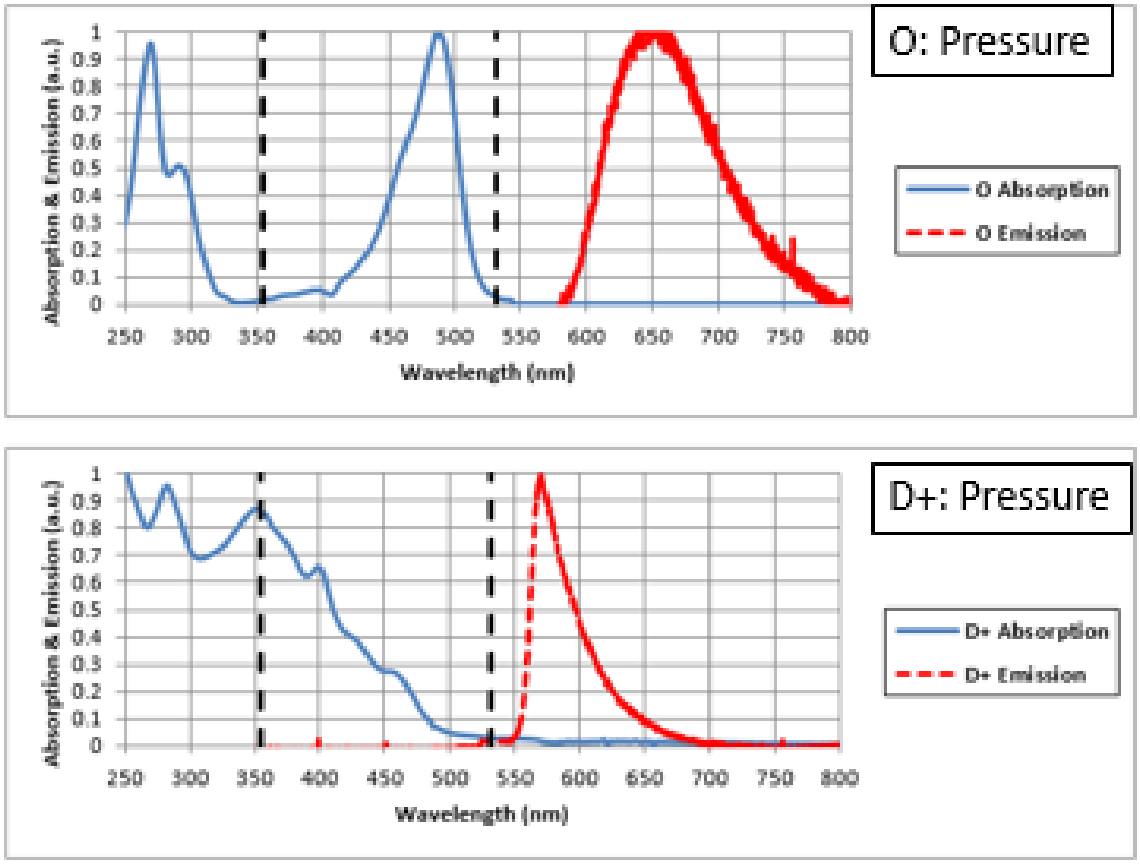

Figure 3.5: Absorption/Emission Spectra for O and D+ Dyes

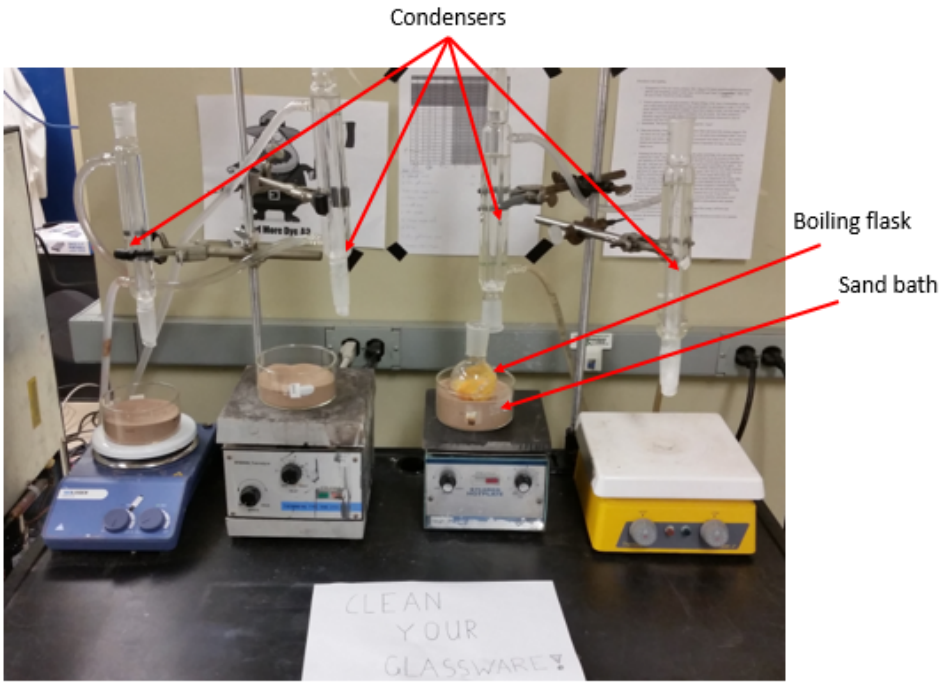

Figure 3.6: Setup used for particle fabrication

Table 3.3: Setup for Fabrication of Particles

Left Hot plate	Mid-Left Hot plate	Mid-Right Hot plate	Right Hot plate
SciLogex MS-H-S	Sybron Thermolyne Type 1000 Stir Plate	VWR Scientific Stirrer Plate (Model # 58849-908)	Thermolyne Cimarec 2

3.1 Particle Dispersion Method

3.1.1 Particles for 532 nm Laser

Initially, efforts were focused on techniques for the synthesis of a viable dual luminophore bead compatible with a 532 nm laser. Variables such as the type of solution

used, amount of solution, concentration of dye per milligram of particle, temperature, and cooking time were adjusted to optimize the production of the beads.

The first effort in creating and testing a particle was a SiO_2 bead loaded with dye B. The process closely followed an in-house manual made by researcher Jonathan Howard. The initial preparation for making particles involved mixing a stock solution of 10 mg of dye B, 15 mL of dichloromethane(DCM), and 10 mL of methanol. 2.5 mL of the solution was mixed with 250 mg of particles, 3.5 mL of DCM, and 4 mL of methanol. The mixture was sonicated in a Cole-Parmer 8891 sonicator and then heated with continuous stirring for 24 hours on a hot plate. The solution was transferred to a glass centrifuge tube and centrifuged for 5 minutes. Care had to be taken in this process because too much centrifuging can create resuspension difficulties.[38] Afterwards, the separated dye solution was removed and deionized water was added to the remaining particles in the tube. The particles were centrifuged and washed a second time and stored in 2-4 mL of deionized water. Polyscience, Inc. recommends storing particles in deionized water as a medium since high concentrations of ions may lead to irreversible aggregation. Freezing beads is also discouraged, as it can cause irreversible aggregation, so this was avoided.[38] The particles were tested in the laboratory's pressure chamber using a miniature fiber optic spectrometer (USB4000, Ocean Optics, Dunedin, FL) and processed through the Spectrasuite Spectroscopy Software (Ocean Optics, Dunedin, FL) to determine their pressure sensitivity.[10] The results, depicted in Figure 3.7, show that dye B was reasonably bright at vacuum, but decreased in intensity at too high a rate 0-50 kPa and was not sensitive enough 50-100 kPa. As an adaptation, it was decided that dye B on AlO_2 might change the pressure response sensitivity.

The next step was to find a reference dye to use with the 532 nm laser. Initially, the options were Rhodamine 6G, rose bengal, sulforhodamine 101, and SiOEP. Stock

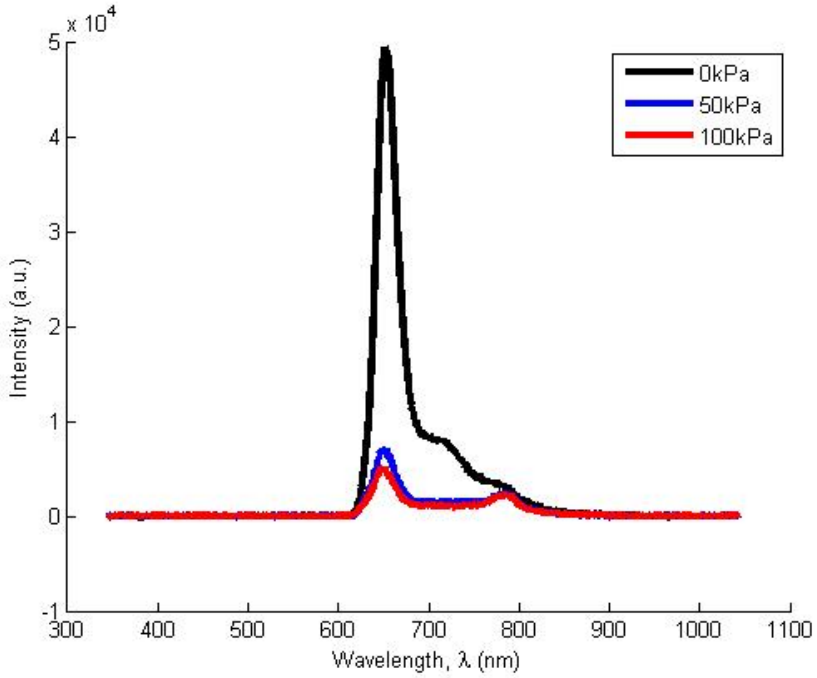

Figure 3.7: Si02 beads with Dye B (650 nm) at pressures 0, 50, and 100 kPa (Oct 2, 2013)

solutions of the reference dyes Rhodamine 6G, sulforhodamine, and SiOEP with dye B were tested in a pressure chamber at 0-100 kPa to determine the viability of each in a dual-dye combination.

Rhodamine 6G has a bright emission around 570 nm and would be spectrally compatible with dye B, which has an emission spectra occurring at approximately 650 nm. Rhodamine 6G was combined with dye B to determine its appropriate ratio. As shown by Figure 3.8, a 1400:1 ratio of dye B to Rhodamine 6G was needed to provide relatively equivalent intensities of emission peaks. This ratio has the potential for large variations in error due to the large difference in amount of dyes. From previous research in the lab, a ratio of around 0.5 mg dye per 100 mg particles has shown good

results for single-dye particles. Because the ratio between dye B and Rhodamine 6G is so large, the ideal dye to particle ratio cannot be reached for both dyes. An AlO_2 particle with dye B and Rhodamine 6G was made. Dye B's emission from the particles was not visible and Rhodamine 6G appeared very weakly, so this dye/particle combination was not considered a viable option.

Rose bengal has a bright emission under 532 nm light. However, its emission spans 550-720 nm, as shown in Figure 3.9. A strong pressure dye with an emission spectra 700-800 nm would be necessary for rose bengal, which was not available. This was not considered a viable candidate for a reference dye.

Sulforhodamine absorbs light at 532 nm, so it was considered a potential solution to the reference dye. However, due to significant emission overlap demonstrated in Figure 3.10, sulforhodomine was not the primary choice for a reference dye. At the desired excitation, sulforhodamine emits more strongly than dye B, so a 20:1 ratio of dye B to sulforhodamine provides more equivalent emission peaks.

Lastly, SiOEP absorbs at 532 nm and a large portion of its emission is spectrally separate from dye B. This was considered a viable alternative to Rhodamine 6G and sulforhodamine. Figure 3.11 shows a ratio of dye B to SiOEP of 1:2. While the ratio could be further optimized, SiOEP was considered to be a viable candidate to use with dye B.

In the following fabrications Dye A was used in lieu of dye B because both dyes demonstrate similar spectra and sensitivity properties, but dye A has a higher absorption peak at 532 nm. A 2:1 ratio A/SiOEP AlO_2 particle appeared to be the optimal configuration, as shown in Figure 3.12. The particle was made in a similar manner to the single dye particles, except now the concentrations of each dye relative to the amount of particles had to change. Stock solutions of $\frac{8 \text{ mg dye A}}{15 \text{ mL DCM}}$ and another of $\frac{8 \text{ mg SiOEP}}{15 \text{ mL DCM}}$ were made. 5.625 mL (3 mg dye A) and 2.8125 mL (1.5 mg SiOEP)

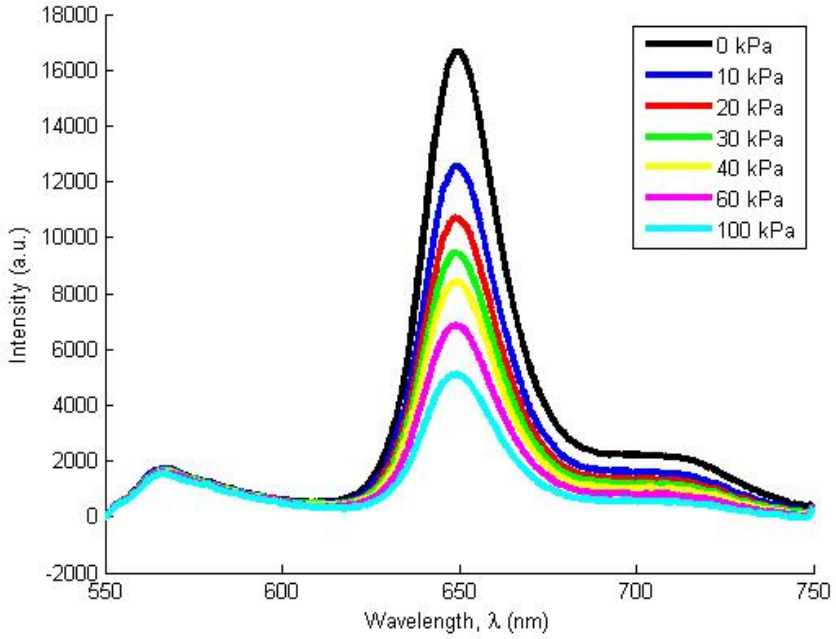

Figure 3.8: Spectra of 1400:1 B (650 nm)/Rhodamine (570 nm) dyes 0-100 kPa (Oct 22, 2013)

were pipetted and sonicated in a 100 mL boiling flask with 100 mg AlO_2 and an additional 3.5 mL DCM and 4 mL methanol for one hour. The flask was submerged in a sand bath to help maintain uniform temperatures across the mixture, and it was placed on the left hot plate with a heat setting of 2 for approximately 24 hours. The condenser was used to help reduce the rate of evaporation.

The ideal ratio of dye to particles for a single-dye bead was considered to be approximately 0.5 mg per 100 mg particles, but with a dual-dye particle with different ratios of dyes, oftentimes this condition could not be met with both dyes. The two dyes seemed to be competing for space on the surface of the particle and thus neither were as bright as their single-dye counterparts. After testing different sets of dual-

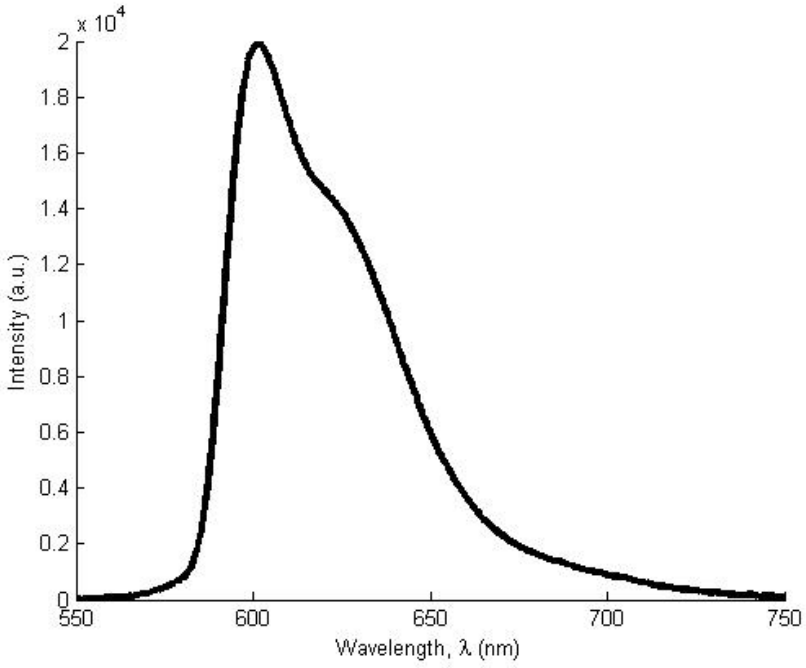

Figure 3.9: Spectra of rose bengal (550-725 nm) dye

dye beads, it seemed that keeping the ratio of the dyes around 1 mg to 3 mg per 100 mg of particles was more effective than keeping the ratio of dyes between 0.5 mg and 1 mg per 100 mg of particles. In addition, the extra solvents added to the solution was changed from equal amounts of DCM and methanol to 4 mL DCM and 8 mL isopropanol. Because isopropanol has a higher boiling point than methanol, the mixture, which was held just under boiling point, experienced an overall higher temperature. This was done to see if heating the particles at a higher temperature had much effect on the performance of the particles.

Tests were run using 1:1 A/SiOEP $Al0_2$ particles to determine the minimum amount of time needed to heat the particles. Throughout the tests, different conditions had to be tweaked as new discoveries were made. At first, intensity measure-

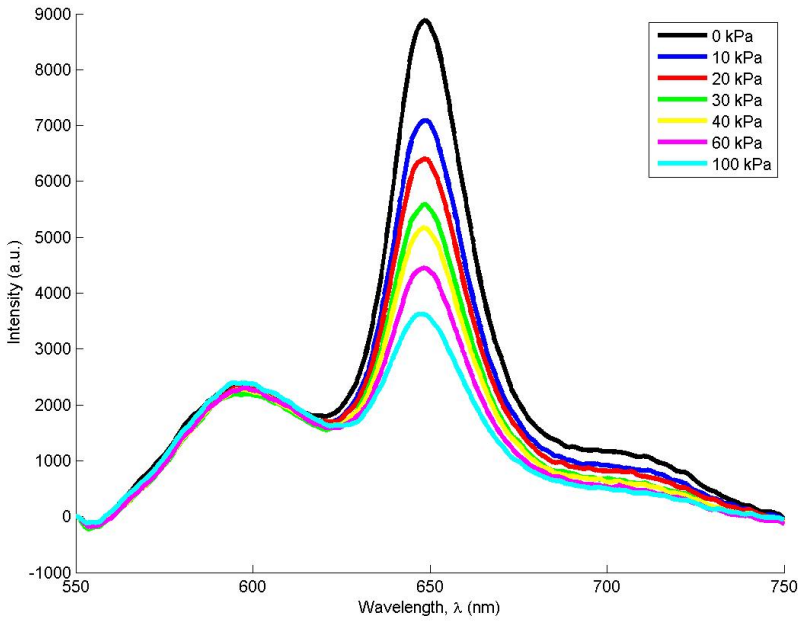

Figure 3.10: Spectra of 20:1 B (650 nm)/Sulforhodomine (605 nm) Dyes 0-100 kPa (Oct 22, 2013)

ments of microscope slides coated in particles were recorded with the spectrometer as a means for comparison between particles. However, each sample slide varied slightly, and it was difficult to standardize the opportunity for excitation across different samples. In addition, samples for the different heating times were taken from different particle batches on different hot plates, which introduced too many variables.

In the next test method to determine the minimum amount of time needed to heat the particles, six sets of 1:1 A/SiOEP $Al0_2$ particles, each to be used as an individual test, were made. Tests 1, 3, and 5 were performed on the left hot plate and tests 2, 4, and 6 were performed on the right hot plate. Solution samples, which contained unloaded dye, were collected from each test set at specific times to compare

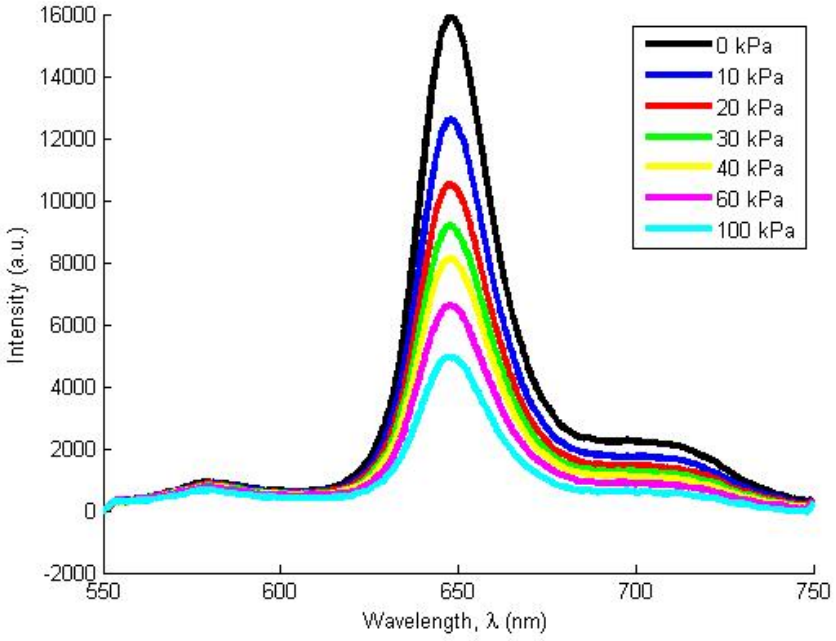

Figure 3.11: Spectra of 1:2 B (650 nm)/SiOEP (580 nm) dyes 0-100 kPa (Oct 22, 2013)

the concentrations of the solutions from each of the six test sets. Specific amounts of DCM and isopropanol were added back to restore the solution's original volume before collecting each sample. Absorption analysis was then performed on the samples from each of the six tests using a Hewlett-Packard 8452A Diode array UV/Vis spectrophotometer. Higher levels of absorption corresponds to higher concentrations of dye still in solution, which ideally would correlate to less dye being loaded to the particles.

It was important to standardize the process as much as possible. Several variables in the experiment had to be accounted for. The boiling flask on the hot plate had to be centered, and it was ensured that the tape covering the joint between the

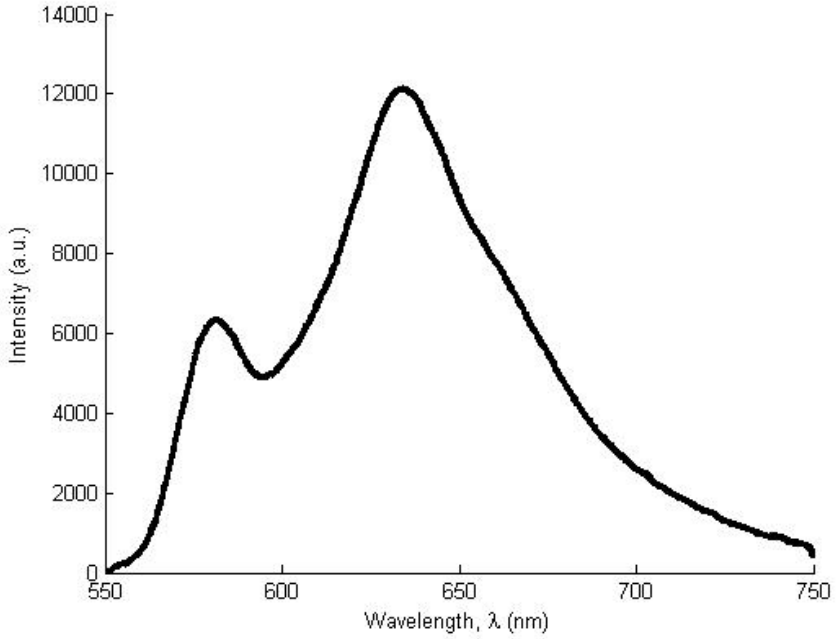

Figure 3.12: Spectra of 2:1 A (650 nm)/SiOEP (580 nm) $Al0_2$ dyes

condenser and the boiling flask was completely sealed with teflon tape to ensure that the evaporated solution could exit only through the condenser. The mixture was completely submersed in sand, the temperatures and stirring speeds for the hot plates used were kept the same, and the initial amounts of dye, particles, and solution were held constant. However, it became apparent that there were more factors. For instance, the depth of the boiling flask in the sand became a factor. At heat setting 3 on the left hot plate, given an inch of sand, the difference in temperature from the bottom to the top varied about 70 degrees Celsius. Depth was controlled carefully, but small variations in the depth could affect the temperature from one test to the next. Heat settings 3 and 2 were used on the left and right hot plates, respectively. The temperature between the left and right hot plates reached equal temperatures at

settings 3 and 2, respectively, but the right hot plate took about twice as long (60 minutes) to reach that temperature. This is shown by Figure 3.13, where a boiling flask with a known volume of deionized water was heated with the aforementioned settings.

A large factor in the solution's temperature was the ratio between DCM and isopropanol. DCM has a boiling point of approximately 40° Celsius while that of isopropanol is about 80° Celsius. The maximum temperature of the solution will be somewhere between those two boiling points, and it will increase as the DCM evaporates off first. To demonstrate this, a three-neck boiling flask was acquired with a mercury thermometer installed in one of the necks through a cork stopper in order to monitor the temperature. One neck was attached to the condenser and the third neck was plugged with another cork stopper. When the plug is removed, enough evaporated DCM was allowed to escape to substantially increase the ratio of isopropanol to DCM, raising the boiling point and thus the solution's temperature. This is shown by Fig 3.14.

The absorption analysis had varied results. Test 1, depicted in Figure 3.15, shows the 0 hour sample with the lowest concentration. This is inconsistent with all of the following tests. In Figure 3.16, test 2 showed a significant decrease in dye concentration in the solution at 18 hours. Tests 3 and 6, as seen in Figures 3.17 and 3.20, respectively, showed 24 hours to be enough time for changing the solution concentration, whereas test 4 showed both 10 and 24 hours to be sufficient, shown by Figure 3.18. Test 5, in Figure 3.19, showed 17 and 24 hours to be sufficient. The solution flasks in tests 5 and 6 were not placed at the bottom of the sand bath, so it is believed that the temperature did not get hot enough for the dyes to load as quickly as in the other tests.

While the exact patterns changed between each test and there were a few outliers,

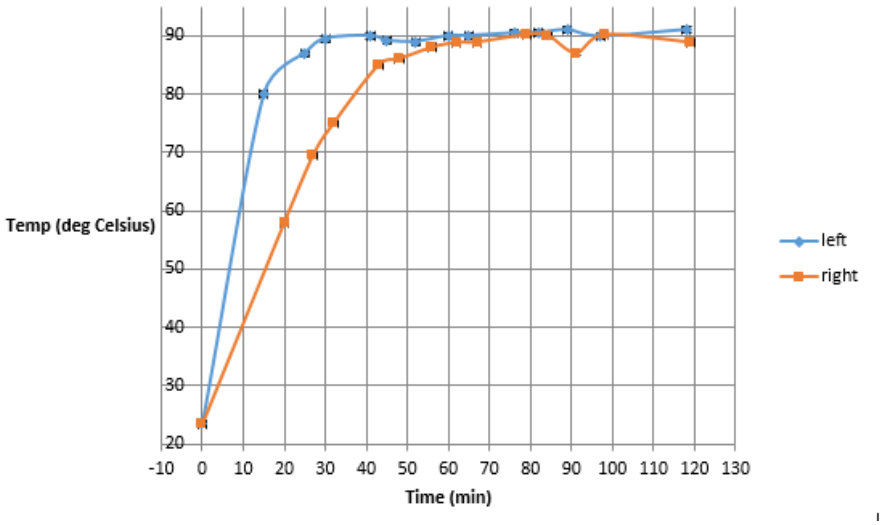

Figure 3.13: Timed temperature change of left (setting 3) and right (setting 2) hot plates (Dec 17, 2013)

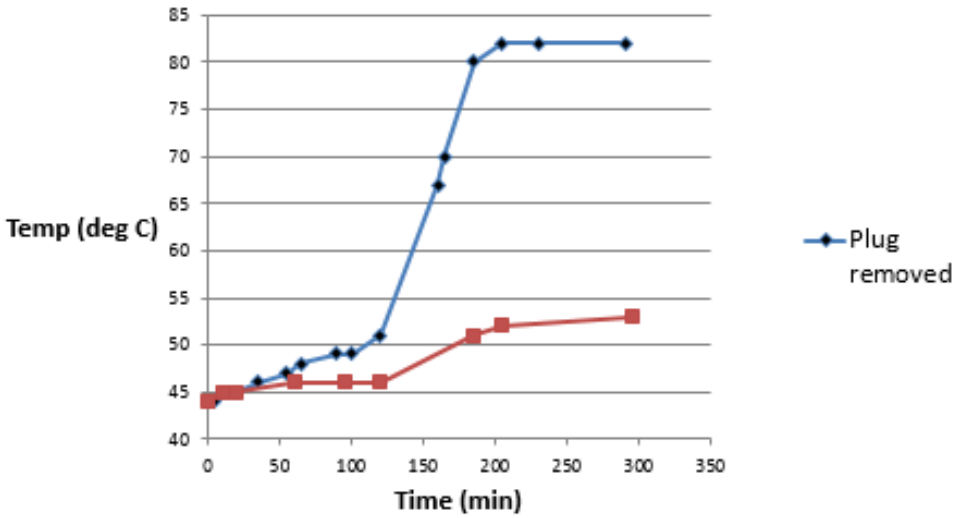

Figure 3.14: Comparison of timed temperature change for left hot plates with and without plug removal at 120-185 minutes

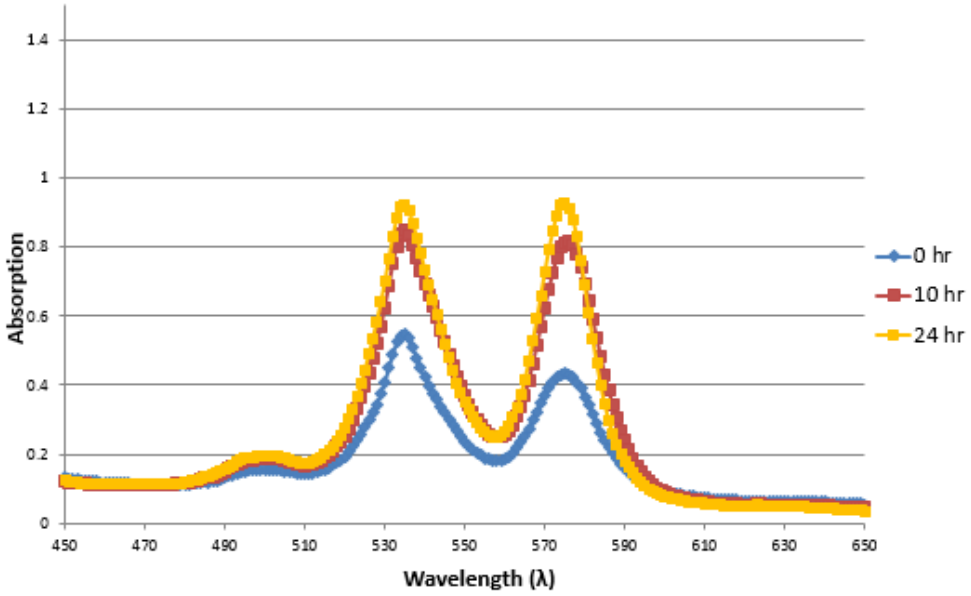

Figure 3.15: Absorption spectra of solution from 1:1 A/SiOEP $Al0_2$ sample on left hot plate at different heating times, Test 1 (Dec 5, 2013)

the general trend shows less dye concentration in the solution after 17-24 hours. A potential reason for the outliers is that the concentration measurements were very sensitive, and small differences in the volume of solution retrieved and added back to a sample after being evaporated may have affected the concentration more than the small change due to dye loading. It is also probable that the absorption tests would not correspond very well to particle performance, because the dye could come out of solution only to load onto the glass walls of the boiling flask, or excessive loading of dye onto the particle could actually cause self-quenching or decreased temporal response. It was determined from these tests that a more reliable standard of performance is to find the particle's Stern-Volmer slope and shock tube response and also to determine if the particle is bright enough to perform these tests.

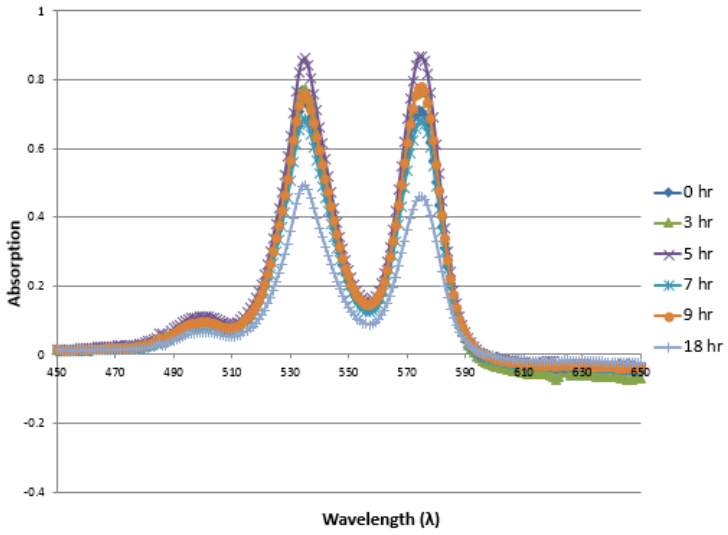

Figure 3.16: Absorption spectra of solution from 1:1 A/SiOEP $Al0_2$ sample on right hot plate at different heating times, Test 2 (Dec 5, 2013)

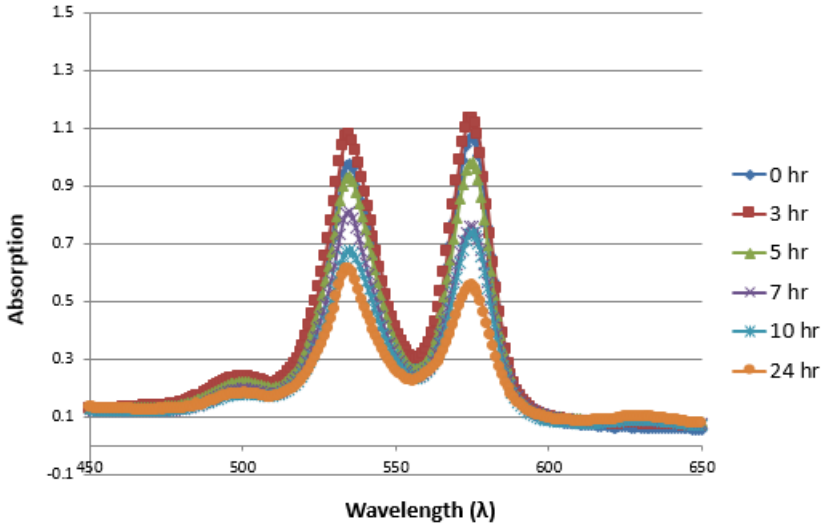

Figure 3.17: Absorption spectra of solution from 1:1 A/SiOEP $Al0_2$ sample on left hot plate at different heating times, Test 3 (Dec 5, 2013)

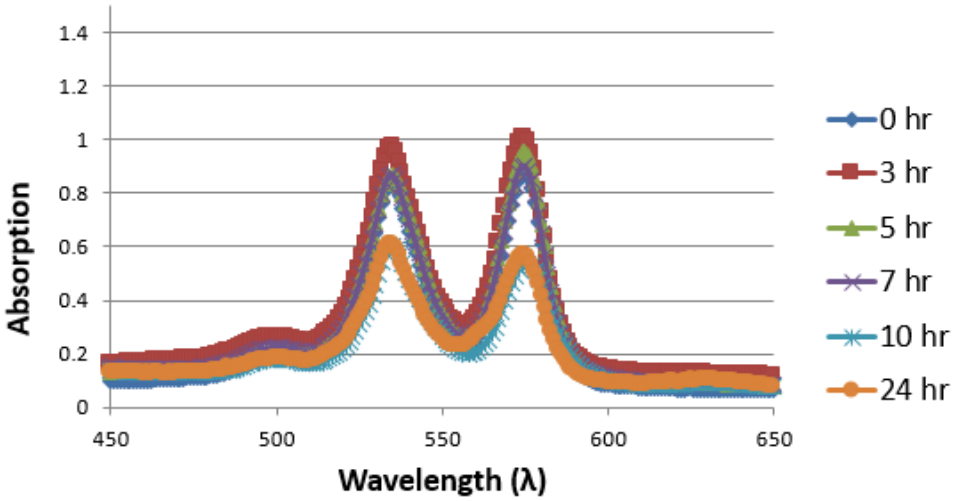

Figure 3.18: Absorption spectra of solution from 1:1 A/SiOEP $Al0_2$ sample on right hot plate at different heating times, Test 4 (Dec 5, 2013)

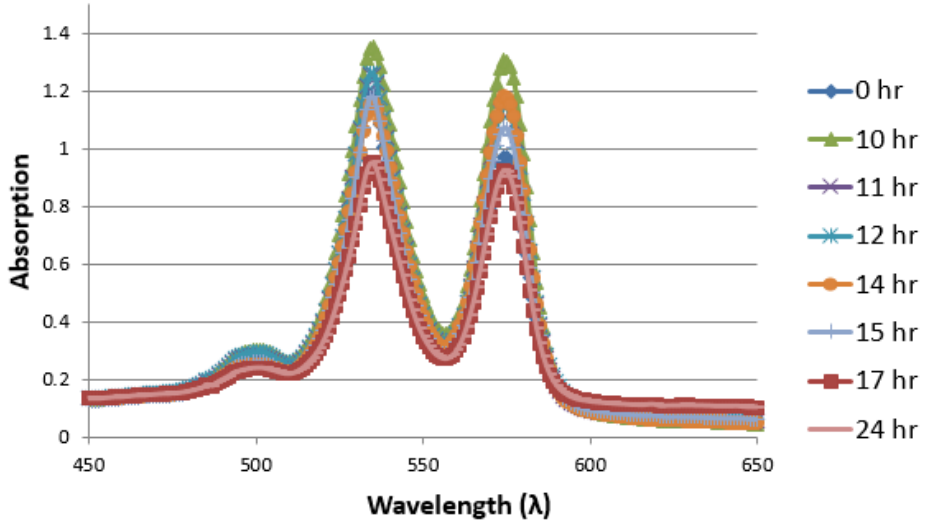

Figure 3.19: Absorption spectra of solution from 1:1 A/SiOEP $Al0_2$ sample on left hot plate at different heating times, Test 5 (Dec 16, 2013)

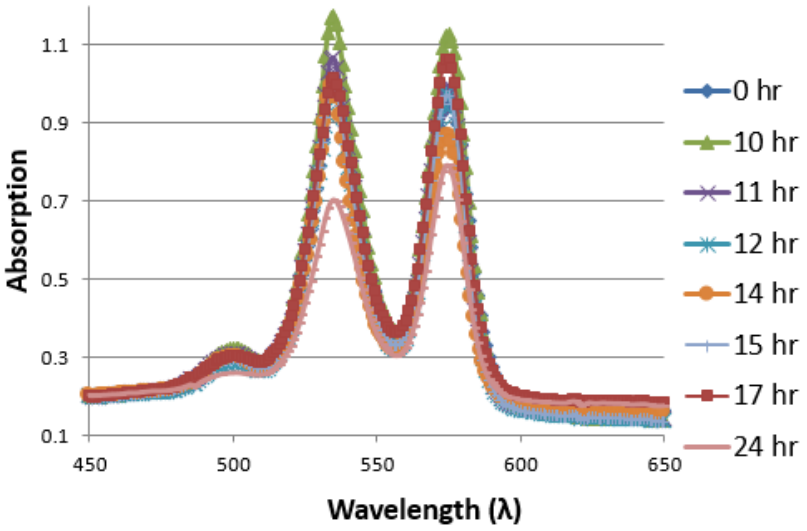

Figure 3.20: Absorption spectra of solution from 1:1 A/SiOEP $Al0_2$ sample on left hot plate at different heating times, Test 6 (Dec 16, 2013)

3.1.2 Particles for 355 nm Laser

At this point efforts for making particles shifted to designing ones for the 355 nm laser, as this allowed for particles with a higher range of emissions. Dye H was used as a compatible reference dye for dye A, and different combinations of the dye were tried on $Al0_2$ and $Zn0_2$ particles. $Al0_2$ and $Zn0_2$ were found to perform very similarly in the bead-making process, with similar slopes and response times. However, like their 532 nm counterparts, these particles were dim and/or not very pressure-sensitive. Figure 3.21 shows the spectra for a 50:1 A/H $Zn0_2$ particle, the brightest and most pressure-sensitive of the group. A duplication of the batch failed to show similar results, so the process, due to perhaps a change in the amount of evaporated solution in the alotted time, was not repeatable.

To determine the effect of dye concentration and time on the bead-making process, a test was running using dye A on $Zn0_2$. Concentrations used were $\frac{8 \text{ mg dye A}}{100 \text{ mg particles}}$,

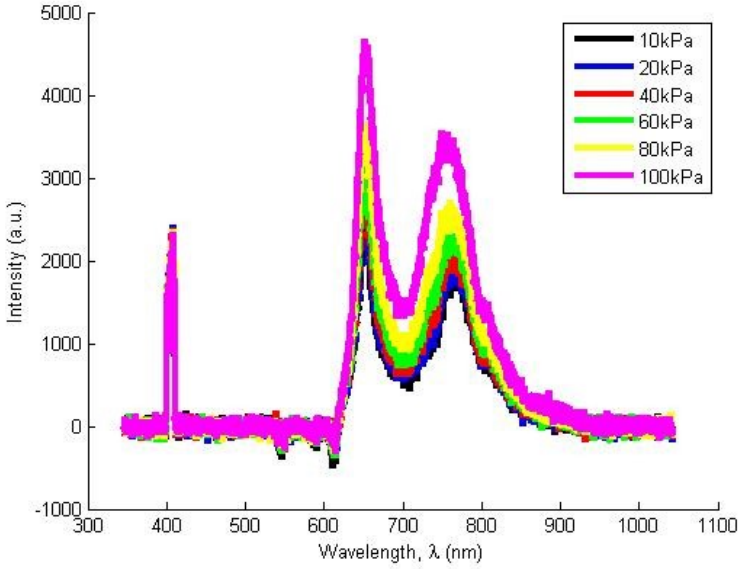

Figure 3.21: Spectra of pressure sensitivity for 50:1 A/H $Zn0_2$ particle

$\frac{1.0 \text{ mg dye A}}{100 \text{ mg particles}}$, and another of $\frac{0.27 \text{ mg dye A}}{100 \text{ mg particles}}$, heated over 2, 7, and 10 hour periods. Unless a particle is magnitudes of orders brighter than another, relative intensity is not a very reliable means for comparison, so Stern-Volmer slopes were used as the standard for comparison. It seems that across different concentrations of dye A for an A dye ZnO_2 particle, the Stern-Volmer slopes didn't change very much. These particles were very dim except for the 0.27 mg dye A sample heated for 10 hours. The concentration seemed to have an effect on the required heating time for loading the dye. The particles with lower concentrations of dye paid a higher price for shorter cook times. For the higher concentration particle heated for 10 hours, the particle may have been overloaded with dye. Table 3.4 shows a list of the particles tested and their corresponding sensitivities to pressure. Figs 3.22, 3.23, 3.24,3.25, 3.26, and 3.27 show the spectra for the brighter of the particle sets.

Table 3.4: Time Dependance of Stern-Volmer

Particle	SV slope
8mg A ZnO 2 hr	.22
8mg A ZnO 7 hr	.25
8mg A ZnO 10 hr	.14
1mg A ZnO 2 hr	Too dim
1mg A ZnO 7 hr	.21
1mg A ZnO 10 hr	.17
.27mg A ZnO 2 hr	Too dim
.27mg A ZnO 7 hr	Too dim
.27mg A ZnO 10 hr	.15

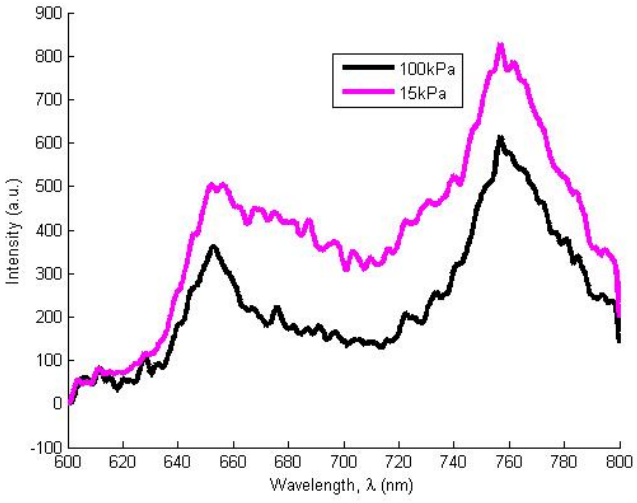

Figure 3.22: Spectra of $Zn0_2$ particle, concentration $\frac{8 \text{ mg dye A}}{100 \text{ mg particles}}$, heated 2 hr

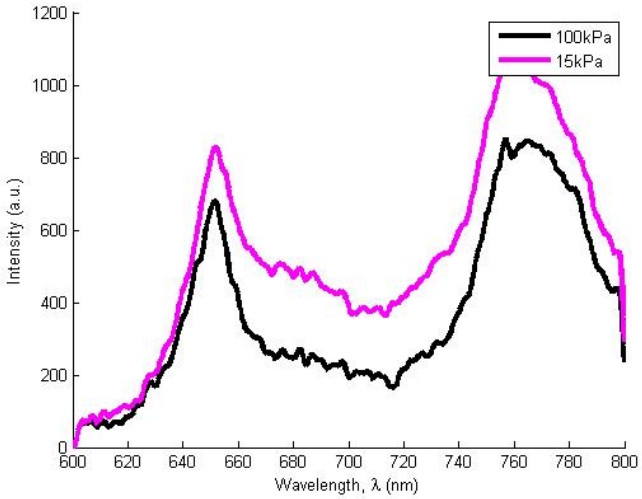

Figure 3.23: Spectra of $Zn0_2$ particle, concentration $\frac{8 \text{ mg dye A}}{100 \text{ mg particles}}$, heated 7 hr

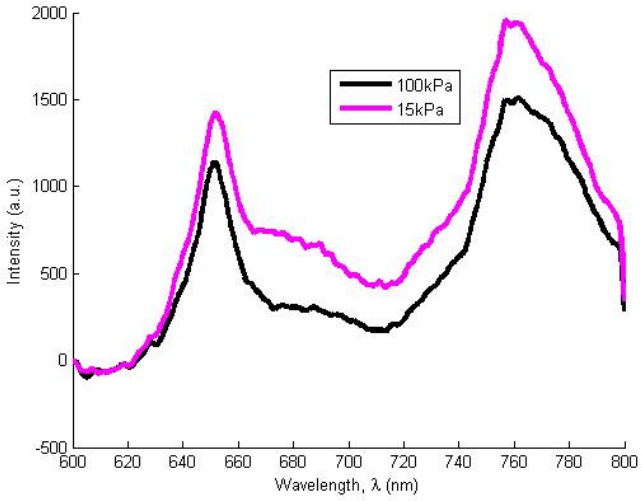

Figure 3.24: Spectra of $Zn0_2$ particle, concentration $\frac{8 \text{ mg dye A}}{100 \text{ mg particles}}$, heated 10 hr

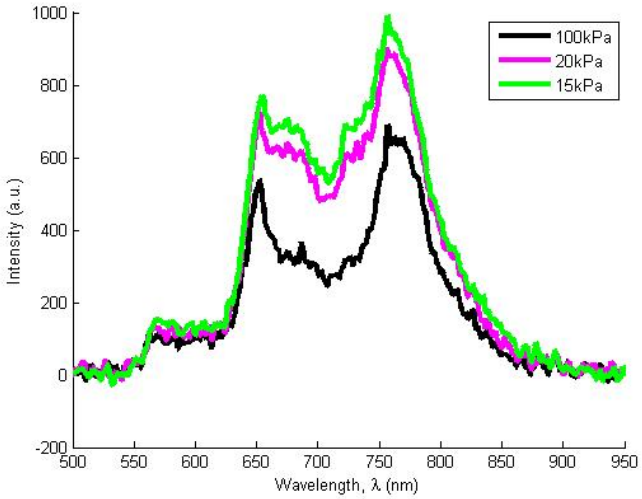

Figure 3.25: Spectra of $Zn0_2$ particle, concentration $\frac{1 \text{ mg dye A}}{100 \text{ mg particles}}$, heated 7 hr

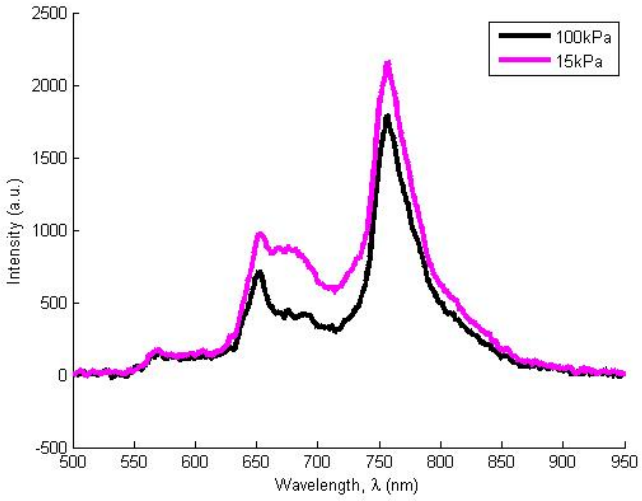

Figure 3.26: Spectra of $Zn0_2$ particle, concentration $\frac{1 \text{ mg dye A}}{100 \text{ mg particles}}$, heated 10 hr

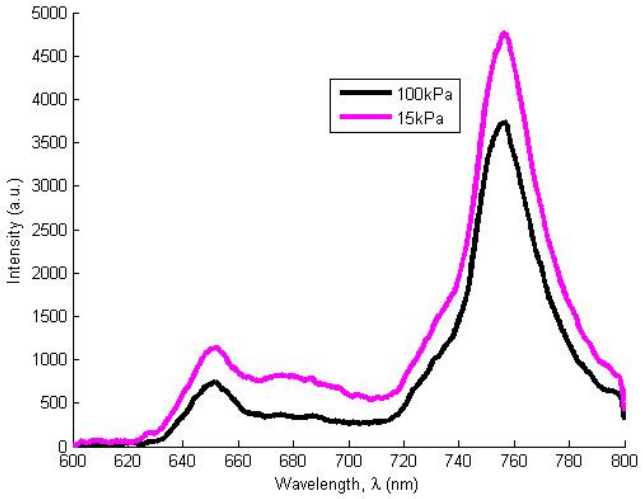

Figure 3.27: Spectra of $Zn0_2$ particle, concentration $\frac{0.27 \text{ mg dye A}}{100 \text{ mg particles}}$, heated 10 hr

3.1.3 Uncharacterized Peak

In some of the particles, an uncharacterized peak has been observed through the spectrometer. The uncharacterized peak has only appeared on oxide particles, to include silica. The exact wavelength it appears at can vary, but it is generally seen at approximately 780 nm. In addition, the ratio of the uncharacterized peak to the pressure dye's peak changes. Unless otherwise mentioned, a 560nm cutoff filter was used to filter out the 405nm laser light. In Figure 3.28, the bead is a dual-dye B/H on $Zn0_2$. The uncharacterized peak emits strongly at 778.5nm. The ratio of magnitude between this peak and dye B is approximately 2.6. Figure 3.29 shows that this peak also appears on the dual-dye particle 50:1 A/H dye $Zn0_2$. Dye H loaded more efficiently on this particle and can be seen up until the point of the cutoff filter. Its uncharacterized peak actually occurs at 763.5nm and the ratio of the peak to A dye is approximately 0.5. Figure 3.21 from the previous section depicts the same 50:1 A/H dye $Zn0_2$ particle with a higher cutoff filter to show that its uncharacterized peak is pressure-sensitive. So far, this peak has been pressure-sensitive for all of the oxide particles so it is hypothesized that the peak is correlated more with the pressure dye. Figure 3.30 shows that B dye by itself on $Zn0_2$ strongly shows the uncharacterized peak. This peak occurs at 780.7 nm with a ratio of approximately 1.57. Since this peak has occurred with only dye B on $Zn0_2$, it leads to further speculation that the peak is pressure-dye related. Figure 3.31 shows that this uncharacterized peak does not show up with the polystyrene beads. Figure 3.32 shows that BH-1 silica from Georgia tech has an uncharacterized peak at 775nm. The ratio is approximately 0.14, comparatively small to the other beads. BH-3 silica from Georgia Tech, shown in Figure 3.33, has a much stronger peak, occurring at 722nm with a ratio of approximately 2.35. It seems for the silica particles that the uncharacterized peak was strong whenever dye B was not as strong, as if some dye B's intensity was being converted

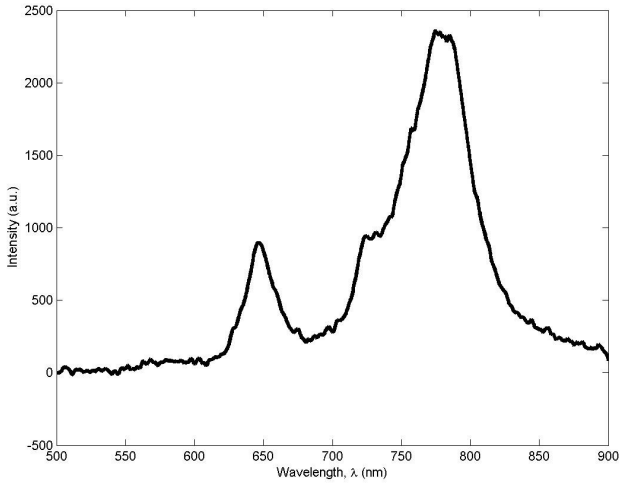

Figure 3.28: Spectra of 50:1 B (650 nm)/H (530 nm) $Zn0_2$ particle with uncharacterized peak (778.5 nm)

to this new peak.

Samples of particles showing the uncharacterized peak were sent to Professor Christian Bruckner's laboratory at the University of Connecticut for further analysis. The new species producing the extra emission band was not able to be isolated, but the peak was related to the loading of the dyes on the particles. The peak only appeared when the dyes were loaded onto the particles, and the peak disappeared from both the dyes and the particles when the dyes were stripped from the particles. The peak appeared regardless of temperature or time spent loading the dyes onto the particles.

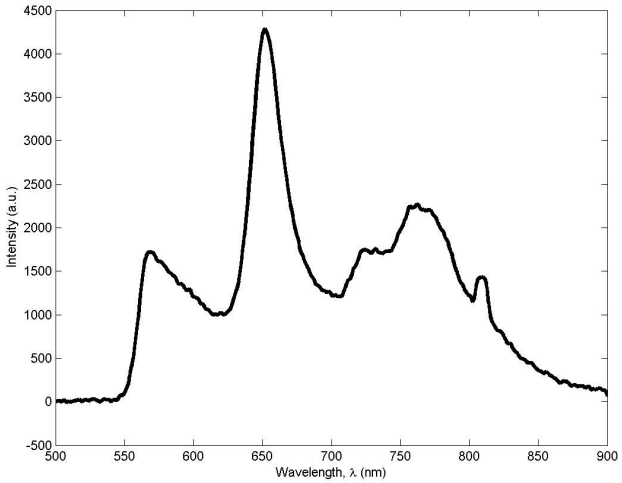

Figure 3.29: Spectra of 50:1 A (650 nm)/H (530 nm) $Zn0_2$ particle with uncharacterized peak (763.5 nm)

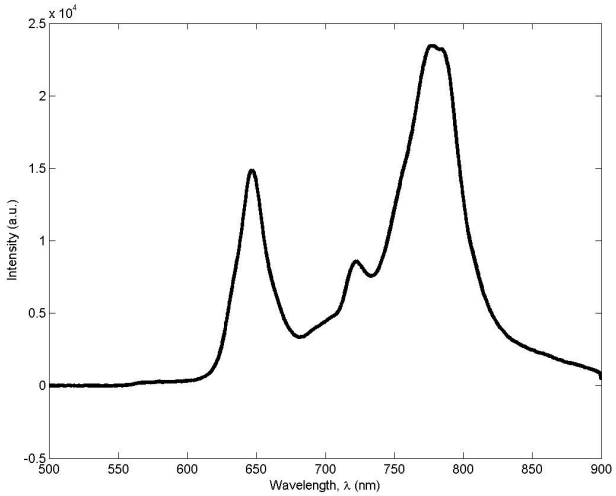

Figure 3.30: Spectra of B (650 nm) $Zn0_2$ particle with uncharacterized peak (780.7 nm)

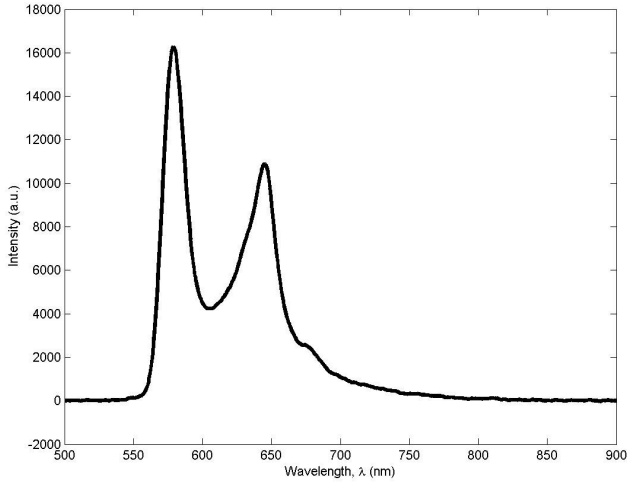

Figure 3.31: Spectra of A (650 nm)/SiOEP (580 nm) polystyrene particle without uncharacterized peak

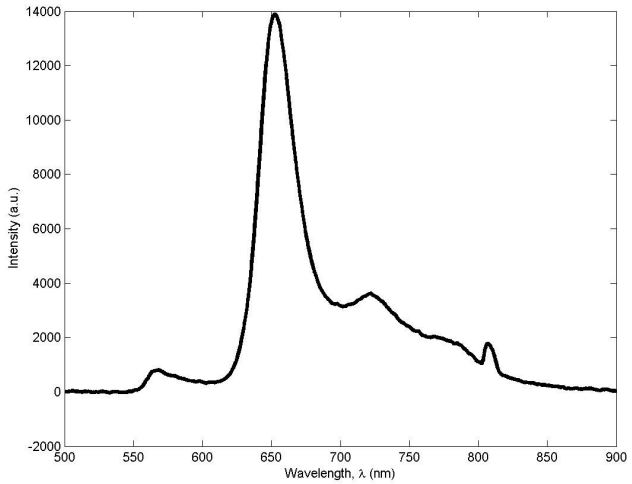

Figure 3.32: Spectra of B (650 nm)/H (530 nm)-1 silica particle with uncharacterized peak (775 nm)

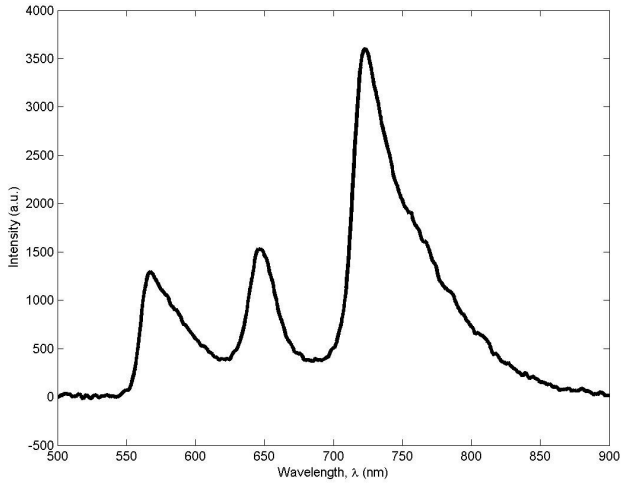

Figure 3.33: Spectra of B (650 nm)/H (530 nm)-3 silica particle with uncharacterized peak (722 nm)

3.2 Forced Dye Loading Through Complete Evaporation

After several iterations of experiments, it became apparent that the method of loading two dyes onto oxide particles through only partial evaporation of the liquid was unreliable at producing bright particles. While factors were controlled to the limits of the equipment, the dual-dye experiments were not replicable. Sometimes more of one dye loaded on the particle than it would a previous time, or not at all. Uncontrollable variables such as daily atmospheric pressure, humidity, or temperature may have had a role in changing the evaporation rates of the solution, and therefore the concentrations of dye coming out of solution and loading onto the particles. A more consistently producible and brighter PSBead composed of a silica microsphere (Cospheric, 2-19 μm diameter) was produced by fellow researcher Gai Ogihara and PSP guru Gamal Khalil. 5 mg of ruthenium dye and dye H (C480) each were combined with 500 mg of silica particles and equal solutions of methanol and DCM. The particles were left

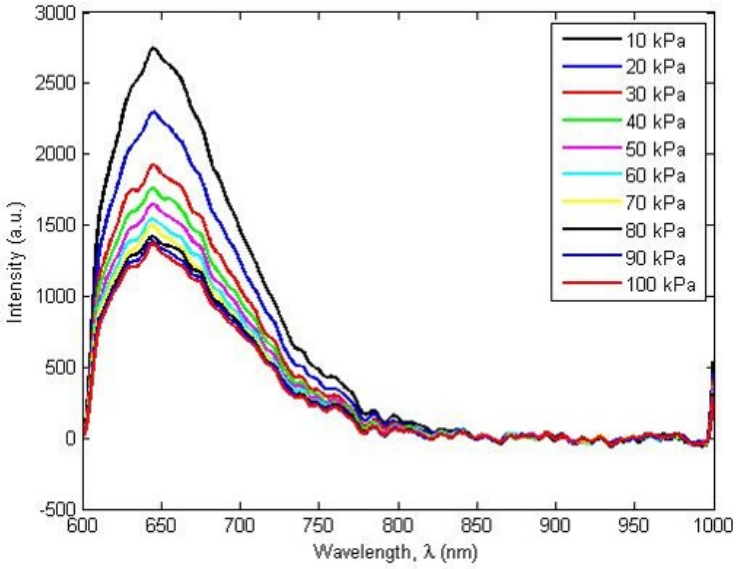

Figure 3.34: spectra of pressure sensitivity for ruthenium (640 nm)/H (C480)(530 nm) on silica particles (co-effort with researcher Jamie Lambie)

to evaporate completely, a process that takes roughly 2-4 days. A benefit to using silica microspheres is that they tend to be more stable in suspension because they are hydrophilic and negatively charged.[38] In addition, these particles did not have the uncharacterized peak. By allowing the solution to completely evaporate, fluctuations in the dye loading due to different amounts of evaporation are eliminated, leaving the dye to load either to the glass boiling flask or to the particles. Ruthenium has a very broad emission spectra, which can be integrated for overall better signal-to-noise.

The spectra of the pressure sensitivity for the ruthenium/H dye silica particle is shown in Figure 3.34. Limitations in the available filters to cut the 532 nm excitation source resulted in wavelengths below 600 nm being cut. The ruthenium/H silica particle was the consistently the brightest and most pressure-sensitive particle developed during this research.

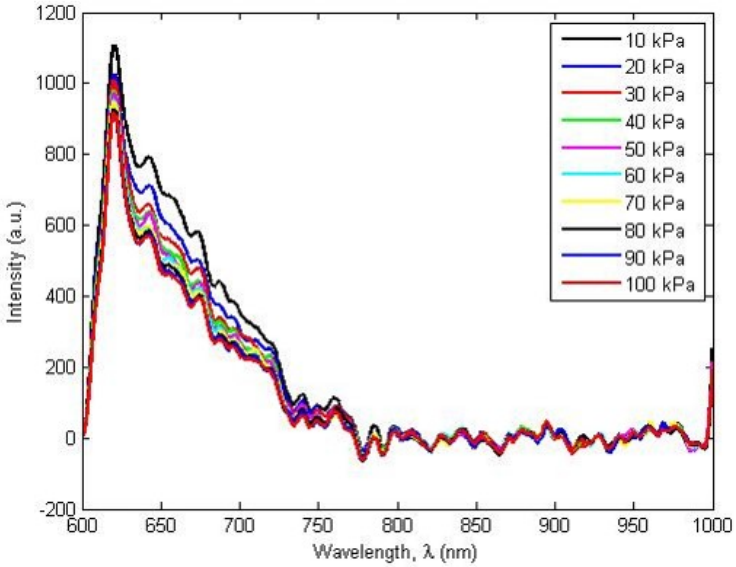

Figure 3.35: Spectra of pressure sensitivity for ruthenium (640 nm)/fluorescein (580 nm) on silica particles (co-effort with researcher Jamie Lambie)

The ruthenium/H dye silica particle could not be used with the 532 nm laser, and with the unavailability of the 355 nm laser, a new particle set had to be made. This led to the ruthenium/fluorescein dye silica particle. Its pressure sensitivity is shown in Figure 3.35. The same filtering system was used to image this spectra, and unfortunately the fluorescein dye was mostly cut. This particle showed very little pressure sensitivity, and it is suspected that this is due to a combination of effects from loading the dyes onto the particle and possibly the fluorescein dye overpowering the ruthenium, which is exacerbated because of their significant spectral overlap.

Chapter 4

EXPERIMENTAL RESULTS

4.1 Response Time Characterization

Out of the dozens of particles that were fabricated, only a few were bright enough to collect resolvable data from a shock tube test. Figures 4.1 and 4.2 show the raw Labview data from previous and current research, respectively, for intensity (plotted inversely) over time for a dye A $Al0_2$ particle made in previous research, as a measure of comparison between this and previous research. It can be seen that the signal was improved in the test conducted under current research. The raw intensity data for the ruthenium/H silica particle is shown in Figure 4.3. Filtered intensity data showing the start time, minimum and maximum lines, and the 63.2% and 90% response times calculated from those lines are shown in Figure 4.4. Figure 4.5 shows a chart of the most successful particles with their 63.2% and 90% response times.

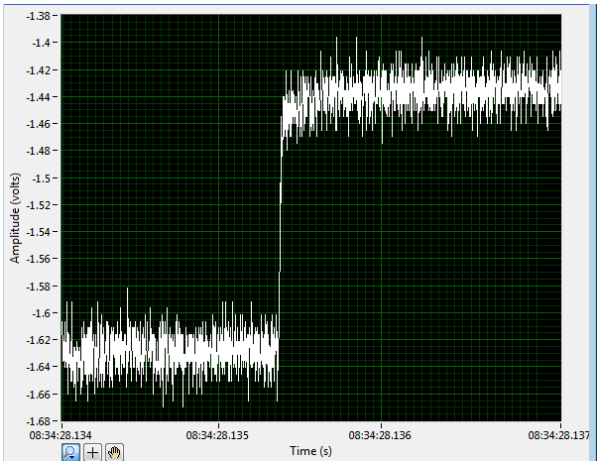

Figure 4.1: Raw Labview data of intensity (plotted with negative values) over time from shock tube test of a dye A $Al0_2$ particle fabricated in a previous research, conducted during a previous research

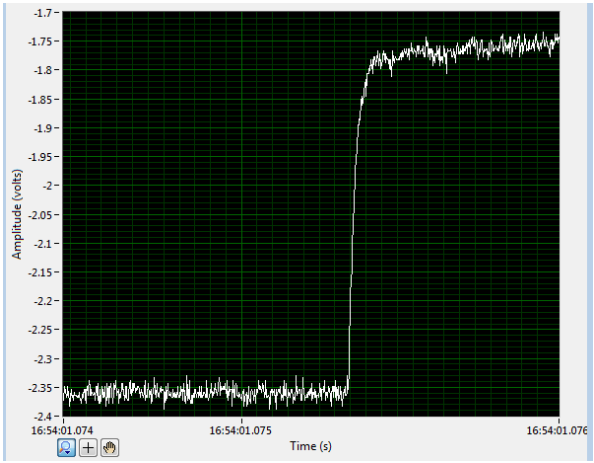

Figure 4.2: Raw Labview data of intensity (plotted with negative values) over time from shock tube test of a dye A $Al0_2$ particle fabricated in a previous research, conducted during current research

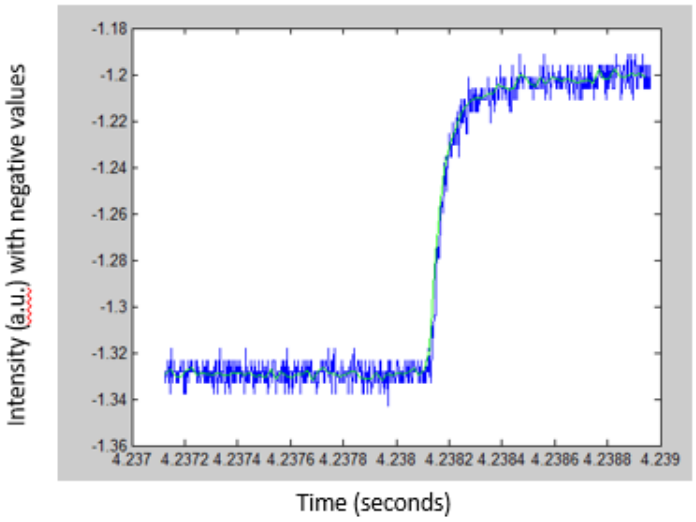

Figure 4.3: Raw data: intensity values for shock tube test of ruthenium/H silica particle

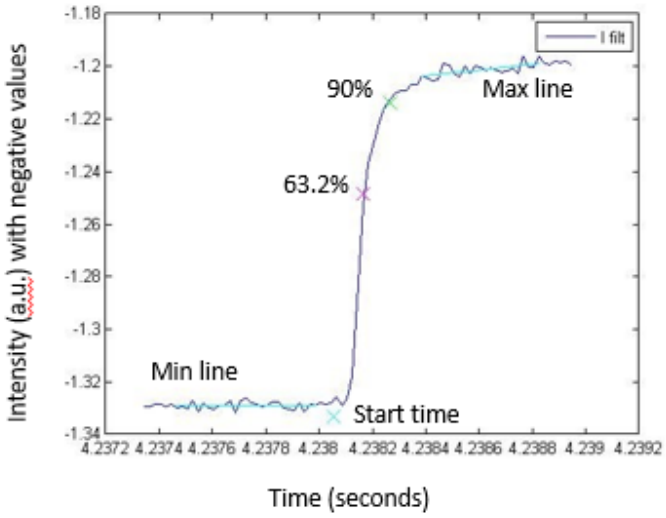

Figure 4.4: Filtered data: intensity values showing maximum, minimum, start time, and 63.2% and 90% response times for shock tube test of ruthenium/H silica particle

Shock tube Results

Sample	Response time (63.2%) µs	Response time (90%) µs
A AlO (134)	46	66
B ZnO	≈218	≈1400
A ZnO	N/A	N/A
B AlO	N/A	N/A
A AlO	N/A	N/A
BH ZnO	N/A	N/A
10:1 A/SiOEP AlO	N/A	N/A
2:1 A/Sioep AlO	54	274
50:1 A/H ZnO	40	60
Ruthenium/H (Ru1C480) Silica	110	210
Ruthenium/fluorescein Silica	N/A	N/A

Figure 4.5: Shock tube results for most successful particle samples

4.2 Stern-Volmer

Stern-Volmer linear-fit curves were generated for particles that were bright enough to get sufficient signal-to-noise. The pressure range shown is 80-120 kPa. Figure 4.6 shows the Stern-Volmer slopes for three consecutive tests of 50:1 A/H $Zn0_2$. These were the best-performing oxide particles fabricated. The mean slope of the particle was 0.23 with a standard deviation of 0.02. Figure 4.7 shows the Stern-Volmer slopes for six consecutive tests of 50:1 B/H $Zn0_2$ (mean of 0.16, standard deviation of 0.02). Overall, these batches of particles performed similarly, but they were much dimmer than the polystyrene particles and not very pressure-sensitive.

Figure 4.8 shows three tests of dye A ZnO_2 and three tests of dye B ZnO_2, both made without using heat. The A ZnO_2 particles were allowed to fully evaporate while the B ZnO_2 particles still had much of its solution left. The A ZnO_2 particles had a mean slope of 0.56 with a standard deviation of 0.10. The B ZnO_2 particles had a mean slope of 0.09 with a standard deviation of 0.03. It is suspected that the B ZnO_2 particles were not given enough time to allow the dye to adequately load to the particles.

Figure 4.9 shows the slope of the ruthenium/H silica particles. These particles consistently demonstrated a slope of approximately 0.3.

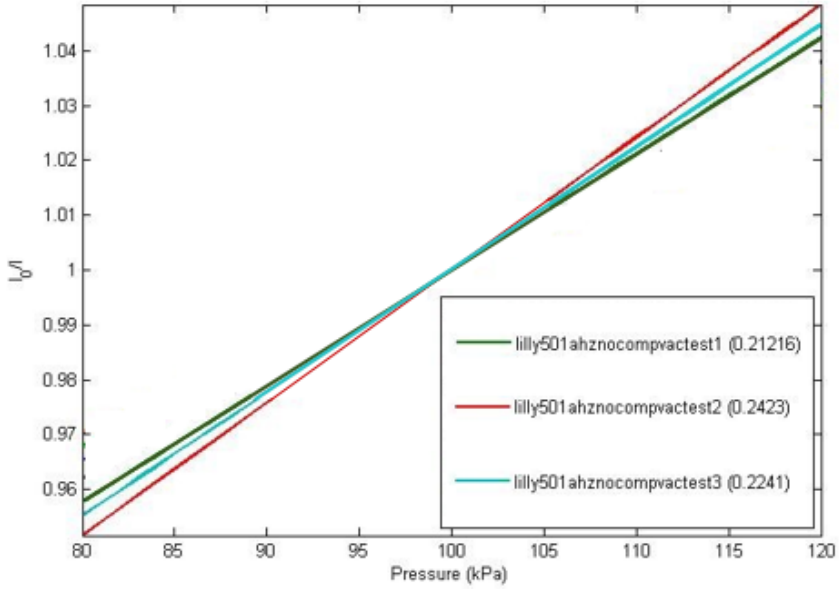

Figure 4.6: Stern Volmer Comparison for 50:1 A/H $Zn0_2$

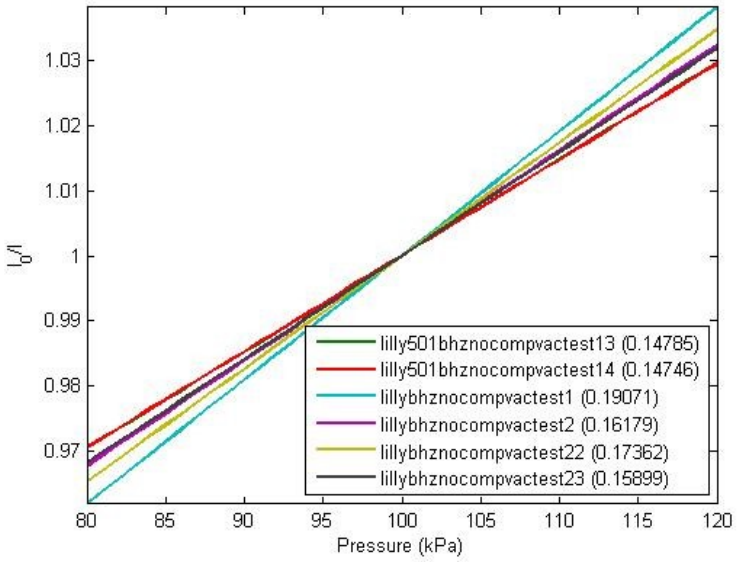

Figure 4.7: Stern Volmer for 50:1 B/H dye $Zn0_2$ particles

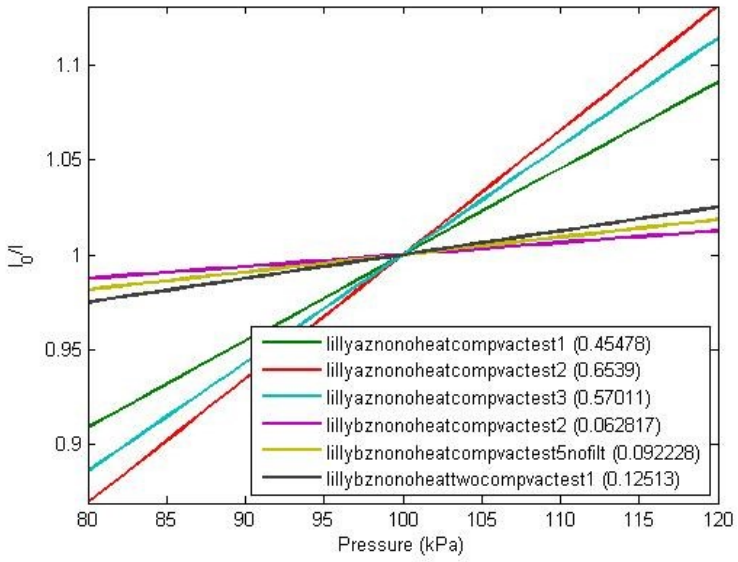

Figure 4.8: Stern Volmer for dye A $Zn0_2$ and dye B $Zn0_2$ particles Without Heat

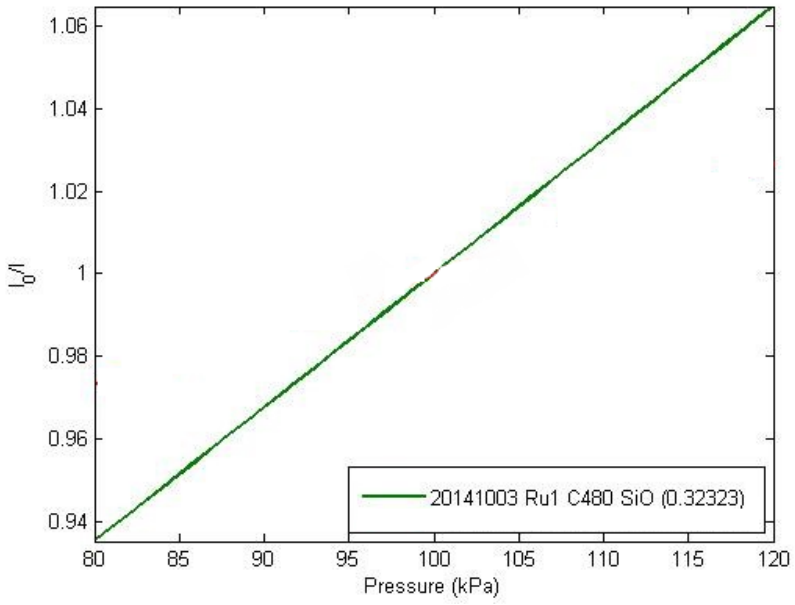

Figure 4.9: Stern Volmer Comparison for 50:1 A/H $Zn0_2$ and B/H $Zn0_2$

4.3 Particle Summary and Discussion

Using an oxide particle for a single dye showed acceptable levels of brightness, pressure sensitivity, and temporal response. However, once a second dye was loaded onto the particle, the emission of each dye was sufficiently quenched so that neither dye was particularly bright, and the pressure sensitivity was not high. Fabrication processes with longer times (at least 24 hours) showed the best results in particle performance. The best-performing particle for overall brightness and pressure sensitivity was the ruthenium/H silica particle, and duplicating this batch was more easily controllable because all of the solution is evaporated out. A summary of the oxide particles produced in this research is shown in Figure 4.10.

Particle	Stern-Volmer
Lilly B AlO with methanol	0.6
A ZnO no heat sample 1	0.56
A ZnO no heat sample 3	0.42
Brian 30:1 A/H AlO discs	0.39
Lilly B Alo with methanol	0.38
Brian 50:1 B/H Alo 100 mg	0.3
Lilly 50:1 B/H Alo with methanol	0.28
Lilly B Zno with methanol	0.28
50:1 A/H ZnO sample 1	0.26
A AlO no heat	0.22
A Zno	.22,.25,.14
A Zno	N/A,.21,.17
A Zno	N/A, N/A, .15
Brian 50:1 A/H Alo 500 mg	0.2
B ZnO hi heat	0.17
K Zno	0.17
50:1 B/H Zno	0.16
A AlO w heat	0.16

Particle	Stern-Volmer
A ZnO no heat sample 2	0.15
30:1 A/H ZnO sample 1	0.1
B ZnO lo heat	0.1
B ZnO Sample 1	0.09
B ZnO no heat	0.09
Lilly 50:1 A/H AlO Sample 1	0.08
Lilly 50:1 A/H ZnO no heat s2	0.08
A ZnO w heat	N/A
Brian A AlO	N/A
Brian 50:1 A/H ZnO Sample 2	N/A
Brian 50:1 B/H Alo 100 mgs2	N/A
Brian 50:1 A/H Alo 500 mgs2	N/A
Lilly 50:1 A/H Alo 500 mgs3	N/A
ruthenium Zno with methanol	N/A
50:1 A/H ZnO no heat	N/A
Brian 50:1 A/H ZnO Sample 1	N/A
Lilly 50:1 A/H ZnO Sample 2	N/A

Figure 4.10: Summary of oxide particles and their slopes

4.3.1 Polystyrene Particles from Previous Researches

The highest standard of comparison for the oxide and silica particles was to A/-SiOEP and A polystyrene particles provided from previous researches in the laboratory. These particles were incredibly bright and pressure-sensitive, but their temporal response was on the order of milliseconds, which cannot be used in turbulent flow applications. The yellow slope in Figure 4.11 shows the sensitivity of the single dye A polystyrene particles, which yielded a slope of approximately 0.81. The dual dye polystyrene particle A/SiOEP's slope, 0.70, is given in Figure 4.12. The polystyrene particles have a 63.2% response time of 12.24 ms and a 90% response time of approximately 17.3 ms. The coated particles are dim and have low Stern-Volmer slopes, averaging around 0.2 in comparison to the 0.7-0.8 slopes seen by the polystyrene particles. The polystyrene particles are several magnitudes of order brighter under 532 nm light. They are different because the polystyrene matrix is completely infused with the dye. This accounts for the slower pressure response because it takes time for oxygen to diffuse through the many layers of polymer and affect the particles' entire luminescence. The coated particles only have a very thin layer of dye, so while it is not very bright, the oxygen can diffuse through the coating faster than it can diffuse through an entire particle. A balance must be found between fabricating a bright particle and minimizing temporal response, because the two variables tend to change inversely. Part of the solution lies in the selection of bright dyes. It would be useful to have two spectrally separate dyes that are both broad in wavelength, so that more light can be integrated across the range of wavelengths. Ruthenium and H dye are both bright and are a promising dye combination for the 355 nm laser. Silica particles have shown promise for brighter particles with acceptable response times.

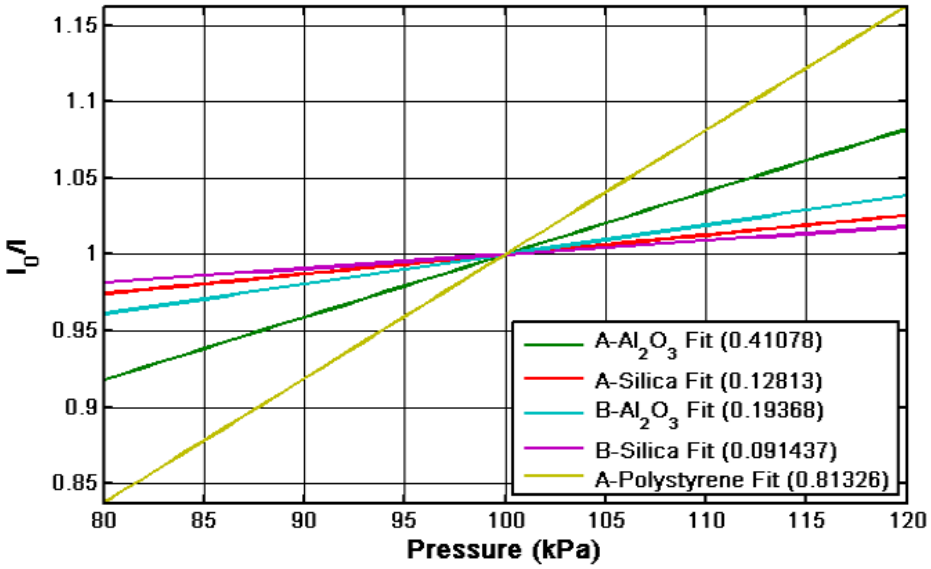

Figure 4.11: Stern Volmer for A polystyrene particles[10]

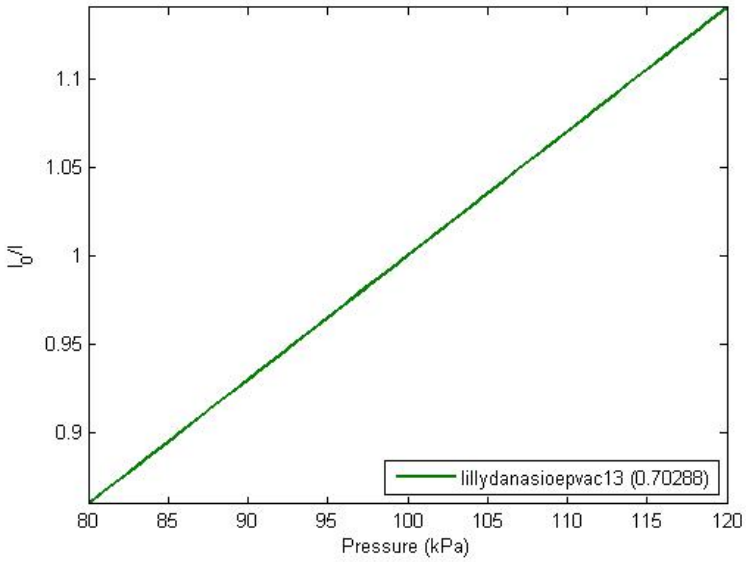

Figure 4.12: Stern Volmer for A/SiOEP polystyrene particles

4.4 Spatially Resolved Film of Particles

4.4.1 Setup Using the Dichroic Filter

In order to validate this setup, A/SiOEP polystyrene particles were tested. Using the windowed ratio-of-ratios method, the particles' light intensity was calibrated to pressure and then used to back-calculate pressure. Figure 4.13 shows the ratio-of-ratio plots for A/SiOEP, with each subplot representing a different pressure on the range 70-130 kPa, by increments of 10 kPa. Figure 4.14 shows a curve fit between the ratio-of-ratios and pressure. Figure 4.15 shows the back-calculated pressures, with each plot representing a different pressure. The standard deviation for the back-calculated pressures was found to be approximately 128 Pa, along the same order of magnitude that previous researcher Daniel Lacroix found.

Researcher Gai Ogihara and Professor Gamal Khalil fabricated D/J and D/G silica particles by forcing dye through a column filled with particles. Due to their brightness, these particles were tested in the setup. Figures 4.16 and 4.17 show processing similar to the A/SiOEP particles for the D/J silica particle. This particle exhibited a standard deviation of 6,955 kPa for pressure back-calculation. This was rather high, and could partially be attributed to a non-homogeneous method of loading the dyes onto the particles as well as their low sensitivity to pressure. Similarly, the D/G silica particle, shown by Figures 4.19 and 4.20, also showed high standard deviations. Figure 4.21 helps to explain part of the large errors. File numbers 1-7 represent pressures 70-130 kPa by increments of 10 kPa. The image displays the average reference and pressure intensities at each pressure. It can be seen that the reference dye is changing with pressure. This occurs because the reference dye is higher in wavelength than the pressure dye, and some of the pressure dye's emission is being absorbed by the reference dye, making it pressure-sensitive. Selecting a higher-wavelength reference

dye poses this risk, and it was determined that the reference dye ideally should be lower in wavelength than the pressure dye to avoid this issue.

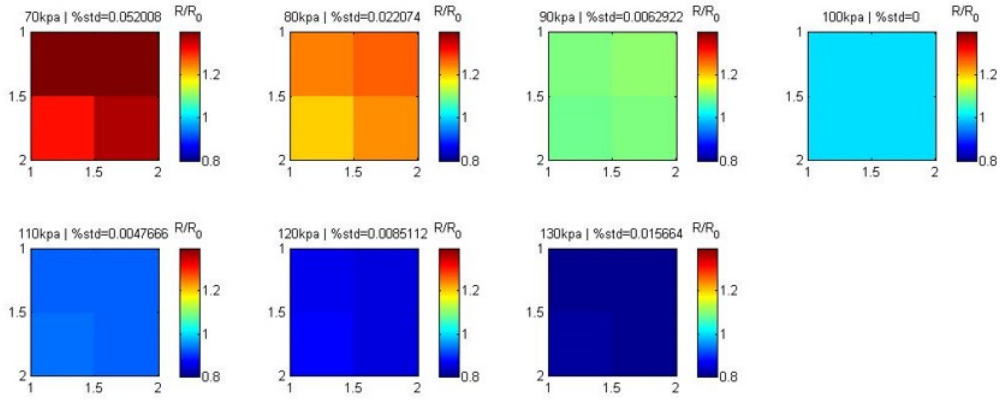

Figure 4.13: Windowed ratio-of-ratios plots for A/SiOEP polystyrene particles

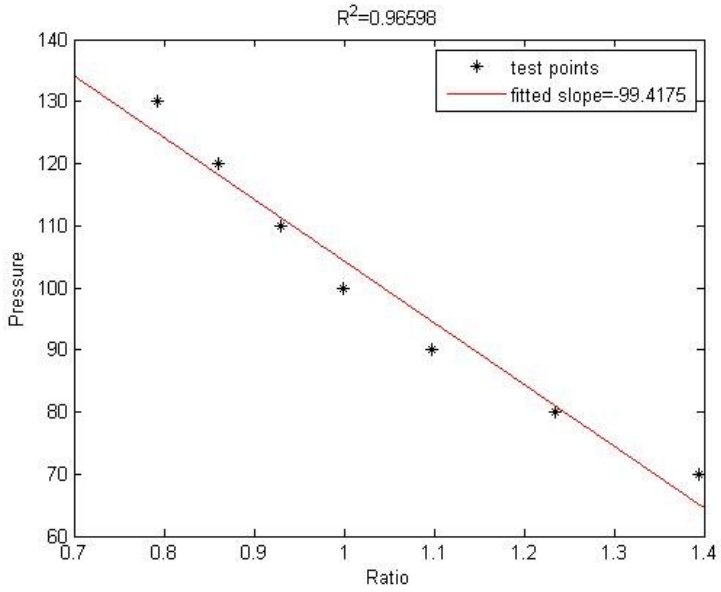

Figure 4.14: Curve fit between ratio-of-ratios and pressure for A/SiOEP polystyrene particles

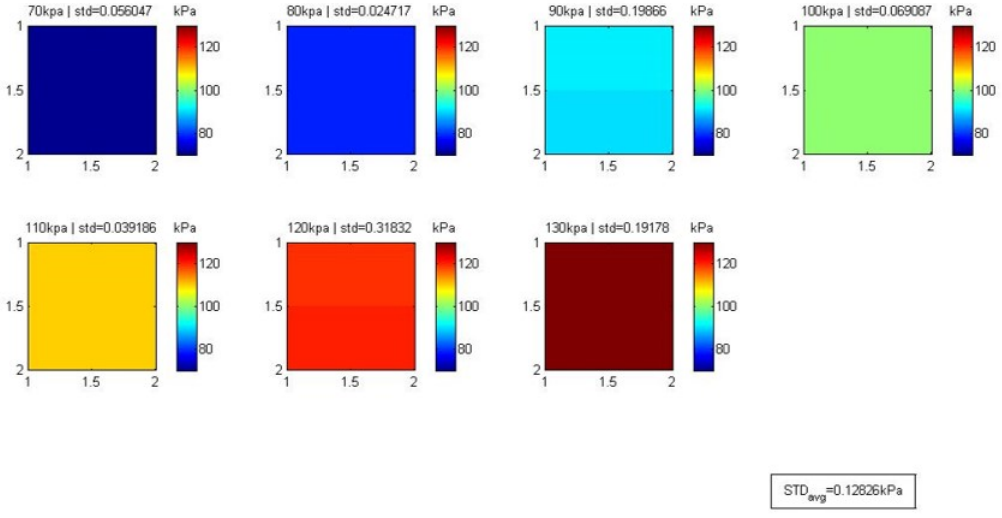

Figure 4.15: Windowed back-calculation of pressure for A/SiOEP polystyrene particle

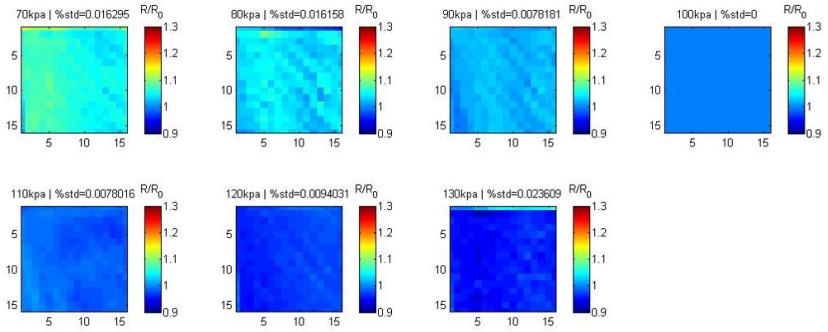

Figure 4.16: Windowed ratio of ratios plots for D/J Silica particles

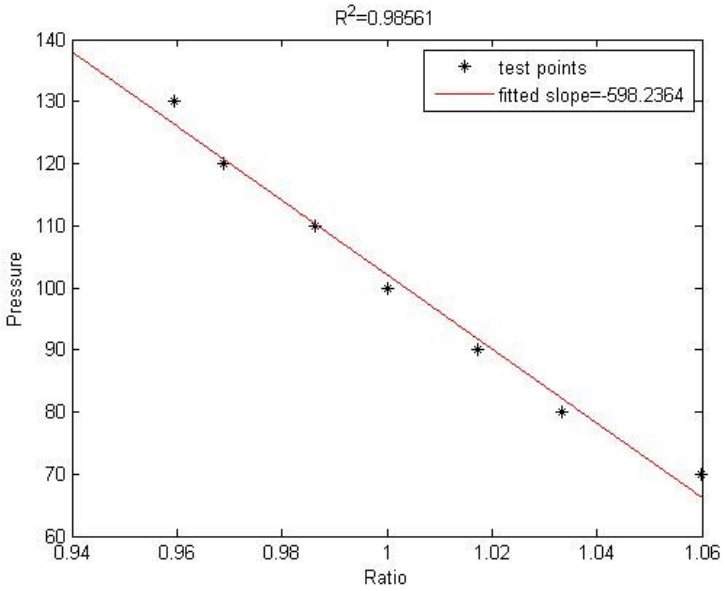

Figure 4.17: Curve fit between ratio of ratios and pressure for D/J silica particles

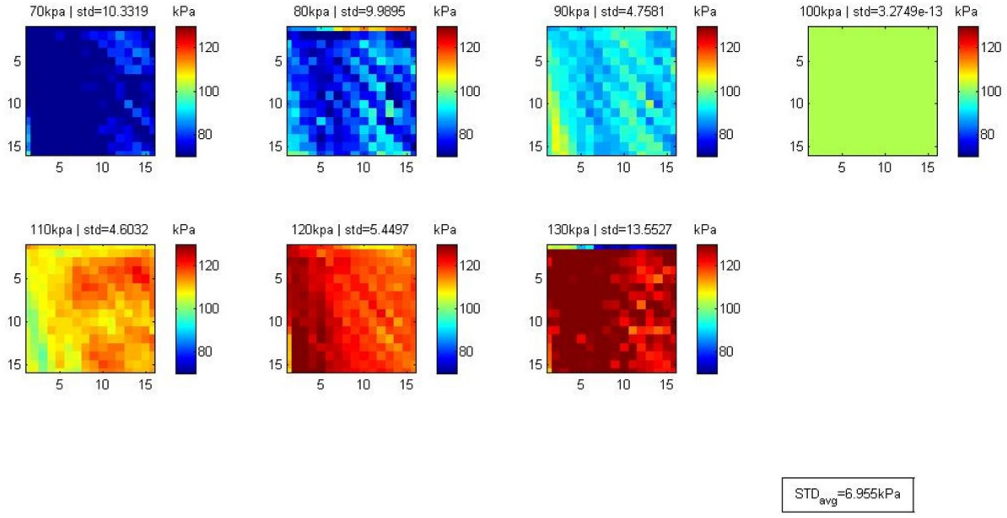

Figure 4.18: Windowed back-calculation of pressure for D/J silica particles

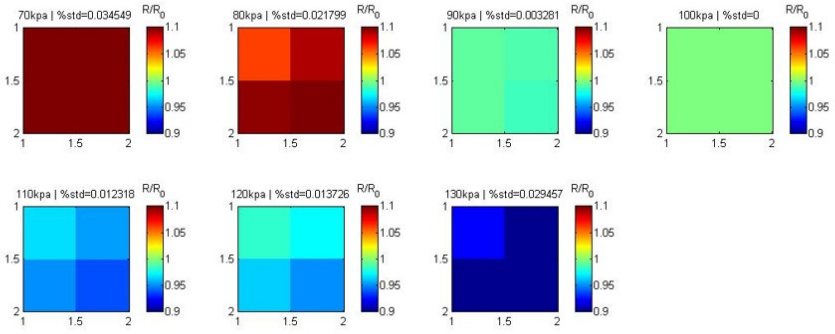

Figure 4.19: Windowed ratio of ratios plots for D/G Silica particles

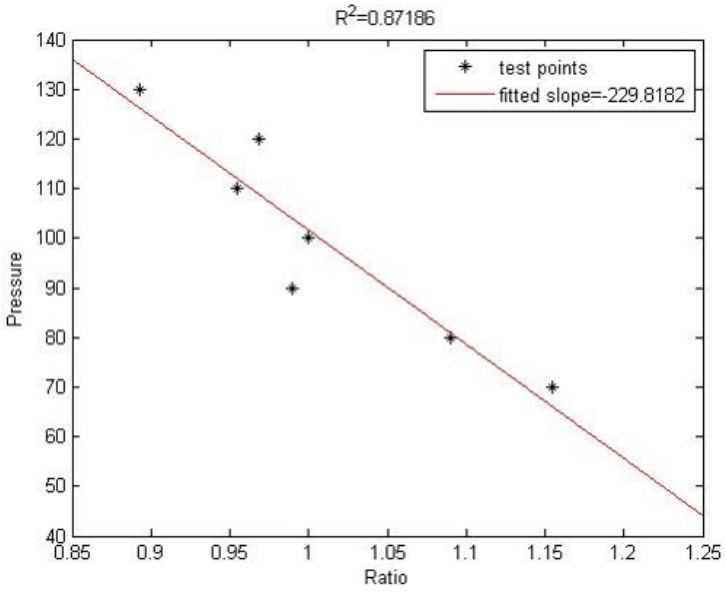

Figure 4.20: Curve fit between ratio of ratios and pressure for D/G silica particles

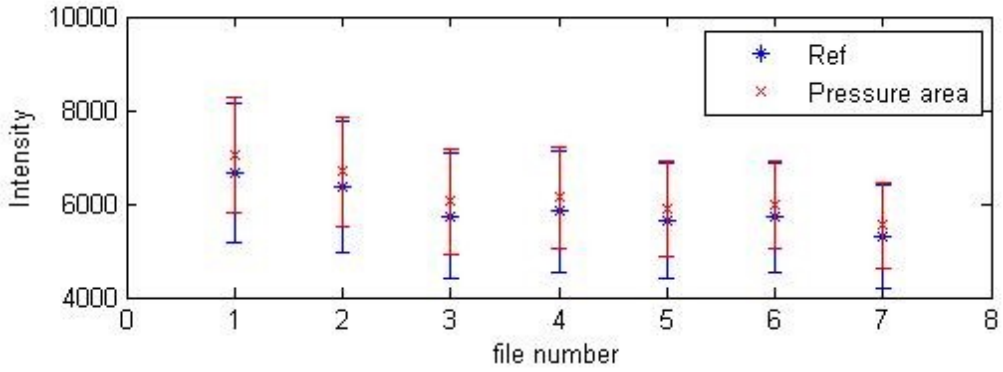

Figure 4.21: Pressure and reference intensity values and ratio of ratio versus pressure for D/G silica particles

4.4.2 Setup Using Cameras on Either Side of the Pressure Chamber

Because this setup used the 532 nm laser, the ruthenium/H silica particles could not be used. An alternative particle had to be fabricated with a reference dye compatible to this excitation source. The ruthenium/fluorescein silica particle was fabricated for use in this setup using the same fabrication method used for making the ruthenium/H silica particles. Because the setup used to conduct Stern-Volmer and shock tube tests was temporarily out of commission, this particle was first tested in this setup. As it turned out upon later analysis, these particles were not pressure-sensitive. Figure 4.22, which shows plots of pressure intensity values at each pressure (80-120 kPa by increments of 10 kPa) for the ruthenium/fluorescein silica particle seen by the Hamamatsu camera, thus demonstrates that the pressure dye did not noticeably change intensity with pressure. Figure 4.23 shows the corresponding intensity values for the reference dye, seen from the Lavision PIV camera. It is important to note that the PIV camera was only reading intensity values around 800 counts out of its 65,000 count range. The fluorescein emission may have just been low in intensity, so it is recommended to use a brighter reference dye such as dye H with this camera.

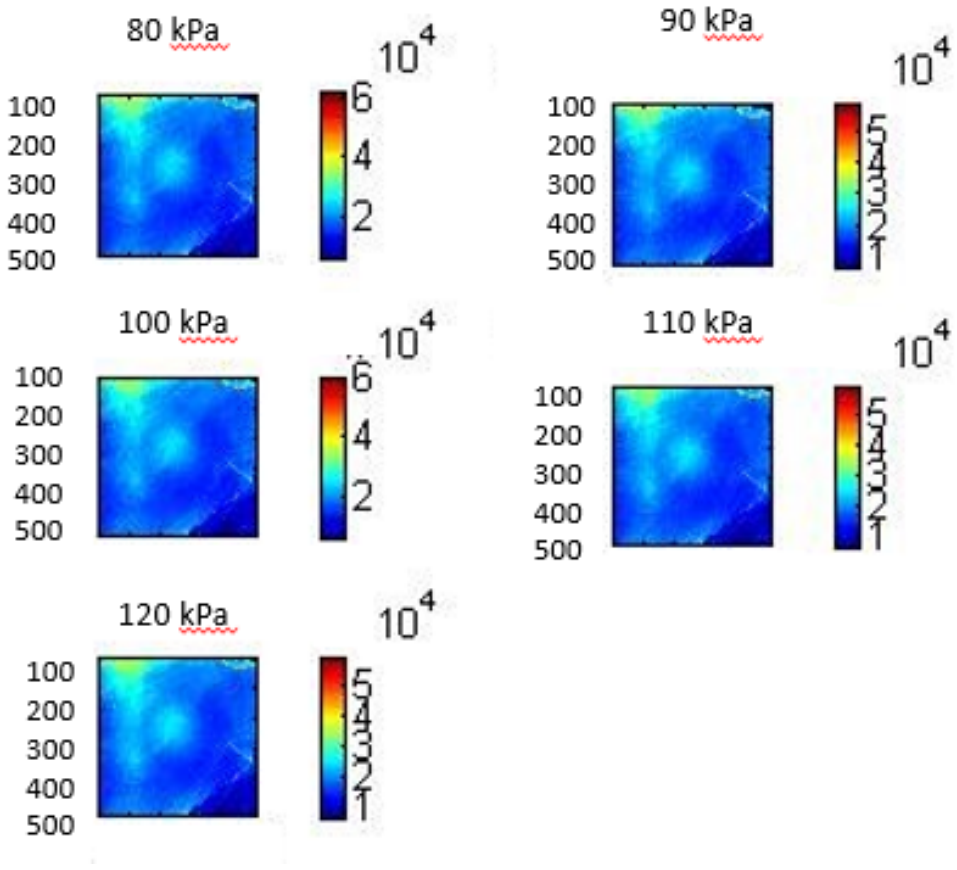

Figure 4.22: Plots of pressure intensity values at each pressure (80-120 kPa) for ruthenium/fluorescein silica particles

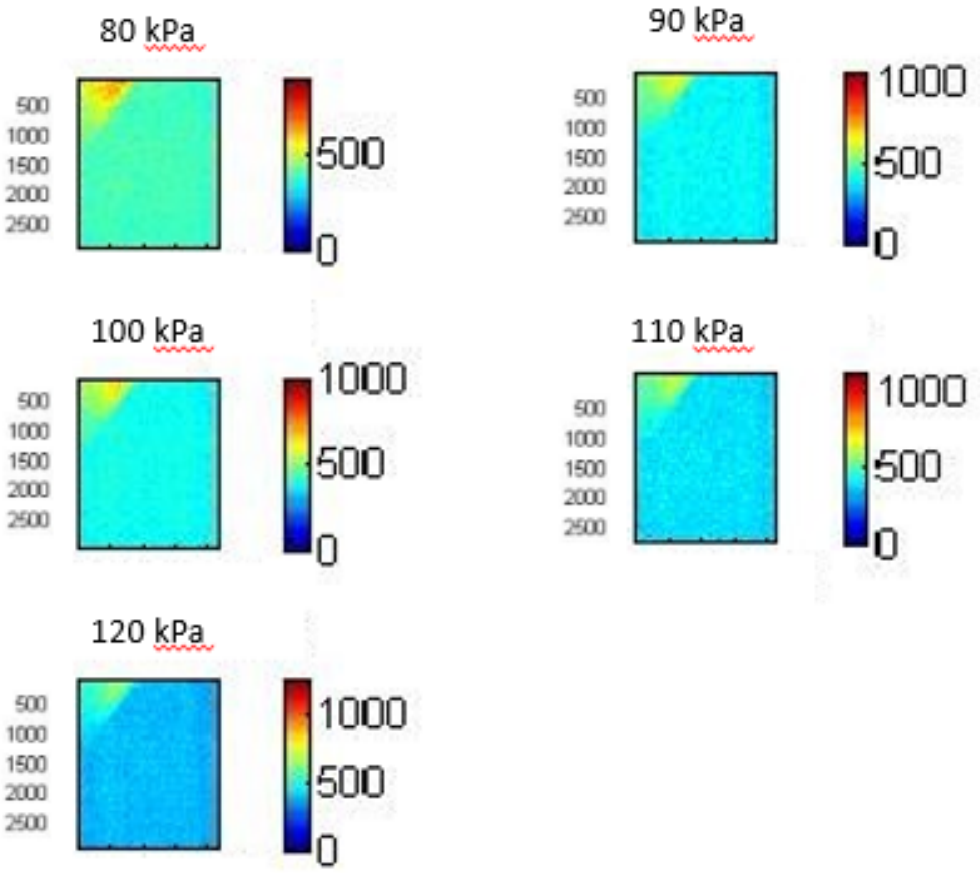

Figure 4.23: Plots of reference intensity values at each pressure (80-120 kPa) for ruthenium/fluorescein silica particles

4.5 Spatially Resolved Individual Particles on Quartz Slide

To help validate this setup's capability for performing pressure-sensitivity tests on aerosolized particles, a quartz slide coated in individual ruthenium/fluorescein silica particles was used. Figure 4.24 shows the particles imaged at atmospheric conditions with the two cameras. The two images look slightly different because the Hamamatsu camera imaging the pressure dye has a lower resolution than the Lavision camera imaging the reference dye. Plots of the pressure dye's and reference dye's thresholded intensity values at each pressure 70-130 kPa are shown by Figures 4.26 and 4.25. The particles were dim compared to the film, with the Lavision camera's intensity counts on the order of its noise count. The ability to get an accurate intensity ratio with an intensity count number this low is questionable. However, both cameras are able to image the particles, and particle identification on these particles would be possible.

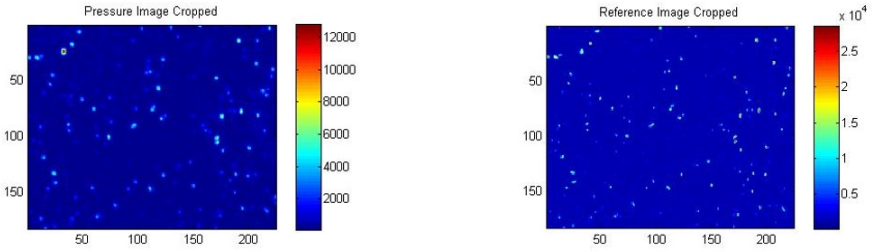

Figure 4.24: Scaled pressure and reference plot at atmospheric pressure for ruthenium/fluorescein silica particles

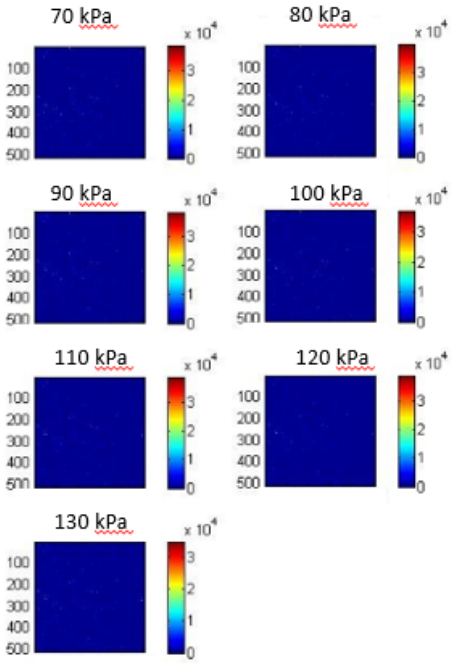

Figure 4.25: Plots of thresholded pressure intensity values at each pressure (70-130 kPa) for ruthenium/fluorescein silica particles

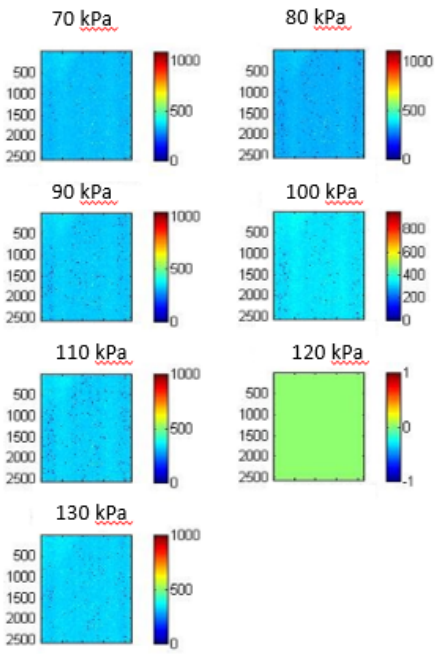

Figure 4.26: Plots of reference intensity values at each pressure (70-130 kPa) for ruthenium/fluorescein silica particles

Chapter 5
SOFTWARE DEVELOPMENT

5.1 Driver code

The Matlab code used to process the data for the spatially-resolved pressure sensitivity tests was originally very lengthy, and the processing required select sections in three different m-files to be run manually, not at all, or sometimes twice after manually changing hard-coded numbers. With a large contribution from fellow researcher Trey Cottingham, this code was updated. The code is now operated from a main driver code, which performs required operations such as flat-field correction and interpolation through sub functions. In the first test setup, 200 frames were taken at each pressure. In the second test setup, this was reduced to 20 frames due to the Lavision camera's program filing framed images in such a way that uses 2 gigabytes of space for seven images of 20 frames each. After reading the images, thresholding is used to eliminate saturated pixels or pixels with intensities low enough to correspond to dark regions, or areas without particles. The images undergo a flat-field correction, and then the frames for each pressure are averaged. Because the Lavision camera's images are 2160 x 2560 pixels and the Hamamatsu's images are 512 x 512 pixels, extra steps are taken to resize the Lavision camera's images. They are first cropped so as to have an aspect ratio of 1, and then they are resized to the Hamamatsu camera's size using the Mathworks imresize function with bicubic interpolation. The region being processed can be cropped further on both images if desired, and then an image registration routine is used to align first all of the pressure images to the pressure image taken at atmospheric conditions, and then all of the references images to the reference image

taken at atmospheric conditions. The reference and pressure images are aligned to each other, and bicubic interpolation is performed for each shift. The ratio-of-ratios method is performed window by window.

5.1.1 Flat-field Correction

Flat-field correction is needed to reduce the effects of photon shot noise, dark current, and small-scale misalignment between the cameras.[1] It accounts for vignetting, a phenomenon commonly seen in cameras where the center of the image is brighter than the edges. The flat-field correction requires subtracting a dark current image and ambient lighting image from the data image, and then dividing the result by a flat-field image, ideally taken from an evenly illuminated scene.[1] The calibration for flat-field correction is performed using equation 5.1.[39]

$$C = \frac{R - D}{F - D} m, \tag{5.1}$$

where C is the corrected image, R is the raw image, F is the flat-field image, D is the dark field, and m is the average value of the corrected flat-field, (F-D).

5.1.2 Image Registration

Image registration is performed to align two or more images to each other so that their intensities can be ratioed. The sub function uses a multi-pass windowed cross-correlation routine that initially aligns the images on a more course scale, and then aligns the images again on a more fine scale.[25] The routine outputs a vector field indicating the magnitude that one window has to shift to align with another. The user is given the option to manually remove outlier vectors.[25]

5.1.3 Interpolation

The vector field from the image registration sub function is used in the interpolation sub function. This routine alters pixel intensities based on the displacements given by the vector field using a cubic interpolation. The interpolation sub function outputs aligned and interpolated images.

Chapter 6

CONCLUSIONS

Several methods of fabrication for dual-dye particles were tested in this research. Pressure-sensitive and pressure-insensitive dyes were loaded onto the particles by mixing them together in a solution with a boiling flask. As the solution evaporated, the dyes, which were dissolved in the solution, precipitated and loaded onto the particles or the flask. Variables such as fabrication time, dye concentrations, solution, temperature, and particle type were controlled. Particles heated with higher temperatures and higher dye concentrations took less time for dye loading to occur. However, fabrication methods in which the dye was loaded to the particle over a process 24 hours and longer tended to have better results, likely due to the increased controllability and uniformity of the loading process. The particles' dye ratio and pressure-sensitivity were highly susceptible to the amount of evaporation of the solution. On a given day, the amount of solution evaporating from the flask might change, regardless of best efforts to keep a uniform temperature by using a sand bath and the same dial settings on the hot plates. Also, each dye had a different solubility in the solution and would not necessarily precipitate or load onto the particles in the same ratio each time. In the end it was determined that the easiest way to control the process was to allow the solution to completely evaporate over several days with continuous magnet stirring, ensuring that a known amount of dye would be coming out of solution while attempting to maintain homogeneity.

Overall, single-dye $Al0_2$ and $Zn0_2$ particles were brighter and more pressure-sensitive than the dual-dye particles. The dual-dye oxide particles were dim and

not very pressure-sensitive. The challenge lies in that the oxide particles are coated only by a thin layer of the dyes. The dyes have to compete for surface area and are limited in luminescence. The concentration of the dyes loaded to the particle can only be increased so much before self-quenching occurs in the small space they occupy. By comparison, polystyrene particles, whether dual or single dye, are very bright and very pressure-sensitive. The dye is saturated through the matrix of the polystyrene, so a much higher amount of dye is available without the same risk of self-quenching. The same characteristic that makes the oxide particles dim, however, makes them fast-responding. Oxygen can penetrate the thin coating of the dye in an oxide particle much quicker than the multiple layers of dyes in the polystyrene particles. The silica particle provides a balance between these two extremes. The silica particles tested in this research had a slower response time than several of the oxide particles, but they were consistently brighter.

Films for in-house pressure-sensitive particles were tested with a two-camera system with a dichroic filter, and processing was performed on these particles. The setup was validated by comparing results of an A/SiOEP polystyrene particle from previous research to the results found from the current setup. It was found that errors in back-calculating pressure can be reduced by using reference dyes that emit at lower wavelengths than pressure dyes, or at least by ensuring that the reference dye is not absorbing the pressure dye's emission.

A new setup was designed to allow for a PIV camera to image the reference dye's fluorescence on the opposite side of the camera imaging the pressure dye's fluorescence. A larger pressure chamber was designed for this setup that incorporated larger windows, included a built-in clamp that could hold larger quartz slides regardless of their thickness, and that has removable side walls for more flexibility in the setup. The pressure chamber was designed and built to accommodate future tests with si-

multaneous pressure, temperature, and velocity measurements.

The ruthenium/H silica particle showed the most promise with the 355 nm YAG laser. It was bright, pressure-sensitive, and had a reasonable time response. However, accommodation was required for the broken 355 nm YAG laser. A 532 nm laser was used in the new setup, and a particle compatible with the 532 nm laser was fabricated and tested. This new particle, the ruthenium/fluorescein silica, was bright but failed to demonstrate pressure sensitivity.

6.1 Recommendations for Future Work

The ruthenium/H silica particle should be tested in the two-camera setup with the 355 nm YAG laser and PIV camera imaging the reference dye. If the PIV camera is not sensitive enough to capture the emission of dye H, the filters on the cameras could be swapped so that the PIV camera images the pressure dye and the Hamamatsu camera images the reference dye. Otherwise, a new set of particles designed for the 532 nm laser will need to be developed and tested. Silica particles were the most viable option from this research and should be used for particle fabrication. One of the issues with the oxide particles was that the dye could only be applied in a thin coating on the outside of the particle. It might be useful to find a particle that can incorporate dyes into the outermost layers of its matrix, but not all the way through like the polystyrene particle.

For the case of aerosolized particles, particle intensity can vary based off of size, laser excitation, density, and nonhomogenous effects in the dye concentrations or ratios on the particle itself. These variations could be corrected in a film with normalization through the ratio-of-ratios method. The current ratioing method may be difficult to incorporate into an environment where the imaging subject is constantly moving. It may be useful to incorporate particle recognition into the processing to

take into account particle size and location so that intensities may potentially be ratioed in a different way.

Lastly, if the setup using the Lavision camera as the reference camera is fully validated with working particles, tests should be performed utilizing the Lavision camera simultaneously for PIV and reference dye ratioing.

BIBLIOGRAPHY

[1] Tianshu Liu and John P Sullivan. *Pressure and Temperature Sensitive Paints*. Springer, 2005.

[2] Jonathan Howard. Bead making and response time: A global report. 2012-2013.

[3] aerospaceweb.org; history. http://www.aerospaceweb.org/design/psp/history.shtml. Accessed: 2014-2.

[4] J Kavandi, J B Callis, M Gouterman, G E Khalil, D A Wright, E Green, D H Burns, and B McLachlan. Luminescent barometry in wind tunnels. *Review of Scientific Instruments Volume 61(11) page 3340-3347*, 1990.

[5] Martin Gouterman. Oxygen quenching of luminescence of pressure sensitive paint for wind tunnel research. *Journal of Chemical Education Vol. 74 No. 6*, June 1997.

[6] James H Bell, Edward T Schairer, Lawrence A Hand, and Rabindra D Mehta. Surface pressure measurements using luminescent coatings. *Annual Reviews Fluid Mechanics 33:155-206*, 2001.

[7] Martin Gouterman, James Callis, Larry Dalton, Gamal Khalil, Youssef Mebarki, Kevin Cooper, and Michel Grenier. Dual luminophor pressure-sensitive paint: Iii. application to automotive model testing. *Institute of Physics Publishing; Measurement Science and Technology 15 (2004) 1986-1994*, 20 August 2004.

[8] Fletcher Kimura, Miguel Rodriguez, Jesse McCann, Brenden Carlson, Dana Dabiri, Gamal E. Khalil, James B. Callis, Younan Xia, and Martin Gouterman. Development and characterization of fast responding pressure sensitive microspheres. *Review of Scientific Instruments 79*, 2008.

[9] Innovative scientific solutions, inc. http://www.psp-tsp.com/. Accessed: 2014-8-18.

[10] Daniel J Lacroix. Development and characterization of pressure-sensitive microbeads for simultaneous barometry and velocimetry for fluid dynamic applications. Master's thesis, University of Washington, 2014.

[11] A. Neal Watkins, Bradley D. Leighty, and William E. Lipford. Development of a pressure sensitive paint system for measuring global surface pressures on rotorcraft blades. *Instrumentation in Aerospace Simulation Facilities*, 2007.

[12] T. J. Bencic. Rotating pressure and temperature measurements on scale-model fans using luminescent paints. *AIAA Paper 98-3452*, 1998.

[13] J W Gregory, K Asai, T Liu, and J P Sullivan. A review of pressure-sensitive paint for high-speed and unsteady aerodynamics. *Proceedings of the Institution of Mechanical Engineers. Part G: Journal of Aerospace Engineering*, 2007.

[14] Fletcher Kimura, Gamal Khalil, Nobuyuki Zettsu, Younan Xia, James Callis, Martin Gouterman, Larry Dalton, Dana Dabiri, and Miguel Rodriguez. Dual luminophore polystyrene microspheres for pressure-sensitive luminescent imaging. *Institute of Physics Publishing; Measurement Science and Technology 17 (2006) 1254-1260*, 2006.

[15] Muhammet E Kose. *Multi-luminophore Coatings for Pressure Sensitive Paint Applications*. PhD thesis, University of Florida, 2005.

[16] Dana Dabiri. Cross-correlation digital particle image velocimetry- a review. *Departments of Aeronautics & Astronautics*, 2006.

[17] Richard D Keane and Ronald J Adrian. Optimization of particle image velocimeters: Ii. multiple pulsed systems. *Measurement Science and Technology 2 963*, 1991.

[18] Shinkichi Abe, Koji Okamoto, and Haruki Madarame. The development of piv-psp hybrid system using pressure sensitive particles. *Measurement Science and Technology 15 1153-1157*, 2004.

[19] Fletcher Kimura, Jesse McCann, Gamal E. Khalil, Dana Dabiri, Younan Xia, and James B. Callis. Simultaneous velocity and pressure measurements using luminescent microspheres. *Review of Scientific Instruments 81*, 2010.

[20] J. R. Lakowicz. *Principles of Fluorescence Spectroscopy*. Plenum Press, 1983.

[21] A. Baron. *On Time and Spatially Resolved Measurements of Luminescence-Based Oxygen Sensors*. PhD thesis, University of Washington, 1996.

[22] G. Dale, A. Baron., C. Tyler, and V. Mastrocola. *Proceedings of the International Congress Instrumentation in Aerospace Simulation Facilities*. ICIASF, 1997.

[23] S.P. Chan, Z. J. Fuller, J. N. Demas, and B. A. DeGraff. Optimized gating scheme for rapid lifetime determinations of single-exponential luminescence lifetimes. *American Chemical Society; Analytical Chemistry 73 4486*, 2001.

[24] L. D. Landau and E. M. Lifshitz. *Fluid Mechanics*, volume 6. Pergamon Press, 1959.

[25] Trey Cottingham. Characterization and optimization of temperature-sensitive microbeads for simultaneous thermometry and velocimetry for fluid dynamic applications. Master's thesis, University of Washington, 2015.

[26] Christopher E. Brennan. *Fundamentals of multiphase flow*. Cambridge University Press, reprint ed. edition, 2005.

[27] R Wan. Phd thesis. *Department of Chemistry, University of Washington*, 1992.

[28] Tianshu Liu, B. T. Campbell, S. P. Burns, and J. P. Sullivan. Temperature- and pressure-sensitive luminescent paints in aerodynamics. *Applied Mechanics Reviews 50(4), 227-246*, 1997.

[29] B. McLachlan and J. Bell. Pressure-sensitive paint in aerodynamic testing. *Experimental Thermal and Fluid Science vol. 10, no. 4, Paper 93-485*, 1995.

[30] Hirotaka Sakaue and John P Sullivan. Time response of anodized aluminum pressure-sensitive paint. *AIAA Journal Vol. 39, No. 10*, October 2001.

[31] A Baron, J. D. Danielson, M. Gouterman, J. R. Wan, J. B., Callis, and B. McLachlan. Submillisecond response times of oxygen-quenched luminescent coatings. *Review of Scientific Instruments*, 1993.

[32] James W. Gregory and John P. Sullivan. Effect of quenching kinetics on unsteady response of pressure-sensitive paint. *AIAA Journal Vol. 44, No. 3*, 2006.

[33] Michael A. Saad. *Compressible Fluid Flow*. Prentice-Hall, Inc., 1985.

[34] L. Coyle. *Lifetime Measurements on Pressure Sensitive Paints: Temperature Correction, Effects of Environment, and Trials on New Luminescent Materials.* PhD thesis, University of Washington, 1999.

[35] J. H. Waite. *Anal. Chem. 56 1935*, 1984.

[36] Jonathan Howard. Development and characterization of pressure- & temperature-sensitive bbead (ptsbeads) & measurement of flow behind a heated cylinder using ptsbeads. *University of Washington*, 2013.

[37] Daniel Levine and George J. Monser. Polarization, ghost, and shading effects in dichroic beam splitters. *Journal of the Optical Society of America Volume 51, Number 7*, 1961.

[38] Microspheres & pparticle handling guide; polyscience, inc.

[39] Princeton Instruments. Flat-field correction. http://www.princetoninstruments.com/cms/index.php/ccd-primer/152-flat-field-correction.

[40] D Dabiri. Digital particle imgae thermometry/velocimetry: a review. *Experimental Fluids*, 46:191–241, 2009.

[41] J Duncan, T Bryce, H Thomsen, D Dabiri, JR Hove, and M Gharib. An extended study of a generalized digital particle image velocimetry (DPIV) processing technique. *Measurement Science and Technology*, 20, 2009.

[42] Chu King Fung. Nikon af-s 85mm f1.4g. 3D Solidworks 2012 Model, February 2013.

[43] GE Khalil, C Costin, J Crafton, G Jones, S Grenoble, M Gouterman, JB Callis, and LR Dalton. Dual-luminophor pressure-sensitive paint I. ratio of reference to sensor giving a small temperature dependency. *Sensors and Actuators B*, 97:13–21, 2004.

[44] GE Khalil, K Lau, GD Phelan, B Carlson nd M Gouterman, JB Callis, and LR Dalton. Europium beta-diketonate temperature sensors: Effects of ligands, matrix, and concentration. *Review of Scientific Instruments*, 75(1):193–206, January 2004.

[45] Daniel Lacroix, Teddy Viraye-Chevalier, Guillaume Seiter, Jonathan Howard, Dana Dabiri, Gamal E. Khalil, Younan Xia, and Cun Zhu. Characterization of multi-dye pressure-sensitive microbeads. *Review of Scientific Instruments*, 84, 2013.

[46] J.R. Lakowicz. *Principles of Fluorescence Spectroscopy.* Kluwer Academic/-Plenum Publishers, New York, 2nd ed edition, 1999.

[47] M. J. Morris, J. F. Donovan, J. T. Kegelman, S. D. Schwab, R. L. Levy, and R. C. Crites. Aerodynamic applications of pressure sensitive paint. *AIAA Journal 31(3) 419-425*, 1993.

[48] Majid Nabavi. Unsteady and pulsating pressure and temperature: a review of experimental techniques. *REview of Scientific Instruments*, 81, 2010.

[49] M. Raffel, M. Willert, and J Kompenhans. *Particle Image Velocimetry: A Practical Guide.* Springer-Verlag, Berlin, 1998.